Synthesis and Characterization of Zeolite A from Kaolin of Ethiopia: Studies of its application as detergent builder and in tannery wastewater treatment

Lijalem Ayele Regassa

A Thesis Submitted to

Department of Chemistry

Presented in Fulfillment of the Requirnments for the Degree of Doctor of Philosophy (Inorganic Chemistry)

Addis Ababa University

Addis Ababa, Ethiopia

November, 2016

ADDIS ABABA UNIVERSITY

SCHOOL OF GRADUATE STUDIES

This is to certify that the thesis prepared by Lijalem Ayele, entitled: **‘’Synthesis and Characterization of Zeolite A from Kaolin of Ethiopia: Studies of its application as detergent builder and in tannery wastewater treatment’’** and submitted in partial fulfillment of the requirements for the Degree of Doctor of Philosophy (Inorganic Chemistry) complies with the regulations of and meets the accepted standards with respect to originality and quality.

Signed by the Examining committee:

Examiner _____Signature _____ Date_____

Examiner _____Signature _____ Date_____

Examiner _____Signature _____ Date_____

Advisor _____ Signature _____ Date_____

Advisor _____ Signature _____ Date_____

_____

Chair of Department or Graduate Program Coordinator

Abstract

SYNTHESIS AND CHARACTERIZATION OF ZEOLITE A FROM KAOLIN OF ETHIOPIA: STUDIES OF ITS APPLICATION AS DETERGENT BUILDER AND IN TANNERY WASTEWATER TREATMENT

Lijalem Ayele

Addis Ababa University, 2016

Zeolite A is a synthetic sodium aluminium silicate often also referred to as Zeolite NaA or Zeolite 4A with LTA framework type. It is the universal type of synthetic zeolite used for detergent manufacturing and water softening to substitute the environmentally unfriendly material sodium tripolyphosphate (STPP). Despite its remarkable potential, the high cost of zeolite A has restricted its effective use in detergents. Based on this, in this work detergent-grade zeolite A has been synthesized using kaolins of Ethiopia; Ansho and Bombowha kaolins. The synthesis was done by two different methods: the conventional hydrothermal and alkali fusion methods. The process parameters for the synthesis of detergent-grade zeolite A, like the metakaolination temperature, alkaline concentration, crystallization time crystallization temperature and gel formation conditions have been systematically studied. The characterization of the synthesized zeolite was carried out by X-ray diffraction (XRD), Scanning electron microscopy (SEM), Thermogravimetric analysis (TGA) and Inductively coupled plasma optical emission spectroscopy (ICP-OES) study confirms its formation. By the conventional hydrothermal synthesis, cation exchange capacity (CEC) exceeding 290 mg of $CaCO_3$/g and average particle size of 3.0 µm, whereas by the alkali fusion method, cation exchange

capacity (CEC) greater than 300 mg of $CaCO_3$ and average particle size of 4.0 µm are achieved, which make the zeolite A obtained as promising detergent builder. The study also included evaluating the detergency action of the powder detergent formulated with the synthetic zeolite A by analyzing some physicochemical properties like foam height, pH value, moisture content and alcohol and water insolubility test. The results show that this detergent has comparable detergency with a known commercial powder detergent.

Wastewater treatment from tanneries is another environmental issue that needs great attention in Ethiopia. In this work we have investigated the removal of Cr(III) from tannery wastewater with Cr(III) > 2000 ppm collected from various tannneries in Ethiopia. This was done using the synthetic zeolite A prepared using kaolin from Ethiopia and other natural adsorbents for comparison. The results indicate that 99.8% removal and about 200 mg/g adsorption capacity of Cr(III) with 100 g/L and 5 g/L adsorbent dosage, respectively. The adsorbent dosage was varied systematically from 2 g/L to 100 g/L. Kinetic and adsorption isotherm studies have been conducted using zeolite A as adsorbent. The removal efficiency of the synthetic material for Cr(VI) was also evaluated incomparison with other natural adsorbents from Ethiopia. In this aspect the natural adsorbents bentonites and synthetic clay materials hydrotalcite ans nano-hydrotalcatite have been found to be efficient. The natural bentonite exihibited the maximum removal of 90% and the hydrotalcite exhibited 100% removal of Cr(VI).

Acknowledgment

First of all, I would like to express my deep gratitude to my supervisor, **Prof. Isabel Diaz**, for her guidance, valuable ideas, optimism as well as sense of humor. In particular, I do appreciate her encouragement and support in my ‘’down face’’ time! It will be an enjoyable memory the time I worked with her.

I cordially thank my supervisor **Dr Yonas Chebude** for his advice, patience and facilitating my PhD work.

I would like to express my sincere gratitude to **Prof. Joaquin Pérez-Pariente** who became my host while I was at the Institute of Catalysis and Petrochemistry (ICP-CSIC), Spain, for his many ideas, good suggestions and also for all discussions concerning our work. My acknowledgment also goes to **Dr Eduardo Pérez,** for his cooperation in many aspects of this work and for his wholehearted advice.

I am very thankful to Dr. Manuel Sanchez and Andres Varela for running SEM of my samples, Conchi for running powder XRD, Isabel Pacheco for running TGA, Javier Agundez for handling all my samples for ICP-OES, and Beatriz Bernardo for her help in using the X-pert software.

I would also like to extend my gratitude to all staffs at Institute of Catalysis and Petrochemistry (ICP-CSIC) for their help and the enjoyable atmosphere, with special thanks to the Molecular Sieves Group: Dr. Luis, Dr. Enrique, Dr. Carlos, Dr. Victoria, Ana, Dr. Almudena, Dr. Irene, Dr. Teresa, Pilar, Claudia, Manuel, and all others whose names are not mentioned.

I am extremely grateful to all PhD students in Chemistry Department AAU for creating an incredible friendly atmosphere as well as their helpful discussion. I would like to particularly acknowledge the Inorganic Chemistry research team for the unforgettable friendship and for the extremely rewarding feeling of belonging to the group: Dr. Wondimagegn Mamo, Guta Gonfa, Kiros Guesh, Taju Sani, Masresha Amare, Tesfaye Haile and Yaregal Awoke.

My best gratitude also goes to Getachew Gizaw, PhD student in University of Uppsala, Sweden for his immediate respones while I needed published journal articles.

I must also extend my acknowledgment to Hawassa Ceramic factory for giving us kaolin samples freely. The Ethiopian Leather Industry Development Institute (LIDI) is also deeply acknowledged for the supply of tannery wastewater. The Research and Development Directorate of the Ministry of Mines is acknowledged for the Bentonite samples, and the Earth Science Department of AAU for the natural zeolites.

I would also like to extend my great thanks and appreciation to Bekas chemicals plc for allowing me to work in their lab and Repi-Wilmar soap and detergent factory for giving me one month internship in their factory.

I am also indebted to Adigrat University for sponsoring me to pursue my PhD study and the Department of chemistry, Addis Ababa University, for providing the necessary resources to accomplish my study and the AAU Graduate Studies Program for supporting me for three months in Spain (ICP-CSIC).

Finally, I wish to thank my family and my colleagues for their unconditionally support and encouragement.

Table of Contents

List of schemes

List of Figures

List of Tables

List of symbols used and Abbreviations

Å……..Angstrom

nm……Nanometer

µm……...Micrometer

θ……..Theta

LTA……Linde Type A

XRD……X-Ray Diffraction

ICP-OES……Inductively Coupled Plasma Optical Emission Spectroscopy

SEM……Scanning Electron Microscopy

TGA……Thermogravimetric Analysis

DTG……Derivative Thermogravimetry

CEC……Cation Exchange Capacity

1,5-DPC……..1, 5-Diphenyl Carbazide

ET-7…….Ethiopian zeolite sample number seven

HT……Hydrotalcite

SBA-15 ……...Santa Barbara Amorphous

AAS……Atomic Absorption Spectroscopy

FAAS……. Flame Atomic Absorption Spectroscopy

UV-Vis……Ultra Violet Visible

TEM……Transmission Electron Microscopy

STEM ……Scanning Transmission Electron Microscopy

HAADF……...High Angular Annular Dark Field

EDS……..Energy Dispersive X-ray Spectroscopy

CHAPTER ONE

1. Introduction

1.1. General introduction to Zeolites

Zeolites are three dimensional crystalline, microporous, hydrated aluminosilicate materials, which have enormous scientific and industrial significance in the areas of separation (purification, drying, environmental treatment), ion exchange (water softener in detergent industry, radioactive waste storage, and treatment of liquid waste) and solid catalyst (cracking of hydrocarbons, catalytic reforming, hydroisomerization, dewaxing of hydrocarbon oils, isoparaffin/olefin alkylation, transalkylation of aromatics, and methanol to gasoline conversion)[1,2,3]. These applications are based on their inherent properties such as uniform pore size/shape, acidic properties, mobile extra framework cation and surface properties like hydrophilicity/hydrophobicity[4]. Zeolite structural formule are based on the crystallographic unit cell:

$$\mathbf{M_{x/n}[(Al_2O)_x(SiO_2)_y]\cdot wH_2O}$$

where M is an alkali or alkaline earth cation, n is the valence of the cation, w is the number of water molecules per unit cell, x and y are the total number of tetrahedra per unit cell, and the ratio y/x usually has values of 1 to 5, although for high silica zeolite where y/x can be ranging from 10 to 100[5].

The history of zeolites began in 1756 when a Swedish mineralogist Cronstedt, discovered the first natural zeolite mineral, stilbite[6]. He noticed an unusual behavior when the silicate mineral was heated. It shows visible loss of water, a phenomena he called

‘intumescences’ and from which the name zeolite, a Greek word meaning ‘boiling stone’ was derived. Until now, over 40 types of natural zeolites have been found (Table 1)[7], but fewer than 30 of them have had their structures solved. Recently, many natural zeolite resources have been discovered around the world, and the applications of these natural species are drawing increasing attention. At present, natural zeolites are widely used in the fields of drying and separation of gases and liquids, softening of hard water, treatment of sewage, and melioration of soils. Despite their easy availability and low cost, natural zeolites cannot meet all the requirements for various industrial applications. This is due to the presence of impurities in natural zeolites, non-uniform pore size in their particles and their low ion exchange capacities[8]. This situation made synthetic zeolites to recieve more attention in industrial sector than natural zeolites[6]. By the end of the 1940s, a number of scientists started to carry out research on massive synthesis of zeolites through mimicking of the geothermal conditions for natural zeolite formation, i.e., high-temperature hydrothermal reactions. Related with this, the growth of the synthetic zeolite market began to take hold in the late 1950s and that ignited the curiosity on the natural form of the mineral[9].

Table 1: Some natural zeolites with their 3-letter code and date of discovery

Natural zeolite	Three letter code used by IZA	Year of discovery	Natural zeolite	Three letter code used by IZA	Year of discovery
Stilbite	STI	1756	Clinoptilolite	HEU	1890
Natrolite	NAT	1758	Offretite	OFF	1890
Harmotome	_	1775	Erionite	ERI	1890
Analcime	ANA	1784	Kehoeite	_	1893
Laumontite	LAU	1785	Gonnardite	NAT	1896
Thomsonite	THO	1801	Dachiardite	DAC	1905
Scolecite	_	1801	Stellerite	STI	1909
Heulandite	HEU	1801	Ferrierite	FER	1918
Gmelinite	GME	1807	Viseite	_	1942
Mesolite	NAT	1813	Yugawaralite	YUG	1952
Gismondine	GIS	1816	Wairakite	ANA	1955
Brewsterite	BRE	1822	Bikitaite	BIK	1957
Epistilbite	EPI	1823	Paulingite	PAU	1960
Philipsite	PHI	1824	Garronite	GIS	1962
Levynite	LEV	1825	Mazzite	MAZ	1972

_ code not assigned

1.1.1. Zeolite frameworks

The zeolites frameworks are generally open frameworks consisting of many channels and/or interconnected voids of discrete size, which are occupied by cations and water molecules. The presence of cations in the zeolite framework is needed to neutralize the negative charge created as a result of isomorphic substitution of Si^{4+} by Al^{3+} in the framework. The mobility of the cations among other behaviors is responsible for the unique properties of zeolite and zeolite-like materials[10]. The zeolite frameworks are built

from an infinitely extending three dimensional network of silicate (SiO_4) and aluminate (AlO_4) tetrahedral linked to each other by the shared oxygen atoms (Scheme 1)[11]. The framework atom is usually silicon (Si) and aluminium(Al), however other metals such as sodium (Na), calcium (Ca), gallium (Ga), germanium(Ge), boron (B) and titanium (Ti) can take the place of Si and Al[12].

Scheme 1: Basic primary building units of zeolite framework

Silicate (SiO_4) and aluminate (AlO_4) tetrahedra are called the primary building units of zeolites. The frameworks can also be considered in terms of secondary building units (SBUs) which are arrangements of linked tetrahedra, often observed in several structures[10]. The SBU is the main unit that describes the zeolites structure with the exception of the water and cation in the framework. These on their own or in combination with other building units, give the zeolites frameworks (Figure 1). The corners of the polyhedra represent tetrahedral atoms.

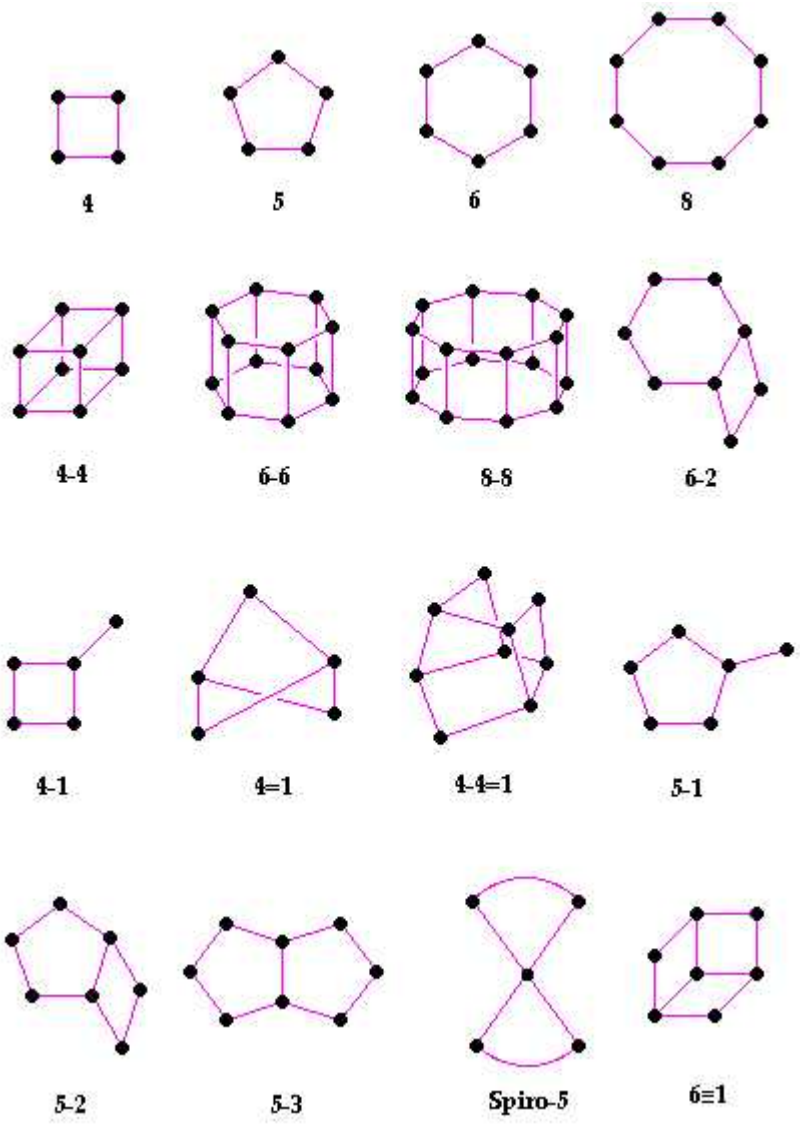

Figure 1: Secondary building units (SBUs) in zeolites framework

These SBUs, which contain up to 16 tetrahedrally coordinated atoms (T-atoms), are derived by assuming that the entire framework is made up of one type of SBU only. Zeolite frameworks are generated from the listed secondary building units (SBUs) and in some cases combinations of SBUs are used to form zeolites. One type of framework can comprise several SBUs. For instance zeolite A is generated using 4 rings or 6 rings. It can

also be formed from double 4 ring building units. Faujasite (FAU) can be obtained from sodalite framework which is made of single 6 member ring or 4-member ring. It can also be generated from double 6 ring building unit[10].

Zeolite structures are also commonly described in terms of the size, geometry and connectivity of the pore space defined by their frameworks. The size of the channels or pore openings (windows) that control molecular access into the pores is given in terms of the limiting ring size[10]. Generally, zeolites can be classified into small, medium, large and ultra large pore materials. The small-pore zeolites such as Zeolite A (LTA), Sodalite (SOD), and Gismondine (GIS) contain the pore opening enclosed by 8 TO_4 tetrahedra (T = Si or Al), with a diameter of about 4.2 Å. Medium pore zeolites (the typical example being MFI) generally feature a 10-ring pore opening with a diameter of approximately 5.5 Å. The large pore zeolites such as Faujasite (FAU) and Mordenite (MOR) have pore openings formed by 12 TO_4 tetrahedra, with a diameter of about 7.5 Å. The zeolites with pore openings comprising more than 12 T-atoms are called extra-large pore zeolites. It is worth noting that 8-, 10-, and 12-rings are common in zeolites. At present, extra-large pore zeolites are still rare, and the largest ring is limited to a 20-ring system, as observed in Gallophosphate Cloverite (CLO)[13]. Examples of the pore structure for the first three types of zeolites pores are given in Figure 2.

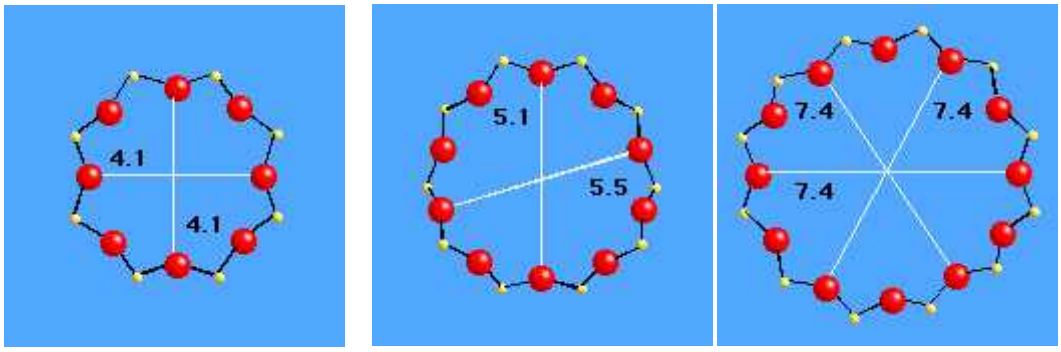

Figure 2: Pore structures of 8 rings, zeolite A, 10 rings, ZSM-5 and 12 rings, zeolites Y

Zeolites are also classified based on their framework symmetry with an identification code of three letters used by the International Zeolite Association (IZA). For example, zeolites X and Y (Faujasite zeolites) that belong to FAU groups[10] have equidimensional channels intersecting perpendicular to each other (Figure 3). The eight interconnected truncated octahedral (β cage) are linked tetrahedrally through double 6-rings (D6R). In each unit cell the cavity diameter is 13 Å[11].

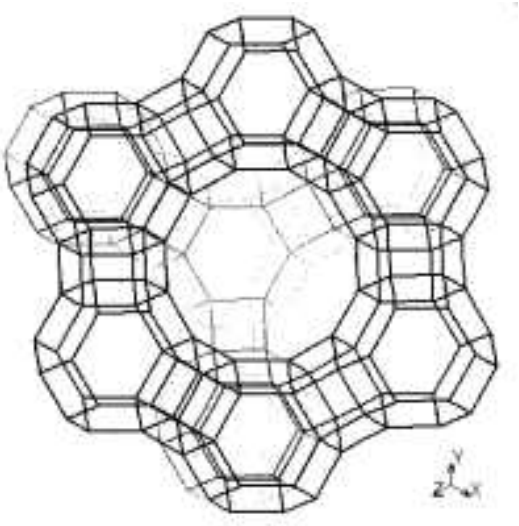

Figure 3: Crystal structure of FAU type zeolites

Similarly, the framework of MFI family which is composed of two members, namely ZSM-5 and silicalite is composed of its characteristic 5-1 unit with D_{2d} symmetry[10]. The symmetry link is via edge sharing to form a pentasil chain. The pentasil chains are connected with an oxygen bridge to form an MFI structure with 10 ring pores, which is also three dimensional (Figure 4). There is an intersecting channel with straight 10 ring channel and sinusoidal 10-ring channel.

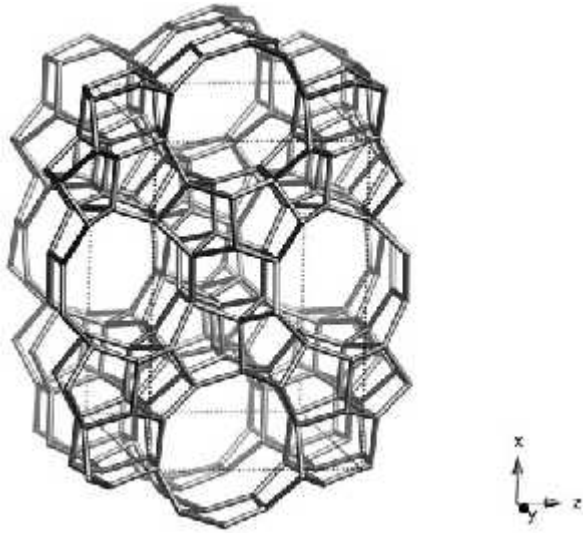

Figure 4: Crystal structure of MFI type zeolite

The 10-ring channel system gives ZSM-5 a unique shape selectivity property, which allows it to be widely used in catalysis and sorption. It is an important source of catalyst in petroleum refining and petrochemical industry and they are even better utilized than zeolite Y[14].

1.1.2. Properties of zeolites

1.1.2.1. Catalytic properties of zeolites

One can safely say that the impact of zeolites in science and technology in the last 50 years has no precedents in the field of materials and catalysis[15]. This is due to the fact that the introduction of zeolites in several industrial processes has brought important economical and environmental benefits. They replaced low-selective and harmful mineral acids and chloro-containing catalysts in several industrial processes, improving the yields and selectivity of the reaction, the quality of the products, the overall life of the catalyst (which is easily regenerable several times before being disposed) and also the energy consumption. The catalytic characteristics of zeolites are due to the combination of intrinsic properties of zeolites[16]. The generation of Brønsted acid sites (Scheme 2) by ion exchange of ammonium hydroxide followed by calcination or the direct ion exchange with mineral acids such as HCl or H_2SO_4 is the most important process in designing of zeolite acid catalysts. As can be observed from the scheme, the Brønsted site is generated at the oxygen bridge in Si-O-Al cluster where the charge compensating cation is a proton[14].

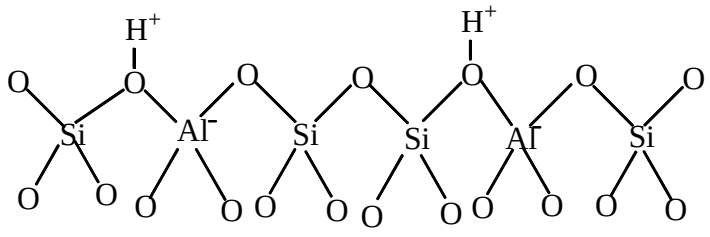

Scheme 2: Brønsted acid sites in zeolites framework

Refining and petrochemical industries have taken the major advantages from the introduction of zeolite catalysts as demonstrated by the fact that these sectors employ more than 90% of the industrial zeolite catalysts. Hence it is possible to say that oil refining and petrochemistry are important industrial sectors, where zeolites find widespread use as heterogeneous acid catalysts and molecular sieves. The role and the increasing importance of zeolite catalysts are examined through the illustration of selected examples of consolidated processes: the Fluid Catalytic Cracking (FCC), one of the most important processes in modern refinery, and the synthesis of cumene, the intermediate in the production of phenol. Finally, the synthesis of 2, 6-dimethylnaphthalene by alkylation of naphthalene and methylnaphthalene is reported as an example of emerging technology, whose development is strongly related to the use of new zeolite catalysts[17].

1.1.2.2. Adsorption properties of zeolites

One of the recognizable features of zeolites is their potential application as adsorbents. Adsorption can be described as a process whereby molecules of a gas or liquid adhere to the surface of a solid. These processes can be used to separate two mixtures of species depending on the affinity of the mixtures toward the solid surface. The solid surface is known as adsorbent while the adhering molecule is called adsorbate. The process of removing the adhered molecules is called desorption and this is achieved by changing the pressure and temperature of the system. This allows the reuse of the adsorbents[18]. Zeolites are among these adsorbents used in separation and purification. Adsorption is an important characteristic of all zeolites that can be attributed to the molecular sieving properties of the materials. Some of the important application of the adsorption and

molecular sieving properties of zeolites include drying agent, gas separation (pollution control) and separation of mixtures such as i-paraffin/n-paraffin system. Zeolites are effective in both liquid and gas phase separation processes and can manage streams containing both percent and even trace contaminant levels, offering potential to reduce these impurities to low ppb levels or better, if required. Other specific utilization of adsorption properties of zeolites include aromatic removal from linear paraffin in the C_{10}-C_{15} range used in linear alkyl benzene production, nitrogenate removal, oxygenate and sulphur removal[12]. Due to their molecular sieve properties, natural zeolites have been widely used as adsorbents in separation and purification processes in the past decades. Application of natural zeolites for water and wastewater treatment by adsorption method has been realized and is still a promising technology in environmental cleaning processes. Adsorption properties of natural zeolites in comparison with other chemical and biological processes have the advantage of removing impurities also at relatively low concentrations and allow conservation of water chemistry. Among the natural zeolites, clinoptilolite is the most abundant and widely used adsorbent in the world[19]. However, because of the SiO_2/Al_2O_3 ratio, pore size as well impurities, the application of natural zeolites is limited. This makes synthetic zeolites to dominate in the area of adsorption. Within this commercial subset of zeolites certain structures, low silica zeolites, especially zeolites A, X and Y tend to dominate in terms of end users application.

1.1.2.3. Ion-exchange properties of zeolites

Ion exchange is an inherent characteristic of most zeolites and has become the highest commercially demanded property of zeolites. It is the property that allows the replacement of a cation held in the zeolite pore by an external ion present in a bulk

solution[12, 20]. The ion exchange property is due to the isomorphous substitution of Si^{4+} by Al^{3+} in a zeolite framework creating a net negative charge. The created net negative charge is balanced by a wide variety of cations such as Na^{+}, K^{+}, Ca^{2+}, Mg^{2+} and others. These positive ions are rather loosely held and can readily be exchanged for others in a contact solution[21]. The exchange reaction between a zeolite and an ionic solution is described as

$$\mathbf{M_1\,(Z) + M_2\,(S) \longleftrightarrow M_2\,(Z) + M_1\,(S)}$$

Where M_1 is the exchangeable cation present in zeolites Z, and M_2 is the saturating ion in solution S. The properties of zeolites as ion exchange materials is widely used and applied in water softening, detergents, waste water treatment and radionuclide separation[22, 23].

1.1.3. Zeolite applications

Due to their compositional variety, uniform pore space, and structural symmetry, zeolites have high surface areas, the ability to sieve molecules based on size and shape selectivity and internal physicochemical properties that can range from acidic to basic and hydrophobic to hydrophilic[24]. The above stated unique characteristics and properties of zeolites make both natural zeolites and synthetic zeolites become an important and integral part of many industrial processes. According to the report of 2010, the global market for natural zeolites grew from 3.98 million to 5.5 million tons and in the same period, the consumption of synthetic zeolites was projected to reach 1.86 million tones[3]. While 90% of natural zeolites are mainly applied in the construction industry, the remaining 10% find uses in processes such as waste water treatment, animal feeding,

horticulture, odor control and other miscellaneous applications[25]. However, due to the large presence of impurities, natural zeolites have limited applications for industrial purposes. For process industries, synthetic zeolites are preferred. This is because in comparison with natural zeolites, synthesized zeolites have many advantages such as high purity, uniform pore size, and better ion-exchange abilities. The ion exchange property of a synthetic zeolite is its most important characteristic, enabling its usage in applications such as detergents, adsorbents and catalysts, and providing scope for future applications such as anti-microbial agent. Synthetic zeolites can be categorized into detergents, adsorbents, catalysts and others by application type[26]. The report in 2014, showed that global synthetic zeolite market is expected to reach 1.76 billion USD in 2020[27]. Detergent application is the largest, accounting for over 65% of the global consumption. Demand for synthetic zeolites in detergents is led by government initiatives to control phosphorus compound pollution in water bodies. Phosphates that are dominantly used in detergents enter water bodies through waste laundry water and increase phosphate burden to the environment. Phosphates are known to be plant growth promoters leading to abundant growth of water algae, thereby endangering marine ecosystem and polluting drinking water[28]. Synthetic zeolites are used as substitutes for phosphates in detergents. The most commonly used synthetic zeolites for detergents of commercial importance to replace sodium tripolyphosphate (STPP) are the synthetic type A, P, X and AX (a co-crystallite composed of 80% zeolite X and 20% zeolite A). While the chemical composition and the basic performance properties of the individual detergent zeolites are almost identical, the individual types have different crystalline structures resulting for instance, in a firmer binding of calcium ions by Zeolite P and a higher magnesium binding capacity of Zeolite

X compared to Zeolite A[29]. Among these, the Linde type zeolites A which comprise 73% of the total production of synthetic zeolites represent a valid alternative in the manufacturing of detergents. This can be attributed to its large ion exchange capacity (CEC), mechanical strength and particular crystal shape.

1.2. Zeolite A

Zeolite A is a synthetic sodium aluminosilicate often also referred to as zeolite NaA or zeolite 4A, with the formula $Na_{12}(AlO_2)_{12}(SiO_2)_{12}\cdot 27H_2O$. It is the universal type of synthetic zeolite used for detergent manufacturing and water softening to substitute the environmentally unfriendly material, sodium tripolyphosphate (STPP)[30]. Zeolite A has the following general properties, which make it suitable for water softening:

- It has the largest ion exchange capacity (CEC) of 5.48 meq/g of anhydrous zeolite.
- Average particle size less than 4 micron and maximum size not exceeding 10 micron. This has made it suitable to pass through the mesh size of clothes and preventing graying thereby.
- Due to the cubic shape with rounded corners and edges of zeolite crystals, zeolite A would not remain on fabrics and is easily removed on rinsing.
- During the deposition of sparingly soluble compounds, zeolite A particles acts in competition with the textile fabrics and reduce incrustation of the laundry.
- The unwanted water soluble molecules from the dirt do not finish up on the other articles but are absorbed on zeolite particles. This inhibits the dye transfer from one cloth to another.

- Toxicologically, zeolite A is safe. The acute toxicity is given as LD_{50} of 10 g/kg (Mouse, oral intake) and toxicity to water organism is greater than 100 mg/L.
- It is environmentally safe with almost zero loading of harmful effect on the environment[31].

1.2.1. Structure of zeolite A

Zeolite A exhibits the LTA (Linde Type A) structure[10]. It has a 3-dimensional pore structure with pores running perpendicular to each other in the x, y, and z planes, and is made of secondary building units with 4, 6, 8, and 4-4 rings. The structure can be described in terms of two types of polyhedra (Figure 5). One is a simple cubic arrangement of octahedron or α-cage and the other is a truncated octahedron of 24-hedron or β-cage. The β-cage is also called the sodalite cage linked by double 4-ring (D4R). The cubic α-cages are placed in the centers of the edges of a cube in the truncated octahedra. These α-cage connect the β-cages, creating a three-dimensional structure having pores of size 4.2 Å. Each corner of the cube (α-cage) is occupied by the truncated octahedra (β-cage) enclosing a cavity with a free diameter of 6.6 Å. The centre of the unit cell is a large cavity, which has a free diameter of 11.4 Å[32].

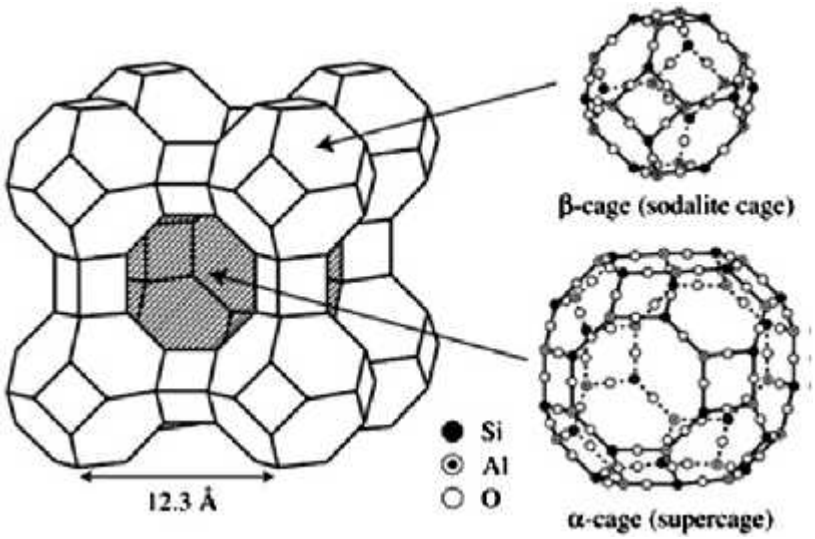

Figure 5: Zeolite A (LTA) structure

A unit cell of zeolite A contains 24 tetrahedra; 12 each of AlO_4 and SiO_4. There are 12 sodium atoms per unit cell; all in the one large cage per unit cell. 8 are located near the center of the 6-rings separating the large β and small α cages, one near the center of each of the eight 6-rings per unit cell. The other four sodium atoms have not been located and they are assumed to be dissolved in the zeolitic water in the large cages. This indicates that the framework structure and most of the cation positions are known for hydrated zeolites A. Fully hydrated zeolite A contains 27 water molecules per unit cell. The theoretical Si/Al ratio in zeolite A is 1 but in many preparations the Si/Al ratio is slightly less than 1[33].

1.2.2. Synthesis of zeolite A

Similar to other types of zeolite synthesis, the synthesis of zeolites A can be traced back to the middle of the 19th century when the earliest synthesis of zeolites was performed in

part by imitating the natural conditions of the formation of natural zeolites, i.e., high temperature and pressure (> 200 ^{o}C and 10 MPa); however, the efforts were not very successful[34]. Chemists at Union Carbide Corporation (UCC), R.M. Milton and D.W. Breck, employed mild hydrothermal synthesis (at about 100 ^{o}C and under self-generated pressure) and achieved a great success in developing a synthetic approach for the synthesis of zeolites. By using hydrothermal synthesis approach, they successfully synthesized unnatural zeolites of types A and X, followed by zeolite Y. Following this, by the end of 1954, zeolites A began to be produced industrially[34]. Despite the fact that different synthesis approaches of zeolite A have been widely reported; hydrothermal, sonochemical (acoustic wave stimulation) and recently ionothermal are the common methods used in the synthesis of zeolites A[35, 36].

1.2.2.1. Hydrothermal synthesis of zeolite A

So far, the hydrothermal synthetic approach is the best way to synthesize a large number of zeolites and microporous materials including zeolite A. It can enhance the effective solvation ability of water, increase the solubility of the reactants, and activate the reactivity of the source materials, leading to the rearrangement and dissolution of the primary gel formed in the first stage and resulting in an increased nucleation and crystallization rate of zeolite synthesis[37]. Moreover, this method of zeolite synthesis led to the growing of perfect and large single crystals allowing controlling the morphology and particle size of the final product, which are important requirements for zeolite A. Basically, the hydrothermal synthesis process of a zeolite consists of two stages: the initial formation of the hydrated aluminosilicate gel and the following crystallization process of the gel. In fact, the crystallization process of the hydrated aluminosilicate gel

is very complicated. No decisive conclusions have been reached for this complicated crystallization process so far. However, regardless of the liquid or solid-phase transformation mechanism proposed before, it is commonly accepted that the crystallization process consists of four steps: (1) condensation of polysilicate and aluminate anions; (2) nucleation of zeolites; (3) growth of nuclei; and (4) crystal growth of zeolites which sometimes results in secondary nucleation. It is still very difficult to obtain a deep understanding of the formation mechanism and the detailed crystallization process of zeolites[6].

1.2.2.2. Nucleation and crystal growth in zeolite A

Crystallization of zeolite A from solution generally occurs via the sequential steps of nucleation of the phase, or phases, dictated by the composition of the solution, followed by growth of the nuclei to larger sizes by incorporation of material from the solution. Nucleation and crystal growth rates typically are governed by a driving force related to the supersaturation of the reaction mixtures[38].

Nucleation involves the formation of aggregation of unstable nuclei from the supersaturated solution prepared from the initial precursor and with time become large enough to form stable nuclei from where crystal growth takes place. Nucleation can be homogeneous, in the absence of foreign particles or crystals in the solution, or heterogeneous, in the presence of foreign particles in the solution (seeds). Both types of nucleation are collectively known as primary nucleation. Secondary nucleation takes place when nucleation is induced by the presence of crystals of the same substance (seeds)[39]. Although the structure and size of nuclei are not definitely verified, the formation of nuclei is essential for zeolite crystallization, regardless of whether they are

formed as a consequence of the supersaturation of source materials or the addition of seeds. Simple aging of synthesis mixtures of zeolite A, even at ambient temperature, facilitates nuclei formation.

Crystal growth is the series of processes by which an atom or a molecule is incorporated into the surface of a crystal, causing an increase in size at the expense of the smallest crystals, acting as nutrients for the growth of the largest crystals[40]. Crystallization generally involves the assimilation of material from solution by a growth process, which begins when the nuclei reach a critical size and the crystals begin to grow.

For zeolite A type formation, it involves the combination of the tetrahedral silica and alumina precursors in the presence of sodium source which acts as a template[41]. These tetrahedral form four and six membered ring secondary building units (SBU). Further combination of these SBUs develops into cages and or zeolite A framework (Scheme 3).

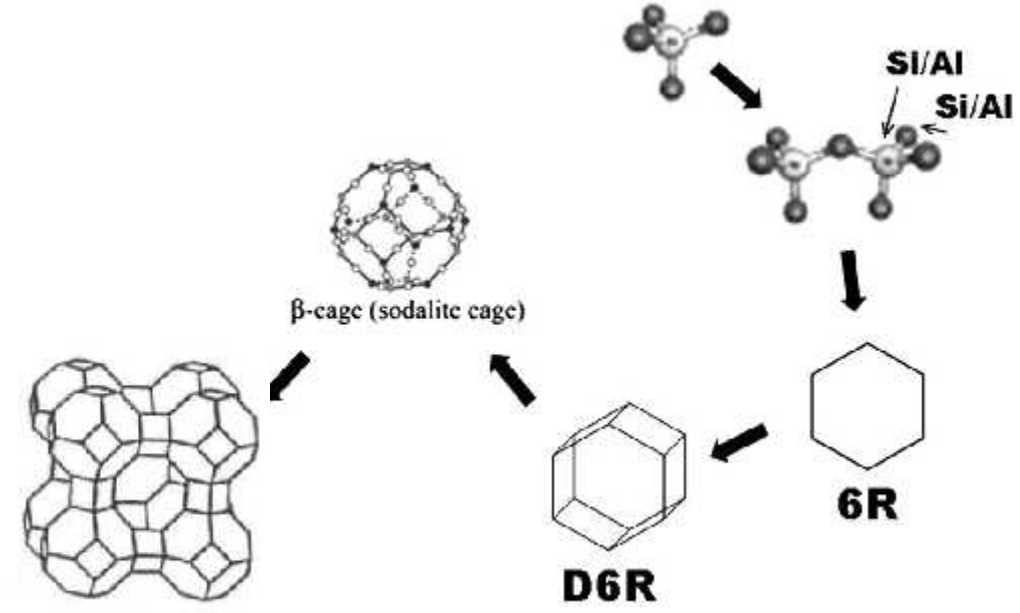

Scheme 3: Schematic representation of the formation of zeolite A

1.2.2.3. Reactants and batch compositions for zeolites A synthesis

Despite the different approaches used in zeolite A synthesis, basic reactants used in the synthesis include silicon source, aluminum source, metal ions, base, mineralizer, and water[1, 12, 34, 42]. Among them, silicon source and aluminum source are the two most important reactants. The silica along with alumina function to provide the primary building units of the framework with the alumina further creating the framework residual charge. The alkali cation is the counter ion which neutralizes the residual charge in the framework and also acts as a guest molecule generating the ion exchanging characteristic. Besides, it can also act as a structure directing agent for the zeolites synthesis which does not involve the presence of organic templates. The common mineralizer is OH^- anion and it provides the necessary environment or media suitable for nucleation and crystal growth. OH^- anion is the most common mineralizer for silica-based zeolites[34].

Frequently used silicon and aluminum sources are:

Silicon source: waterglass: $Na_2O \cdot xSiO_2$, where x is modulus (molar ratio of Na_2O to SiO_2); sodium silicate $Na_2SiO_3 \cdot 9H_2O$, Ludox-AS-40 colloidal sol: SiO_2 40 wt%, fumed silica: Aerosil-200, tetramethylorthosilicate (TMOS): $Si(OCH_3)_4$, tetraethyl orthosilicate (TEOS): $Si(OC_2H_5)_4$

Aluminum source: Sodiumaluminate: $NaAlO_2$; aluminium hydroxide (gibbsite): $Al(OH)_3$, aluminium nitrate: $Al(NO_3)_3 \cdot 9H_2O$, aluminum isopropoxide: $Al(O\text{-}^iC_3H_7)_3$, metallic aluminium.

The more cost effective naturally available clay minerals, coal fly ash and industrial waste can be used as a combined source of alumina and silica with or without pretreatment[34].

The rate of zeolite crystallization, types of products formed, and their particulate properties (morphology and crystal size distribution) depend on a large number of parameters. Di Renzo et al.[43]classified these parameters as crystallization conditions (temperature, stirring, seeding, gel aging, alkalinity, the ratio between framework-forming elements, template concentration) and composition-dependent parameters (temperature, stirring, seeding, and gel aging). In general the key parameters that affect zeolite A crystallization are: alkalinity (concentration of the base), gel formation and aging conditions/time, crystallization temperature and time, seeding, structural directing agent (SDA) and reaction container. The effects of each parameter are covered in many literatures[44-46]. However, for our research interest we discuss the effect of alkalinity, aging of the synthesis gel, crystallization temperature and time.

Alkalinity effect

Alkalinity is an important variable during the hydrothermal synthesis of zeolite and can significantly affect the crystallization. Most zeolite synthesis is usually performed under basic or strongly basic conditions. Many zeolites including zeolite A can be crystallized from the basic $Na_2O–Al_2O_3–SiO_2–H_2O$ system. For this specific system of zeolite synthesis, alkalinity is defined as the OH^-/Si ratio or the concentration of base (H_2O/Na_2O). Basically, increasing the ratio of OH^-/Si leads to a higher solubility of silicon and aluminum sources, which will alter the polymerization state and their distribution. Moreover, a higher alkalinity can decrease the polymerization degree of the silicate anions and speed up the polymerization of the polysilicate and aluminate anions. Thus, increasing alkalinity will shorten the induction period and nucleation time and speed up the crystallization of zeolites. Studies in the synthesis of zeolite A (LTA) from

the precursor gel with the effect of different alkalinity (H_2O/Na_2O = 20, 30, 40) on the crystallization rate (including induction period and growth rate) and particle size of the product have been conducted[1,34,45]. Clearly, with an increase of alkalinity the crystallization process is speeded up, the particle size is decreased, and the distribution of the particle size is narrowed due to an increased nucleation rate and an increased polymerization rate between polysilicate and aluminate anions.

Aging effect

Aging is defined as the gap in time between the aluminosilicate gel formation and the starting of crystallization of zeolites. During the aging course, the aluminosilicate gel is expected to be chemically and structurally reorganized increasing the supersaturation level necessary for zeolite nucleation. Thus, the purpose of aging is to adjust synthetic conditions such as temperature and time to assist the transformation of gel to the zeolite structure and to speed up nucleation. Seeds of crystalline zeolites form inside the gels during the process of aging. This process accelerates gel crystallization. Increasing time of gel aging leads to shortening the induction period, acceleration of the crystallization process, increases final product's purity and leads to a decrease in the size of final product's crystals. The first studies to link these time-dependent gel aging effects with control of crystal size were those of Freund and of Zhdanov and co-workers. These investigations showed that room temperature aging of aluminosilicate Na-A and Na-X gels resulted in both an acceleration of the crystallisation and a decrease in the crystal size of the product, thus linking the aging process directly to the number of nuclei formed[47]. A more recent example for zeolite A concerned the effect of aging on microwave-mediated synthesis. It was found that products from short aging times (5min)

were amorphous after 5 min microwave heating at 100 ^{o}C, whereas zeolite A could be crystallized in 1 min at 120 ^{o}C after overnight aging of the synthesis mixture, crystal size of the products decreased with aging time, again suggesting that, during the aging process, structured elements related to the nucleation process are being formed[48].

Crystallization temperature

Crystallization temperature is one of the most frequently studied synthesis condition having substantial effect on the crystallization of a particular zeolite A. The change in temperature can affect the polymeric state of silicate and aluminate ions, the dissolution, and the transformation of the gel. Besides it also acts as the generator of the autogenous pressure that can have an impact on the crystallization and structure of the zeolites. Increase in temperature influences basic properties of zeolites such as the phase, change in induction period and increase in the crystallization rate[49]. Moreover, the variation of crystallization temperature can affect many other factors during the synthesis, such as the polymerization reaction between the polysilicate and aluminate anions contained in the liquid phase of the gel; the polymeric state of the silicates; the formation, dissolution, and transformation of the gel; the nucleation and crystal growth; and the phase transition of metastable phases resulting in the formation of zeolites with different pore structures from a single synthetic system. The formation of various zeolites from the synthetic system Na_2O-SiO_2-Al_2O_3-H_2O at different temperatures will serve as an example. Studies by many zeolite chemists since the 1950s indicate that zeolites A could be crystallized in the temperature range of 100 to 150 ^{o}C[50]. Zeolites with small pore system such as Sodalite (SOD) could be formed when the crystallization temperature reaches 200 to 300 ^{o}C; and when the crystallization temperature is higher than 300 ^{o}C, very-small-pore

zeolites such as Analcime (ANA) and Natrolite (NAT) and nonporous Albite (A_B) and Nepheline hydrate (N_H) are the main products[6]. Therefore, controlling of crystallization temperature during hydrothermal synthesis is an important task.

Crystallization time

Crystallization time is also an important parameter that controls the type of final zeolite product obtained. The major objective in the synthesis of zeolites and other porous materials are attaining the desired synthetic material in a minimum time as much as possible. Moreover, due to the matastable nature of zeolites A, optimization of the synthesis time is one vital task for zeolites synthetic chemists. Dyer[12] stated the two ways the effect of crystallization time play a part in the formation of zeolite from reacting species or gels:

- An induction time during which the reaction mixture is held near ambient temperature prior to moving up to the crystallization temperature often optimizes zeolite yield (as in X and Y synthesis).
- There is the possibility of crystallization of different zeolites from one reaction mixture at different times. This is because of the fact that all zeolite are metastable species whereby the initial zeolite formed is an open structure which with time are transformed into more dense or closed structure. Similar to crystallization temperature, controlling the crystallization time for the synthesis of zeolite A should be an important task. Based on this, the different studies on the effect of synthesis parameters indicated the metastable zeolite A could be converted to the more stable phase hydroxysodalite as the time of crystallization is increased[51].

Following the above mentioned synthesis parameters, large number of papers and patents have been reported on the synthesis of zeolite A by different synthesis approaches using different starting materials. Mohamed et al.[52] reported the synthesis of zeolite A from fumed silica and sodium aluminate precursors. The optimum conditions for the synthesis of zeolite A were studied to obtain a high ion-exchange capacity and an affinity for heavy metal ions. The findings revealed that the optimum conditions for synthesis of zeolite A were SiO_2/Al_2O_3 = 2, H_2O/SiO_2 = 150 and Na_2O/SiO_2 molar ratios = 1.15 at 110 ^oC with 4 days crystallization time. Concerns about energy consumption, carbon economy and production costs have called the attention of researchers to seek for cheaper raw materials for zeolite A synthesis other than pure synthetic starting raw materials. Based on this, the hydrothermal synthesis of zeolite A has been conducted using industrial wastes such as cupola slag and aluminum sludge[53], coal fly ash[54] and other aluminosilcate sources clay minerals such as kaolin[55]. S. M. Holmes et al.[56] demonstrated the direct synthesis of pure zeolite-A using 'virgin' Nigerian kaolin. The method involves a rapid and low temperature metakaolinization step followed by chemical conversion directly into pure zeolite A. The synthesis step acts as the purification step removing the 80% quartz impurity simultaneously with zeolite growth. This was done by refining the synthesis gel to remove the denser quartz portion by decantation. The whole process is designed to be both economical and straight forward to facilitate commercialization. M. Gougazeh and J. -Ch. Buhl[57] reported the synthesis of zeolite A by hydrothermal transformation of natural Jordanian kaolin. The synthesis at various concentration of NaOH was investigated at 100 ^oC for 20 h. Mixtures of zeolite A, quartz and hydroxysodalite (HS) was obtained. Zeolite A was the main product with the NaOH concentrations of 1.5-3.5 M.G. García et

al.[58] reported a novel method called alkali fusion followed by hydrothermal synthesis method to produce zeolite A with excellent optical properties from clays material. Discoloration of zeolite A powder is a common problem when natural raw materials such as kaolin clay are used as starting material for the synthesis of zeolite A that can be mentioned to the formation of colored iron compounds. The product obtained comprised of intergrown zeolite A crystals with cubic habit and the brightness was as high as 94.5%. S. H. Park et al.[59] also recently reported eco-friendly hydrothermal synthesis of zeolite A from synthesis cakes prepared by removing the liquid phase of aged synthesis mixtures. The volume and weight of the synthesis cake prepared using a filter press were about one-eighth and one-fourth those of the mixture, respectively. This implies that the reactor volume and energy input required for the hydrothermal reaction can be reduced by the same respective factors, allowing the eco-friendly synthesis of zeolites.

These are few of many works reported on the possibilities of synthesizing zeolite A from cheaper raw materials by hydrothermal method of synthesis. Hence in this PhD project the synthesis of zeolite A from locally available kaolin from Ethiopia is conducted. Moreover, the practical application of the synthetic products in different scenario is tested.

1.3. Motivation of the study

Regardless of the different synthesis approaches used for the production of zeolite A using various starting raw materials, the conventional way of its synthesis is performed by hydrothermal crystallization process using commercial chemicals, silicates and aluminates that act as sources of silica and alumina[34]. However, these chemicals are not the most cost-effective raw materials. The use of a low cost and locally abundant material

such as kaolin (china clay) as a combined source of silica and alumina is rather inviting. It was shown that clay as a precursor to zeolite A synthesis has a comparative cost advantage of 15% over a commercial chemical such as sodium silicate. An advantage of the clay process lies not in making more economical detergent-grade zeolites, but in making shaped zeolites for certain adsorbent applications. For example, clay can be extruded, pelletized or otherwise agglomerated. The resulting product retains its original shaped structure and has good mechanical strength[60]. Besides, this study is important since we are using a highly abundant natural clay material (kaolin) of Ethiopia for production of value added chemical compound zeolite A. This synthetic work, is a new area or research in Addis Ababa University (even in Ethiopia) that has been advised to be tackled given the interest of the our local industrial partners from detergent factories. Zeolite A can be used in detergent industry to substitute the environmentally unfriendly phosphate based material (STPP) and as an adsorbent to treat wastewater. On the other hand, leather industry is currently becoming one of the booming industrial sectors in Ethiopia which is contributing substantially towards national economy. However, the challenge coming with the expansion of tannery is the management and treatment of effluents coming out from these factories. Based on this national problem there is room for the application of this synthetic zeolite A made from kaolin of Ethiopia in the treatment of tannery wastewater. Hence our research objectives are designed and set based on the research gap observed in the area of value adding and using of such raw materials available in our country for different applications. Moreover, this work could be taken as part of technology transfer approach in research.

1.4. Objectives of the study

1.4.1. General objective

The principal aim of this research project is the synthesis and characterization of optimized zeolite A from kaolin minerals available in Ethiopia following characterization and beneficiation of the raw minerals. It is also our aim to investigate the practical application of the synthesized zeolite A in detergent as a builder and as adsorbent for chromium removal from tannery wastewater and synthetic wastewater in comparison with other natural and synthetic adsorbents.

1.4.2. Specific objectives

- Characterize and purify the raw kaolin from Ethiopia.
- Synthesize and characterize zeolite A from both raw and purified kaolins.
- Optimize the synthesis parameters and methods in order to obtain zeolite A with high crystallinity and rounded edges.
- Investigate the practical application of the synthesized zeolite A for its application in the manufacturing of detergents.
- Investigate the efficiency of the synthesized material for Cr(III) removal from tannery wastewater and Cr(VI) from aqueous solution of chromium in comparison with other locally available natural and synthetic adsorbents.

1.5. Organization of the Thesis

This thesis consists of six chapters. Chapter One presents a general introduction to zeolites, description of the intended zeolite A, motivation of the study, aim and objectives of the research. Chapter Two contains information on all the characterization techniques used in the work. Chapter Three presents the studies carried out on the systematic synthesis of zeolite A using kaolin from two Ethiopian deposits following two synthesis routes: the conventional hydrothermal synthesis route and the alkali fusion followed by hydrothermal synthesis route. The processes include the study of the raw kaolin, the purification processes, metakaolinization and the synthesis processes are explained in this chapter. In Chapter Four the characterization of the synthetic products is exhaustively presented and discussed. Chapter Five report the detail application of the synthesized zeolite A in detergents as a detergent builder. This chapter includes the detergent formulation using the synthesised zeolite A as a builder and the physicochemical tests used in measuring the efficiency of the formulated detergent. The last chapter (Chapter Six) presents comparative study undertaken in the application of zeolite A and other clay based materials in the removal of chromium from tannery waste and synthetic wastewater. Finally, few additional XRD patterns not included in the main body are appended.

CHAPTER TWO

2. Characterization Techniques

In this chapter the different techniques used in this study are briefly described. The techniques used are: Powder X-ray diffraction (PXRD), Inductively Coupled Plasma Optical Emission Spectroscopy (ICP-OES), Scanning Electron Microscopy (SEM), Scanning Transmission Electron Microscopy (STEM), Thermogravimetric Analysis (TGA), Cation Exchange Capacity (CEC) and Atomic Absorption Spectroscopy (AAS).

2.1. Powder X-Ray Diffraction (XRD)

X-ray diffraction (XRD) is widely utilized to elucidate the structure of crystalline materials[61]. It is a technique used to confirm the structural characteristics of a synthesized specimen providing with a unique fingerprint of samples under investigation. XRD is based on the principle of scattering phenomena, whereby crystals perform the function of diffraction grating toward an incident X-ray. The atoms in the crystals scatter the X-rays in all directions[62]. The diffraction of X-rays in crystals was discovered in 1912 at the University of Munich by Max Theodor Felix Von Laue which earned him a Nobel Prize for Physics in 1914. In his work, he showed that X-rays are electromagnetic radiation of short wavelength similar in dimension to those of the bond distance in crystals which can act as a diffraction grating for incoming X-rays[63]. English physicists Sir W.H. Bragg and his son Sir W.L. Bragg developed a relationship in 1913 to explain why the cleavage faces of crystals appear to reflect X-ray beams at certain angles of incidence. They described for a crystalline solid that the waves are scattered from lattice planes separated

by the interplanar distance d. When the scattered waves interfere constructively; they remain in phase since the path length of each wave is equal to an integer multiple of the wavelength. The path difference between two waves undergoing constructive interference is given by 2dsinθ, where θ is the scattering angle (Figure 6).

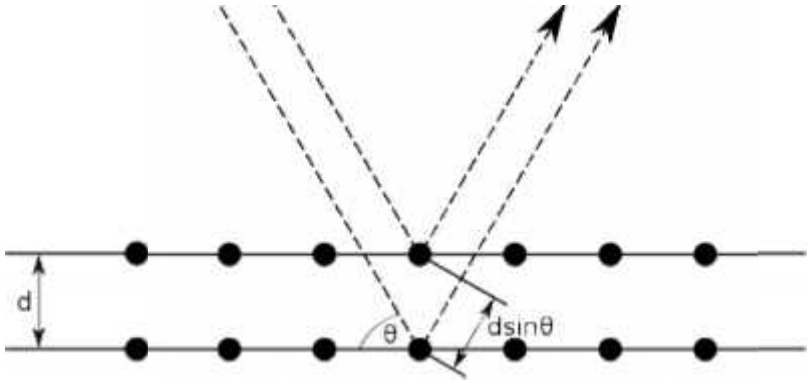

Figure 6: Diffraction of X-rays from crystals

This leads to Bragg's law which describes the condition for constructive interference from successive crystal crystallographic planes (hkl) of the crystalline lattice which is given by the equation:

$$2d \sin \theta = n\lambda$$

This is called Bragg's law; n is generally taken as unity, d is the interplanar spacing of the atoms, λ is the wavelength of the incident X-ray. Crystalline materials contain infinite number of lattice planes and of different Miller indices, and hence various d-spacing can be calculated from the modification of the Bragg equation for any crystal system. A diffraction pattern is obtained by measuring the intensity of scattered waves as a function of scattering angle. Very strong intensities known as Bragg peaks are obtained in the

diffraction pattern when scattered waves satisfy the Bragg condition. Using the Bragg peaks it is possible to calculate the crystallinity of crystals. Therefore studying the diffraction of X-ray is used to generate information about the structural properties of any crystalline material[64].

In an XRD machine, the X-ray tube is where electrons are emitted from the cathode (a glowing tungsten filament) and are accelerated through the vacuum where they strike a metal target anode (Figure 7).

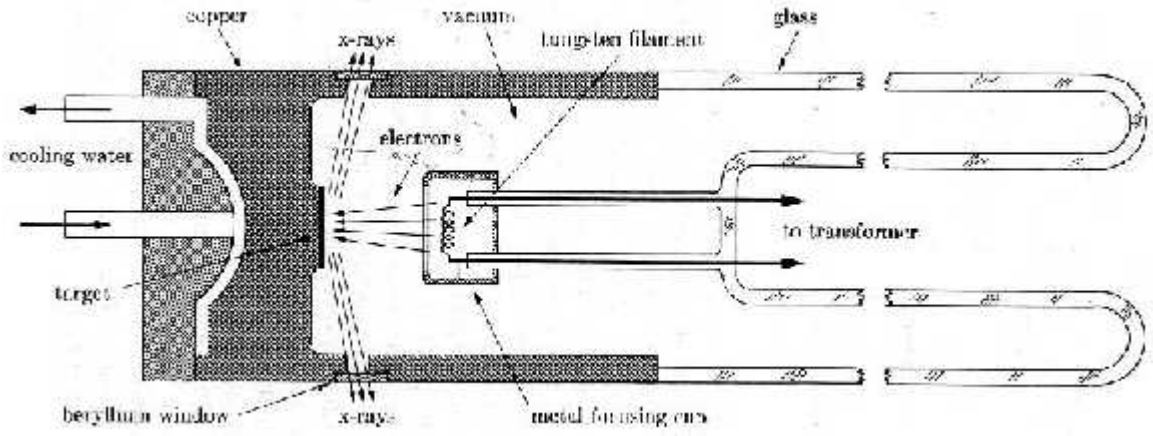

Figure 7: Cross-section of a typical X-Ray tube

Several metallic elements are used as anode such as chromium (Cr), molybdenum (Mo), cobalt (Co) and copper (Cu). Cu is commonly used in powder X ray diffractometers. The energy of the produced X-ray by the listed metal target are within the range of 4.21 kV corresponding to wavelength of 3.1-0.59 Å[65]. Powder x-ray diffraction is the main characterization tool used in identifying crystalline samples like zeolites during synthesis and modification stages. With powder XRD, the long range atomic structure of a zeolite

can be resolved. Each zeolite type has a specific XRD pattern as a finger print. Each pattern can provide important structural information such as crystal size, strain or stress in the sample or material and degree of crystallinity[66].

In this study, the analysis of the kaolins, metakaolins and zeolites powder samples were carried out using the XRD machine model of X'pert Pro PANalytical with a Cu K_α radiation and Ni filter, which has a wavelength of 1.54056 Å. The instrument setting for each test at room temperature was: tension = 45 kV, current = 40 mA, number of steps = 4368, total run time 19.3980 s and 2 intervals between 4.0087^o to 89.9737^o. Samples for the X-ray analysis were prepared by placing 0.2-0.5 g of the powder sample in an aluminum holder. The sample holder surface should be smoothed off to absorb the X-ray beam regularly. The diffraction pattern is plotted within the XRD machine by generating a scan with continuous scanning mode for the intensity of peak (I_{rel}) as the Y-axis versus (2θ) as the X-axis.

2.2. Inductive Coupled Plasma Optical Emission Spectroscopy (ICP-OES)

Inductively coupled plasma optical emission spectroscopy (ICP-OES) is a powerful analytical tool for the determination of metals in a variety of different sample matrices[67]. It can also help in the determination of major, minor and trace compositions in various materials including kaolin and zeolite. It is a type of emission spectroscopy that uses the inductive coupled plasma to produce excited atoms and ions that emit electromagnetic radiation at wavelengths characteristic of a particular element. It is a flame technique with a flame temperature in a range from 6000 to 10000 K. With this technique, liquid samples are injected into a radiofrequency (RF)-induced argon plasma using one of a variety of nebulizers or sample introduction techniques. The sample mist reaching the

plasma is quickly dried, vaporized, and energized through collision excitation at high temperature. The atomic emission emanating from the plasma is viewed, collected with a lens or mirror, and imaged onto the entrance slit of a wavelength selection device[68]. In this study, the elemental composition analysis of kaolins and synthesized zeolite A were carried out using ICP-OES Optima 3300 DV Perkin Elmer instrument. Alkali fusion method of digestion was used for the digestion of the kaolin and zeolite samples. For this process, the flux fusion was using lithium borates ($Li_2B_4O_7$-$LiBO_2$) and potassium iodide (KI) and the solution was filtered after the digestion period. Following the filtration process, the samples and standards were quantitatively transferred to volumetric flasks and then introduced into the ICP plasma. Initially, the range of standards prepared was run on the ICP to generate a typical calibration curve. The sample solution was then analyzed and the emitted radiation was focused into the spectrometer. The emission signal was directly converted into concentration by using the calibration curve in the ICP computer with an analytical error of ± (0.01-0.05).

2.3. Scanning Electron Microscopy (SEM)

Scanning electron microscopy (SEM) is one of the most versatile instruments available for the examination of the morphology of solid materials including kaolin and zeolites[69]. The configuration of a typical SEM shows that it is made up of an electron gun situated on the top of the column which generates an electron with energy level in the region of 0.1-30 eV (Figure 8).

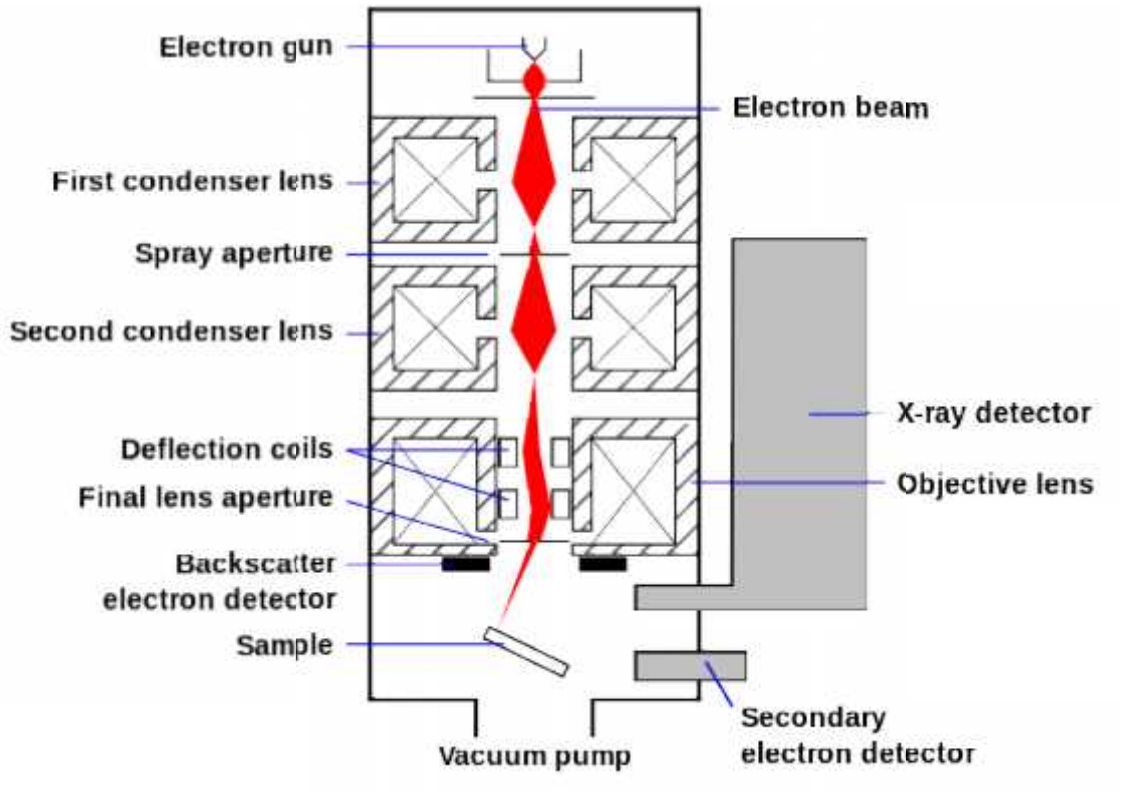

Figure 8: A schematic diagram of a scanning electron microscope

A high vacuum is usually provided to aid electron transport without interference or scattering by air. An electron beam scanning coil and signal detection system are also needed for the image processing of the sample surface. SEM works under the principle of interaction between the specimen and the electron beam producing a signal from secondary electrons and backscattered electrons which can be used to produce images. Secondary electrons are electrons produced when the incident electron beam collides with a sample atom electron and knock it out of its shell. It is weak in energy (nearly 100 volts). Backscattered electrons are electrons formed when the incident electron beam collides with a nucleus of a sample atom and it bounces back out of the sample as a backscattered electron. These electrons have high energies and because a sample with a

higher density will create more of them, they are used to form backscattered electron images, which generally can discern the difference in sample densities[70].

The morphology analysis of the kaolins, metakaolins and zeolite A samples synthesized from kaolin of Ethiopia were carried out using a NOVA NANO SEM 230 (FEI) scanning electron microscope with the VCD detector in high vacuum. The output voltage from the electrons gun is 3000 V and the actual voltage reaching the sample is 2000 V. With this detector the signal were collected from both secondary and backscattered electrons simultaneously. Although sample coating is important in many SEM analyses, in our case the analysis was done without couting under high vacuum. In addition to the morphological analysis, the particle size of the kaolins, synthetic and the standard zeolite A samples were estimated using this technique.

2.4. Thermogravimetric Analysis (TGA)

Thermogravimetric analysis (TGA) is the method in which the effect of heat on the mass of a sample with time is studied to obtain quantitative information. It is an analytical technique used to determine a material's thermal stability and its fraction of volatile components by monitoring the weight change that occurs as a specimen is heated[71]. The measurement is normally carried out in air or in an inert atmosphere, such as helium or argon, and the weight is recorded as a function of increasing temperature. In this particular study, the thermal stability analysis of the starting kaolins, metakaolins and the synthesized zeolite A was carried out in air with a Perkin-Elmer TGA 7 instrument in the temperature range of 30-900 ^{o}C and at a heating rate of 20 ^{o}C/min by taking sample of 4 to 5 mg weight.

2.5. Cation Exchange Capacity (CEC)

The cation-exchange capacity (CEC) is the measurement of the number of exchangeable sites within the zeolite pore. It is one of the most important properties of clay minerals and zeolites that determines their practical application in different areas[72]. CEC results from the presence of loosely bound cations of alkali and alkaline earths elements, often called exchangeable cations. These loosely bound cations are easily exchanged when the zeolites are in contact with solutions of "saturating" or "indexing" ions[20]. Although different methods have been reported to measure cation exchange capacity, in this study cation exchange capacity measurement of the kaolin and sodium form zeolite A was conducted using GLP 22 multimeter calcium ion selective electrode. For this particular study, 0.5 g zeolite A is first dried at 110 °C for 1 h to remove its inherent moisture. Then it was cool down to room temperature in a desiccators, precisely weighed again and poured into a beaker containing 500 mL of 0.005 M $CaCl_2 \cdot 6H_2O$. The pH of this solution is brought up to 10.0 by addition of 5 mL of a 5% ammonia solution. The removal of Ca^{2+} ion from the solution was measured with initial water hardness of 500 mg $CaCO_3$/L, being this value considered as very hard water. The mixture obtained is vigorously agitated under room temperature for 15 minutes. The zeolite is then filtered off and the residual Ca^{2+} concentration is measured in the filtrate.

2.6. Atomic Absorption Spectrometry (AAS)

Atomic absorption spectrometry (AAS) is an analytical technique that measures the concentration of an element. It is the process involving the absorption of light by free atoms or ions of an element at a wavelength specific to that element[73]. In atomic

absorption spectroscopy, emission, absorption and fluorescence energy is put into the atom population by thermal, electromagnetic, chemical and electrical forms of energy and is converted to light energy by various atomic and electronic processes before measurement. It is useful not only for the identification but also for the quantitative determination of many elements present in samples. The technique is specific, in that individual element in each sample can be reliably identified and it is sensitive, enabling small amounts of an element down to parts per billion of a gram in a sample[74]. In this study flame atomic absorption spectrometer (FAAS) Analytik Jena ZEEnit700 P model was used for the analysis of chromium(III) in tannery wastewater before and after treatment with different adsorbents including kaolin from Ethiopia and zeolite A.

2.7. Scanning Transmission Electron Microscopy (STEM)

Transmission electron microscopy (TEM) is a microscopic technique in which a beam of electrons is transmitted through an ultra-thin specimen, interacting with the specimen as it passes through it[75]. TEM functions by generating a primary electron beam of high energy and high intensity that passes through a condenser to produce parallel beams that irradiate the sample. Magnified images of the sample are formed by combining the transmitted electrons using an electromagnetic objective lens. TEM is primarily used to give information on topography, morphology and crystal structure at atomic resolution[76]. It can also be used for bulk composition when coupled with EDS and/or EELS[77]. STEM combines both scanning and transmission modes and utilizes scanning coils to illuminate a small area of the sample from which bright or dark field images are obtained. STEM can be combined with the high-angle annular dark field (HAADF) detector to provide Z-contrast images which can distinguish atoms of different atomic number[78] (Figure 9). The

image brightness is dependent on the square of the atomic number (Z^2) of the atoms present. Elemental composition of a sample can also be determined by combining EDS and EELS analysis with STEM images.

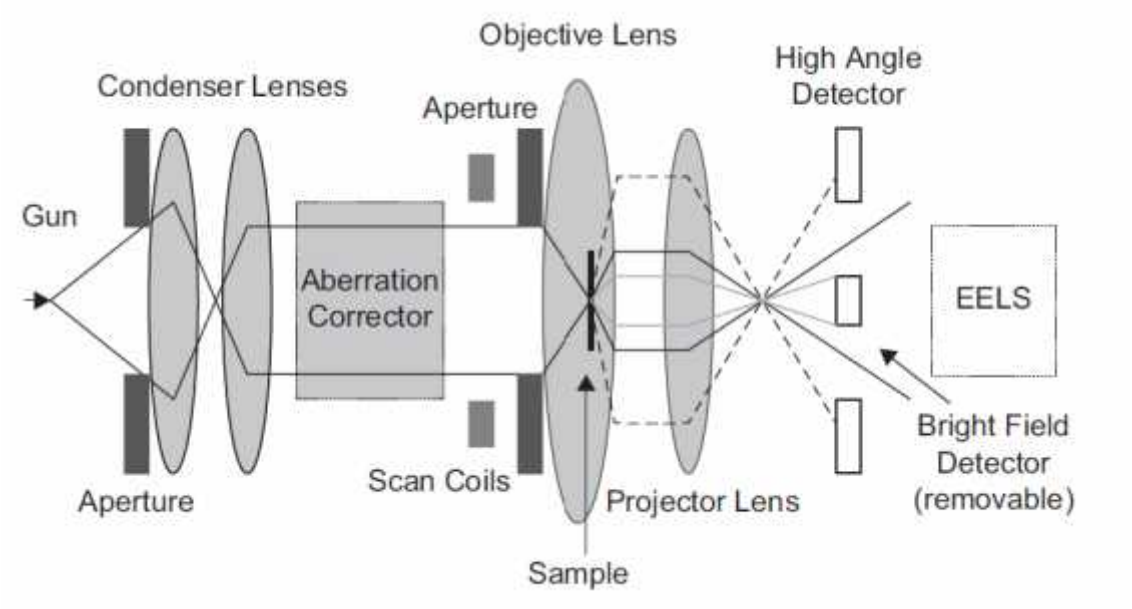

Figure 9: Schematic of an aberration-corrected STEM

In Figure 9 electron trajectories at the edge of the apertures are indicated with solid lines. High-angle scattering used to form the Z-contrast image is indicated with dashed lines and low-angle scattering used to form the bright-field image is indicated with gray lines[78]. In this particular work, STEM/HAADF was performed in a spherical aberration corrected FEI Titan XFEG, which was operated at 300 kV equipped with a corrector for the electron probe allowing a maximum resolution of 0.8 Å; the microscope was also equipped with an EDS detector and a Gatan Tridiem energy filter (for EELS measurements). Prior to observations, the samples were crushed, dispersed in ethanol and placed onto a holey carbon copper microgrid.

CHAPTER THREE

3. Synthesis of Zeolite A from Clay Mineral (Kaolin)

3.1. Introduction

Zeolite A is an important member of low silica synthetic zeolites having unique properties and applications in ion exchange, catalysis, adsorption and separation processes. The commercial production of zeolite A for detergent application, for which it has the highest demand, is mainly achieved by aluminosilicate hydrogel route using sodium silicate and sodium aluminates as a starting raw materials[79]. Nevertheless, its use as adsorbent and builder in detergents requires a competitive price in comparison with phosphates and other possible sequestering agents, which are relatively cheap. In order to overcome this challenge, many researchers and investigators have reported the synthesis of detergent grade zeolite A from economical raw materials. Among these cheaper raw materials: clay minerals, coal ashes, municipal solid wastes and industrial sludge have been widely used. K.S. Hui and C.Y.H. Chao[80] reported the synthesis of pure, single phase, high crystalline, chamfered-edge zeolite 4A from coal fly ash for use as a builder in detergents. A. R. Chaudhur et al.[81]also described synthesis and characterization of detergent-grade zeolite A from Indian clay. M. P. Moisés et al.[82] also reported synthesis of zeolite A from sugarcane bagasse ash.

Kaolin is among clay minerals extensively used for the synthesis of detergent grade zeolite A. This is due to the compositional similarity between zeolite A and kaolin with Si/Al ratio of 1[83]. Moreover, kaolin is a well placed material and is regarded as the next generation industrial mineral because it is more abundant and environmentally friendly

than the other precursors used in zeolite production. Its application in the synthesis of zeolites has continued to receive tremendous research interest.

Kaolin is a commercial term used to describe a white clay mineral composed essentially of kaolinite, $Al_2Si_2O_5(OH)_4$, produced by chemical weathering of aluminum silicate minerals like feldspar[84]. Kaolins chemical composition can vary from one deposit to another or from one location to another in terms of Si/Al molar ratio and the concentration of impurities[85]. Minerals of kaolinite are characterized by the theoretical chemical composition (%) of: SiO_2 (46.5); Al_2O_3 (39.6); H_2O^+ (13.9)[86].

Although originally valued for the manufacture of white ware ceramic, the principal use of kaolin is now in the filling and coating of paper. The mineral is also used to a lesser extent as filler in paint, rubber and plastic while its wider use is in other applications[87]. The potential application of kaolin as industrial mineral is determined by the properties such as particle size distribution, mineralogical composition and structural order-disorder or crystallinity of kaolinite. Among these the particle size distribution is a key factor for the industrial uses of kaolinite. Coarse particle clays differ from fine-particle clays in physical and optical properties. The particle size distribution controls whiteness, gloss, ceramic strength, shrinkage and the paper-filling and paper coating properties such as the mechanical, optical and printing characteristics of the paper sheets[88].

Structurally, kaolin can be viewed as a continuous two dimensional structure consisting of one tetrahedral silica sheet and one octahedral alumina sheet in 1:1 structure in which the silicate layers (Si_2O_5) are bonded to aluminum hydroxide layers ($Al(OH)_4$), called Gibbsite layers, where each aluminum atom occupies the centre of an octahedron with oxygen atoms and hydroxyl groups in the vertices (Figure 10). The other surface is made

of a silica-type structure called silica layer, where each silicon atom occupies the center of a tetrahedron with oxygen atoms in the vertices. Therefore, one side of the layer (gibbsite side) has hydroxyl groups whereas the other side of the layer (silica side) has oxygen atoms[89].

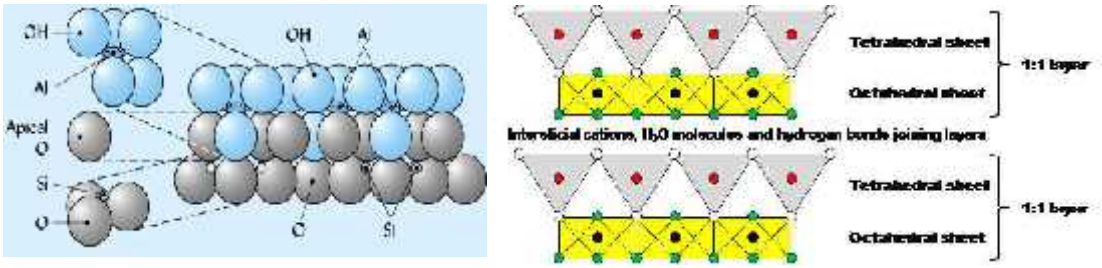

Figure 10: The two dimensional structure of kaolinite

Kaolin is a non expanding clay mineral in which different layers are held together by hydrogen bonding which occurs between the plane of basal oxygen atoms within a tetrahedral sheet and the plane of hydroxyl group within the octahedral layer. In nature, kaolinite has a net negative charge resulting from the broken edge of the clay crystal. The surface of clay mineral generally can be thought to be hydrophobic, however in kaolinite, the presence of hydroxyl group and defects introduce hydrophilicity[90]. Some of the basic physical properties of kaolin include: it is soft, has low viscosity at high solids content in many systems, is readily weted and dispersed in water and some organic systems, and can be produced with a controlled particle size distribution. Some of the important physical constants of kaolin are: specific gravity, 2.60; index of refraction, 1.56; hardness (Mohs scale), 2; fusion temperature, 1850 ^{o}C; dry brightness, 78-92%[85].

3.2. Metakaolinization of Kaolin

The synthesis of zeolite A from kaolin involves two basic steps: metakaolinization, which is the calcination of kaolin at high temperature to change chemically stable kaolin into a very reactive but amorphous material, metakaolin and zeolitization, which is the hydrothermal treatment of the calcined kaolin with sodium hydroxide[91]. Metakaolin ($Al_2O_3 \cdot 2SiO_2$) which is the calcined product of kaolin $Al_2Si_2O_5(OH)_4$ with Si/Al ratio of 1 is a convenient starting material for the synthesis of zeolite A. In the synthesis of zeolites A, kaolin needs to be made reactive through a process called metakaolinization or dehydroxylation before zeolitization can take place. This process consists of calcination of kaolin to form metakaolin in the temperature range of 550-900 ^oC. Metakaolinization directly involves the loss of hydroxyl group and this is followed by rearrangement of the octahedral layer to tetrahedral orientation in the calcined clay[92]. During calcination, the silicon atoms experience a range of environments of differing distortion due to dehydroxylation. The aluminium atoms mostly transform from octahedral to tetrahedral geometry. As the calcination temperature increases, the structure becomes more distorted, and finally amorphous silica is liberated. For kaolinite, dehydroxylation might result in the disturbance of the Al $(O, OH)_6$ octahedral sheet by the outer hydroxyls, but does not much affect the SiO_4 tetrahedral sheet due to the more stable inner-hydroxyl groups. Only a small part of AlO_6 octahedra is maintained, while the rest are transformed into much more reactive tetra and penta coordinated units. The outer hydroxyls of octahedral sheets may be more easily removed by heating than inner ones that will maintain a more ordered SiO_4 tetrahedral group in structure during dehydroxylation[93]. Hence metakaolin with (IV) Al coordination and amorphous in nature

is a necessary path toward zeolite A synthesis from kaolin. The best conditions for obtaining a very reactive metakaolin have been discussed by several authors and reported as between 600-900 °C[94]. Different research results indicated that if the temperature is too low, hydroxysodalite could be formed, whereas for higher temperatures (> 900 ^{o}C), zeolite NaP could be formed. Metakaolin is thermally stable up to 925 °C. Increasing the calcination temperature up to 950 ^{o}C leads to transformation of metakaolin to aluminium silicon spinel phase also called gamma alumina type structure. Further increase of temperature to 1050 ^{o}C results in the spinel phase nucleates and transform to mullite and highly crystalline cristobalite (Scheme 4).

$2Al_2Si_2O_5(OH)_4 \longrightarrow 2Al_2Si_2O_7 + 4H_2O$ 600-900 ^{o}C

Kaolin Metakaolin

$2Al_2SiO_7 \longrightarrow Si_3Al_4O_{12} + SiO_2$ 925-950 ^{o}C

Metakaolin Spinel

$3Si_3Al_4O_{12} \longrightarrow 2Si_2Al_6O_{13} + 5SiO_2$ 1050 ^{o}C

Spinel Mullite Cristobalite

Scheme 4: Kaolin transformation into different phases with increase in temperature[95]

The presence of impurities, like quartz, anatase and mica makes “low grade” kaolin. The appearance of quartz peaks indicates the presence of some of the silica in the form of free quartz. In the same trend, the anatase presence is a common feature of most calcined kaolins due to TiO_2 crystallization at the high temperature of calcination[96]. This

associated mineral requires removal or reduction because it generally reduces the commercial value of the mineral. Hence purification is very important before usage. The most common and simplest method of enriching the kaolin content of raw kaolin sample is fractionation by sedimentation. The refining process of kaolin is clearly divided into two groups, namely removal of foreign material by chemical method and refinement by sedimentation to remove larger impurities, especially for quartz which is trapped within the mineral aggregates. However, addition of chemicals in the treatment process can impair the properties of the parent material. Therefore, the use of chemical treatment should be the last resort. Some of the well known techniques to purify kaolin are: selective flocculation, high gradient magnetic separation, flotation purification and particle size separation by sedimentation[97].

3.3. Kaolin deposits of Ethiopia

Exploration for kaolin in Ethiopia was carried out mainly at the granites and pegmatite rocks which have been the main sources of kaolin for the ceramic industry in Ethiopia. Economic kaolin resources of the country are mostly associated with these rocks. Kaolins hosted by sedimentary rocks are reported in Blue Nile river basin, Ogaden basin and Mekele outlier. Assessment of the economic aspects of these occurrences had been discouraged due to their low clay content. Acidic volcanic rocks (such as rhyolite or trachyte) in central and northern Ethiopia, and the coal related clay sediments of northwest Ethiopia, near Chilga are a source of kaolin in Ethiopia[98]. As the current information from office of Tigrai region mine and energy shows, there is large deposition of kaolin that can be estimated to 9 x 107 m^3 which is not yet exploited for any purpose[99]. These and the other kaolins which have been investigated in the different parts of the

country are summarized in Table 2 and Figure 11.

Table 2: Kaolin occurrence in different parts of Ethiopia

Place	**Longitude**	**Latitude**	**Region**
Belesa	37° 58'E	7° 35'N	SPNNRS
Awzet	38° 07' 48" E	11° 45' 00" N	Amhara
Debre Tabor	38° 00' 36" E	11° 50' 02" N	Amhara
Gypsite Mariam	37° 35’ 24” E	11° 45’ 36” N	Amhara
Kerker	37° 24' 43" E	12° 42' 40"N	Amhara
Bombowha	38° 46'30" E	06° 05' 20" N	Oromia
Kombelcha	42° 08' 50" E	09° 27' 58" N	Oromia
Ansho	37° 38' 28" E	7° 20' 6"N	SPNNRS
Adwa	38° 57' 44" E	14° 19' 54"N	Tigrai
TsadaMidri	38° 12' 55" E	14° 26' 42"N	Tigrai

SPNNRS – Southern People Nations and Nationalities Regional State.

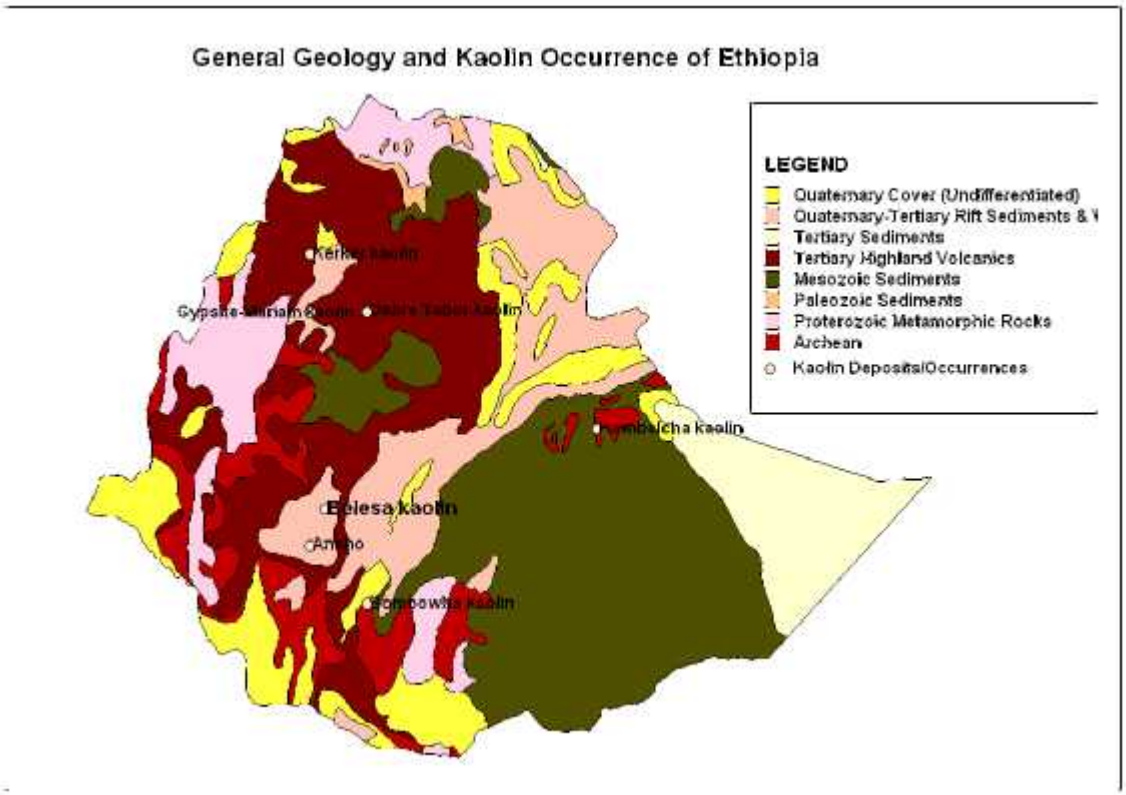

Figure 11: General Geology and Kaolin deposit of Ethiopia

Among these kaolins, intensive exploration has been carried out at Bombowha and Kombolcha areas and both of them are related to acidic intrusive rocks. According to Mengistu and Fentaw[100], the Kombelcha kaolin occurs as blankets extending over large areas overlying the granites, whereas the Bombowha kaolin occurs on kaolinized pegmatites and granites. All the pegmatites and granites occur in deformed metamorphic rocks. The Bombowha kaolin was found to be an important raw material for the ceramic factory without purification. Regardless of the wide geographical coverage and

abundance of kaolin mineral in Ethiopia, excluding the recently reported kaolin of Tigrai region, its exploitation is limited to an annual production of about 4, 000 metric ton.

Based on the report by U.S. Geological Survey Minerals Yearbook[101], the annual kaolin production in Ethiopia is summarized in the following Table 3.

Table 3: Annual Kaolin Production in Ethiopia (metric tons)

Year	2002	2003	2004	2005	2006	2007	2008	2009	2010	2011
production	3,534	3088	4251	4,300	1641	1400	1,275	3,534	3,600	4,000

3.4. Purification and calcination of Ansho and Bombowha kaolins

Among the different types of kaolin available in Ethiopia, the present study used Ansho and Bombowha kaolins for synthesis of zeolite A. The samples were collected from *Hawassa ceramic factory,* located in the southern part of Ethiopia. For the purpose of discussions the Ansho kaolin is represented by 'A', Bombowha kaolin by 'B' and the commercial kaolin used as standard kaolin is designated as 'S'. Initial characterization of the raw kaolins was carried out using XRD, ICP-OES elemental analysis, SEM and the thermal stability analysis by TGA.

In the purification of the raw kaolins, two basic routes have been followed: the physical route and the chemical routes. In the physical route we have used the mechanical separation methods: separation by sedimentation, ultrasonic suspension and magnetic

separation for the removal of magnetic iron. In the chemical method we have used the low concentrated hydrochloric acid (HCl) for the removal of some remaining impurities and to minimize non structural iron in the raw kaolins.

3.4.1. Physical method of purification

In this method of purification, 20 g of the raw kaolin soaked with 50 ml of the ultra pure (milli Q) distilled water. The mixture was allowed to age for four days with constant stirring. In this process of sedimentation, the water on the top was decanted and replaced with the fresh one periodically. On the fourth day the lower density suspension which is mainly composed of kaolinite was decanted to other beaker and the denser one which is predominantly quart was discarded. The suspended mixture was separated through centrifugation and dried. Then the dried materials were subjected to ultrasonic suspension by mixing with water in the ratio (2 g: 200 mL) at a temperature of 40 ^{o}C for 30 minutes. Following the ultrasonic suspension process, the removal of non structural iron was done by magnetic separation at different time intervals of magnetic stirring. The suspension with lower density was decanted and filtered and finally dried overnight in an oven at 110 ^{o}C. The dried kaolinite was crushed and sieved to 75 µm particle size using 200 µm mesh size sieve.

3.4.2. Chemical method of purification

To remove non structural iron and improve the whiteness of the starting raw kaolin, chemical treatment was conducted for the physically purified kaolin by treating it with 1 M HCl for 1 h at 100 ^{o}C with stirring.

3.4.3. Calcination of kaolins

The transformation of kaolin to metakaolin was carried out by calcining both the raw and purified kaolins. This was done using time and temperature programmed muffle furnace (CARBOLITE) which was initially heated to a temperature of 600 or 900 ^{o}C at heating rate of 10 ^{o}C/min. Immediately after the furnace attained the intended temperature of calcination, a crucible containing 5 g of the sample was loaded into the furnace and was removed after the intended duration of calcination and allowed to cool. The calcined product obtained was characterized using XRD and SEM. The thermal stability of the kaolin and metakaolin was determined using thermogravimetric analysis (TGA).

3.5. Synthesis of zeolite A from kaolin

The synthesis of zeolite A from the kaolin sources of Ansho (A) and Bombowha (B) has been carried out by using the uncalcined kaolin and the calcined (metakaolin) formed at two different calcination temperatures (600 and 900 ^{o}C). The synthesis process was done following two methods: the conventional hydrothermal and alkali fusion followed by hydrothermal method. Before doing the synthesis by either of the two methods, the synthesis without pre activation (calcination) of the kaolins was conducted to assess the importance of preactivation of kaolin prior to the zeolitization process. For the optimization of the best synthesis condition, the effects of different reaction parameters have been studied. The effect of metakaolinization temperature, alkaline (NaOH) concentration, gel formation temperature and aging time and the crystallization temperature and time were studied. Solution of sodium hydroxide with different

concentrations (1, 2, 2.5, 3, 3.5, 4 and 6 M) were used as source of Na_2O and metakaolin as a combined source of alumina and silica.

3.5.1. Conventional hydrothermal synthesis

In the conventional hydrothermal method of synthesis, the metakaolin which is formed by calcination with the conditions of 600 and 900 ^{o}C for 3 h undergo alkaline treatment. This was done by mixing 1.25 g of metakaolin and 25 mL aqueous solution of different concentration of NaOH under different gel forming condition to obtain aluminosilicate gel. The aluminosilicate gel formed was subsequently aged at static condition[102]. The aged gel undergoes crystallization under static condition with varying crystallization time and temperature (Scheme 5).

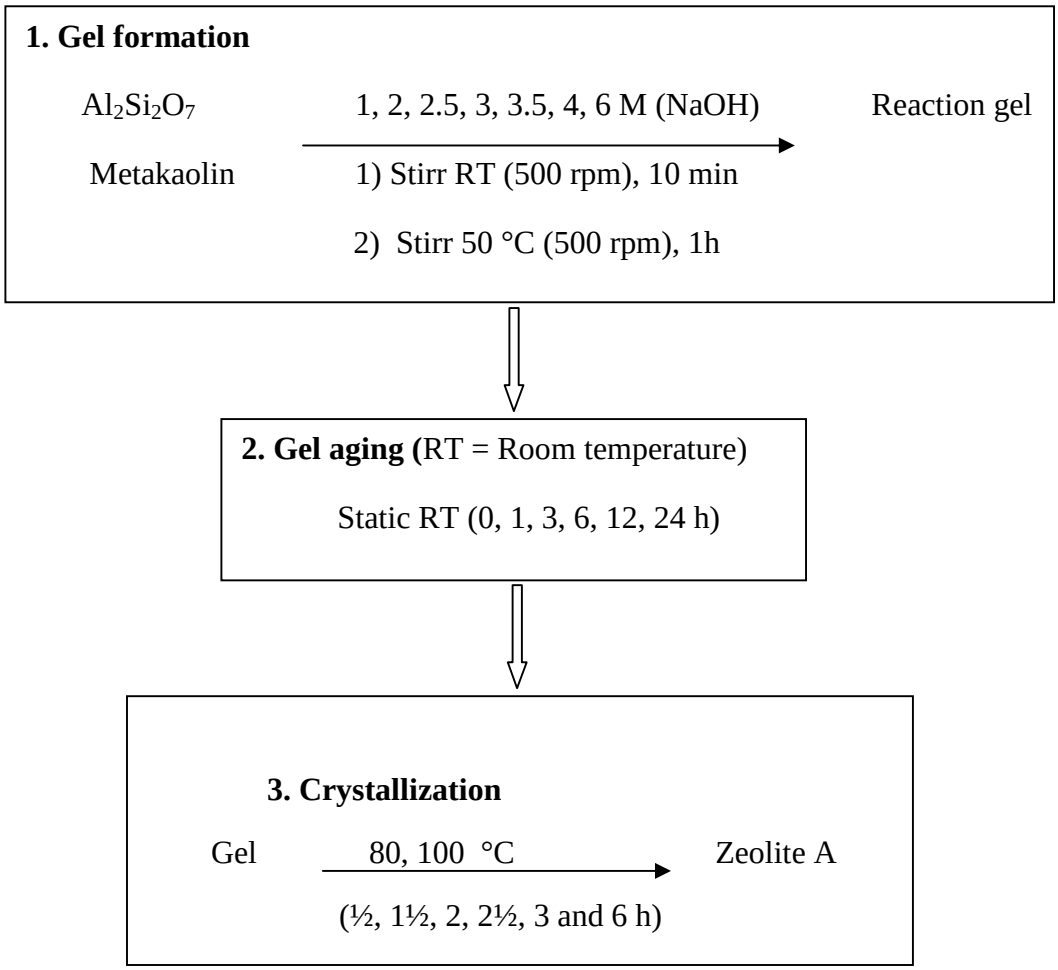

Scheme 5: Flow diagram of the conventional hydrothermal synthesis of zeolite A

Once the activation time was reached, the reactors were removed from the water bath and quenched in cold water to stop the reaction. The hydrogel pH was measured before and after the hydrothermal synthesis. The synthesized product was then washed with ultra pure distilled water until pH = 10 was attained in the wash water. Then the products were dried in an oven at 80 ^{o}C for 24 h and collected in plastic containers for characterization.

3.5.2. Alkali fusion followed by hydrothermal synthesis

In this method of zeolite A synthesis, alkali fusion (solid-state reaction) step was introduced before the calcination step to extract aluminium and silicon from the starting raw kaolin. This method has the advantage of the kaolin and other impurities like quartz are expected to be completely activated and converted to zeolite A due to alkali and thermal activation. Thus, 1.25 g of the raw kaolin was dry-mixed with 1.5 g of NaOH (solid) for 30 min followed by calcination at 600 ^{o}C for 1 h in a crucible put in a muffle furnace. Then the fused product was ground in a mortar and mixed with 12.5 mL of the ultra pure distilled water and stirred (500 rpm) at 50 ^{o}C for 1 h for gel formation[103]. Gel forming condition and crystallization temperature and time was based on the optimized conditions attained in the conventional hydrothermal method. However, the optimization of gel aging time under static condition was undertaken similar to the conventional synthesis method (Scheme 6). Finally, the product obtained was filtered, washed and oven dried over night at 80 ^{o}C and collected in a plastic container for characterization. For comparison commercial zeolite A was purchased from Industrias Químicas del Ebro (Spain). The synthetic samples are labeled with ‘R’ when prepared from raw kaolin, ‘P’ from purified kaolin and ‘F’ from alkali fusion method in which only raw kaolin is used. Then the amount of NaOH is stated as ‘xM’ wherein ‘x’ represents different molar concentrations of NaOH is used. The aging time is indicated as ‘yG’ in which ‘y’ is the time kept in statics at room temperature while aging and finally ‘zh’ where ‘z’ represents the different crystallization time followed in this study.

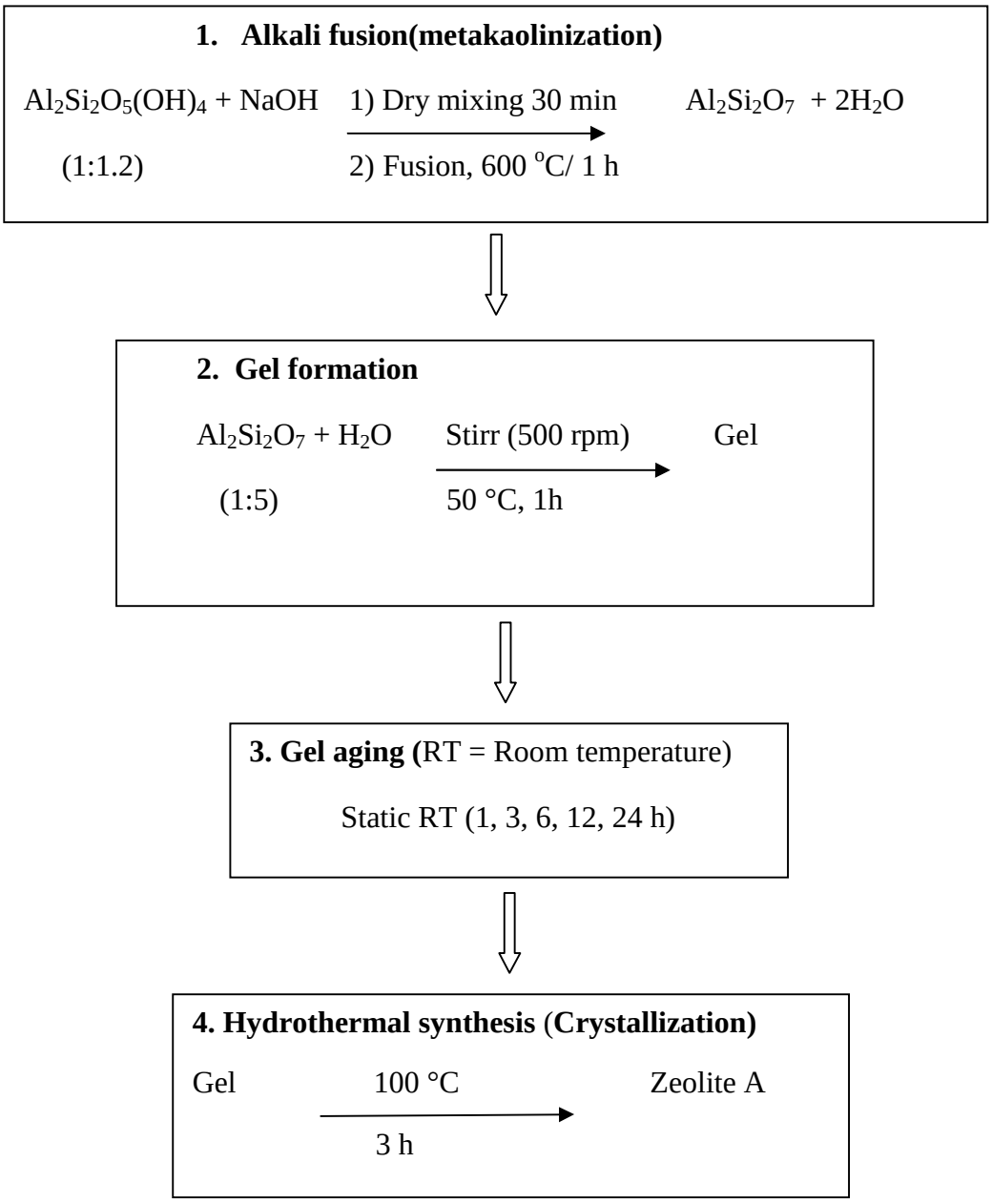

Scheme 6: Flow diagram for the alkali fusion followed by hydrothermal synthesis of zeolite A

CHAPTER FOUR

4. Results and Discussion

4.1. Purification of the raw Ansho (A) and Bombowha (B) kaolins

We have initially analyzed the collected raw kaolins to know the quality and chemical compositions before planning any purification method. We have used commercially available CAOBAR kaolin (S) as standard for comparison. The XRD patterns of the raw Ethiopian kaolins along with the standard are shown in Figure 12. The profiles correspond to that of kaolinite, having a layered structure with d_{100} at 12.34° and d_{200} 24.64°, which are the characteristic peaks of kaolinite[104]. There is also good agreement in the X-ray diffraction patterns of the raw kaolins and the commercial kaolin, despite the presence of the characteristic diffraction intensities of quartz (Q) and mica (M) at 2θ (°) value of 26.6 and 8.9, which are the common impurities found in kaolins.

The scanning electron micrographs (SEM) analysis of the raw kaolins (Figure 13) showed the presence of typical hexagonal platy morphology of kaolinite crystals. Standard kaolin shows a more regular hexagonal morphology of kaolinite crystals[105].

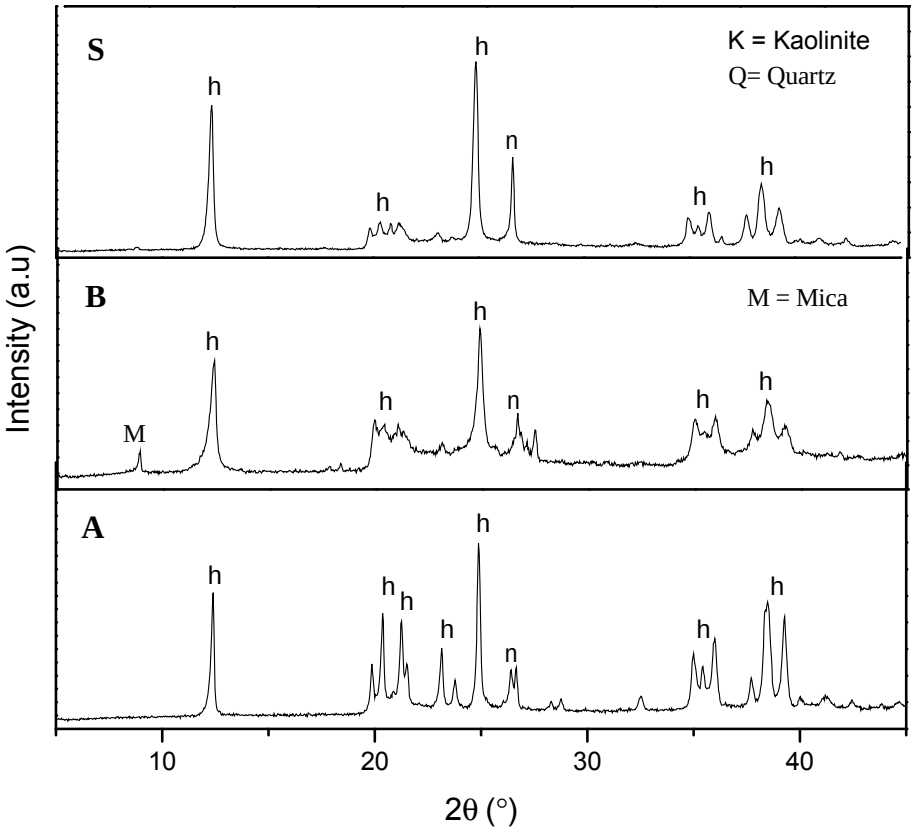

Figure 12: XRD patterns of A, B and S kaolins

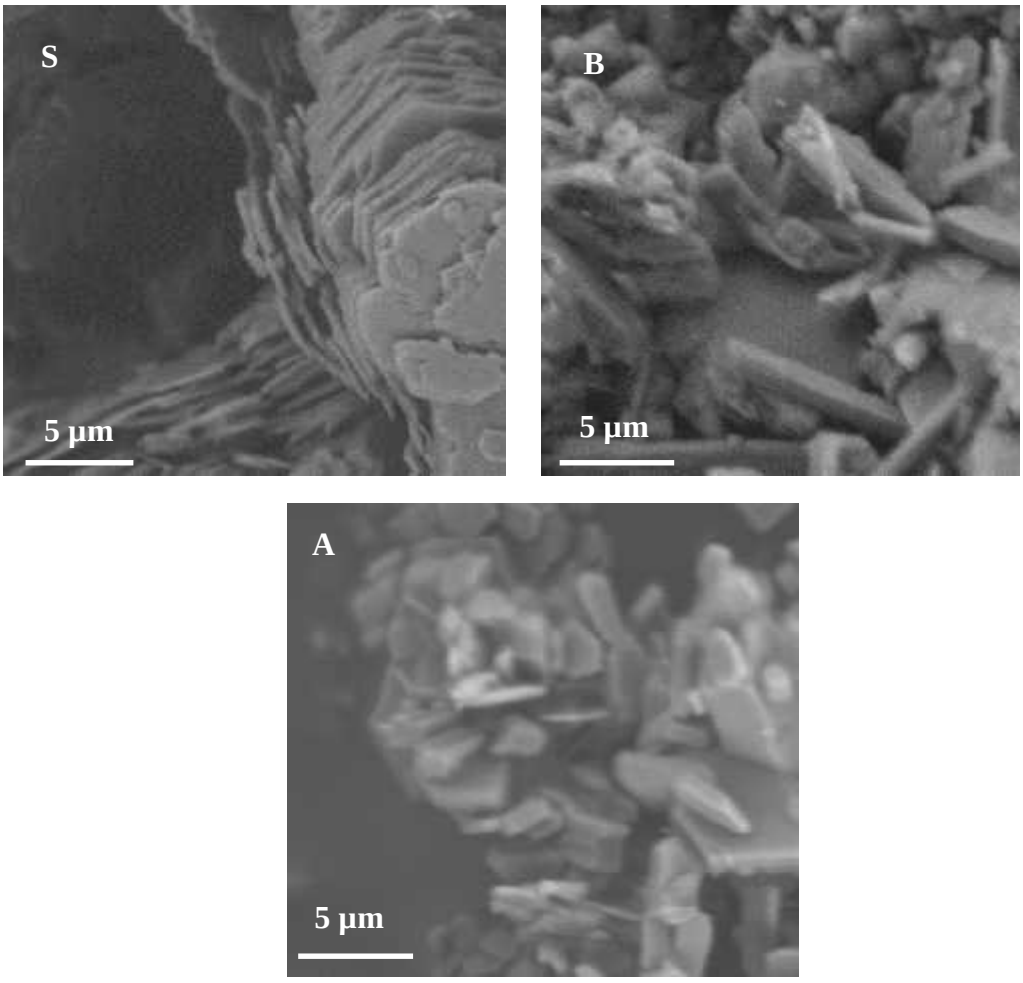

Figure 13: SEM micrographs of the standard kaolin and the raw A and B Ethiopian kaolins

The raw kaolins exhibited low crystallinity compared to the commercial kaolin, 60% and 36% relative percent crystallinity for A and B types of kaolins, respectively. This indicated that our starting raw A kaolin is fairly good, but type B kaolin is of low grade. Thus, both types were subjected to purification methods in order to evaluate the inpact in the final zeolite A synthesis. Following the purification process described in section 3.4, improvement in the crystallinity was observed in both kaolins. However, the

characteristic X-ray diffraction peaks of the impurities persisted. The relative percent crystallinity increased to 67% and 50% for A and B kaolins, respectively. This is verified by the chemical composition analysis done with ICP-OES (Table 4) and phase composition results obtained from the X-pert high square software analysis (Table 5).

From the chemical composition analysis (Table 4), it is noted that the purification of the raw kaolins resulted in the improvement of the quality of both kaolin types. This improvement can also be identified by the variation in Si/Al ratios, which is now closer to 1 and in good agreement with the literature value[86]. The decrease in the Si/Al ratio could be attributed to the successful separation of quartz based on the density differences during the beneficiation process. Moreover, for kaolin type A, purification of the raw kaolin resulted in appreciable reduction of compounds of iron from 2.1 to1.3 wt%, which corresponds to about 38% removal of iron species. This is also true for B type kaolin, in which 27% iron species removal is achieved. The remaining unremoved iron could be structural iron that could be trapped between the lamellae of kaolin by substituting octahedral aluminum. From the table, it can also be observed that there is removal of Na_2O and K_2O following the purification processes. The reductions have occurred as a result of washing off soluble salts of sodium and potassium during the purification.

Table 4: Chemical composition (wt %) of the raw and purified A and B kaolins

Oxides	Kaolin types (wt%)				Literaturevalue
	Ansho (A)		Bombowha (B)		
	Raw	Purified	Raw	Purified	
SiO_2	54.7	52.8	54.9	54.9	46.52
Al_2O_3	34.0	36.0	36.1	33.8	39.53
TiO_2	0.6	0.3	0.0	0.0	-
Fe_2O_3	2.1	1.3	1.1	0.8	-
CaO	0.0	0.0	0.0	0.0	-
MgO	0.0	0.0	0.0	0.0	-
Na_2O	0.2	0.0	0.1	0.1	-
K_2O	0.2	0.0	1.1	0.9	-
Si/Al	1.4	1.2	1.3	1.2	1.0
Lossonignition (LoI)	12.9	12.9	13.7	13.7	13.95

Table 5: Phase composition result from X-pert High Square software analysis

Kaolintype	Kaolinite	Quartz	others
A- Raw	67	27	6
A-Purified	77	19	4
B-Raw	37	25	38
B-Purified	55	18	27

Although the physical treatments of the raw kaolins resulted in an improved material upon the removal of impurities like quartz, there are other impurities that imparted color

to the kaolin, which are predominantly due to iron that still persists in the mineral phase. In order to remove these species and improve the whiteness of the kaolin, chemical treatment was carried out using 1M HCl for 1 h at 100 ^{o}C. The treatment resulted in a whiter version of the kaolins, although the chemical method does not bring remarkable improvement in the overall quality of the kaolins.

The thermal stability data of the starting kaolins was obtained from thermogravimetric analysis (TGA). Its thermal decomposition is illustrated in the TG and the first derivative (DTG) curves shown in Figure 14. The transition of kaolin to metakaolin has been observed near 540 ^{o}C for both types of kaolin. The main weight losses identified are: first loss below 400 °C, 1.51 wt% for A and 1.87 wt% for B kaolin corresponding to the release of loosely absorbed water on the surface of kaolin, the weight loss in the range of 400–700 °C which is 11.39 and 11.83 wt% for A and B type kaolins can be correlated with a pre-dehydration process, which takes place as a result of the reorganization in the octahedral layer of the kaolin and is due to the dehydroxylation of the structural OH of the kaolin. This is the step at which metakaolin is formed by a gradual loss of structural water through diffusion accompanied by a concomitant change in aluminum coordination from six- to four[106]. According to Varga et al.[105], the transformation of kaolin into metakaolin by dehydroxylation results in structural disturbances through the breaking of unstable bonds. As a result, the ordering of the structure is lost as dehydroxylation progresses. From the graph, progressive decomposition of the metakaolinite occurs up to 900 °C. The total weight loss on ignition (LoI) calculated from the thermogravimetric analysis is 12.9 and 13.7 % for A and B kaolins, respectively.

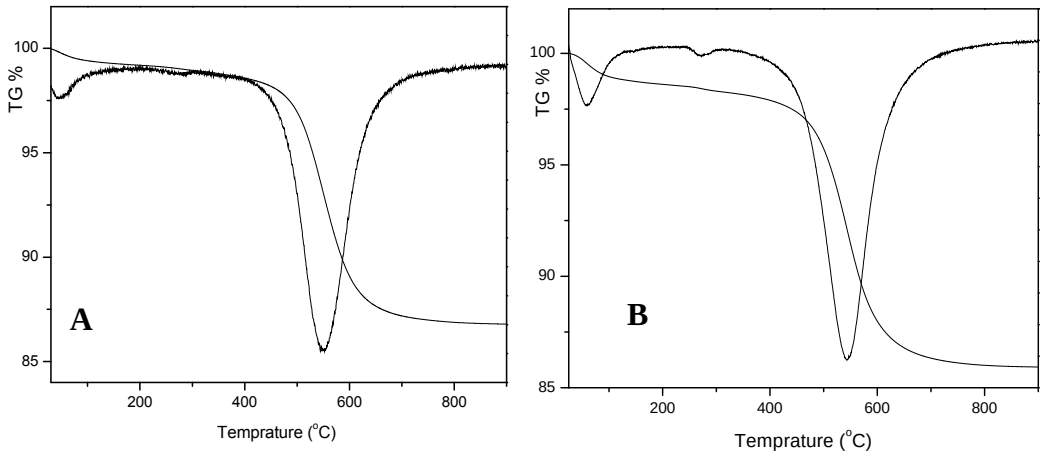

Figure 14: Thermogravimetric analysis (TGA/DTG) of A and B kaolins

4.2. Metakaolinization of kaolin

The preliminary step in the synthesis of zeolite A from kaolin is the thermal activation of chemically inert crystalline kaolin to obtain more reactive and amorphous phase, metakaolin. As explained in the synthesis part, we used 600 and 900 ^{o} C/ 3 h calcination (metakaolinization) for the conventional hydrothermal synthesis and dry mixing followed by alkali fusion at 600 ^{o}C/1 h for the alkali fusion, followed by hydrothermal method of synthesis. The XRD patterns exhibit a significant change in comparison with the pattern of untreated kaolin (Figure 15), which is characterized by the disappearance of the diffraction peaks of kaolin, accompanied by the appearance of amorphous aluminosilicate (a broad featureless bulge extends between 2θ (°) of 15 to 40), which is the characteristic X-ray diffraction pattern of metakaolin[104]. The presence of intense diffraction peaks is due to the quartz and mica which remained intact upon the calcination temperatures in this work.

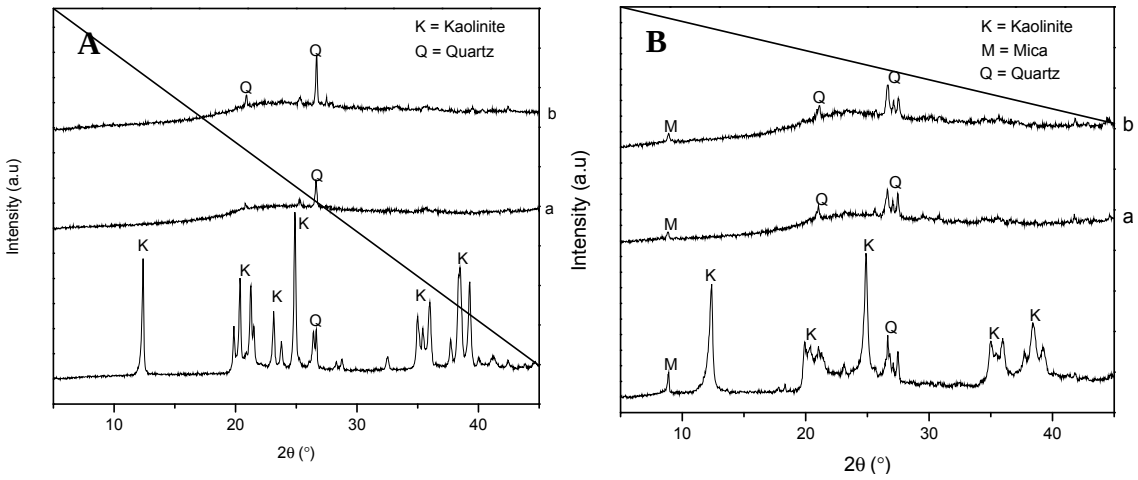

Figure 15: XRD patterns of kaolins A and B. (a) calcined at 600 ^{o}C (b) and at 900 ^{o}C

As it can be observed in the profiles, the characteristic peaks of impurities such as quartz and mica remained crystalline even at 900 ^{o}C calcination. Similar result is also observed for the commercial kaolin calcined at 600 ^{o}C (Figure 16). The graph shows the stability of quartz phase in the calcined standard kaolin.

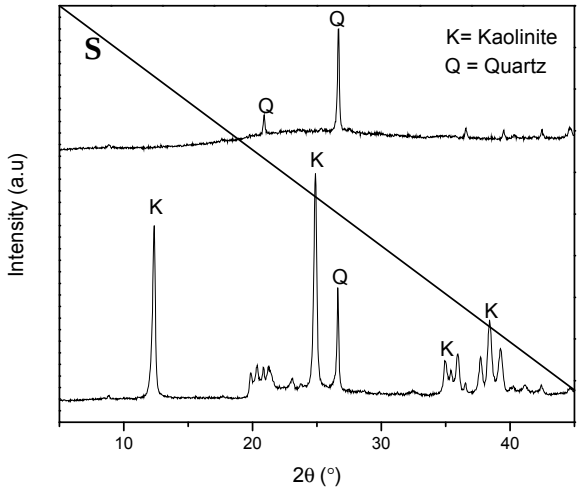

Figure 16: XRD pattern of 600 ^{o}C calcined standard kaolin (CAOBAR)

The transition of crystalline kaolin to amorphous metakaolin was also verified by scanning electron microscopy. The SEM micrographs in Figure 17 indicate the partially shapeless morphology corroborating the disappearance of kaolin and the formation of glassy structure of metakaolin.

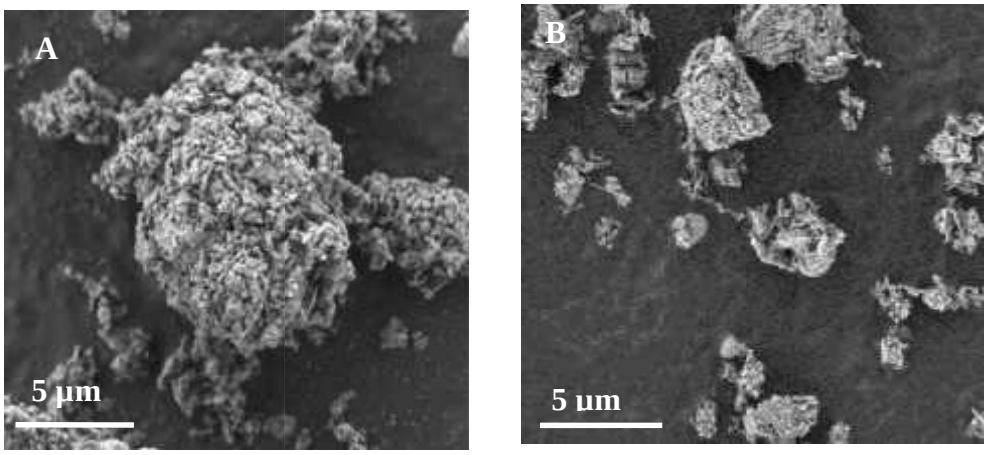

Figure 17: SEM micrographs of metakaolins obtained from A and B kaolins

The thermograms plotted in Figure 18 correspond to the metakaolins formed at 600 and 900 ^{o}C. As can be observed, the lines marked (a) correspond to the calcination at 600 ^{o}C and (b) the calcination at 900 ^{o}C. The graph indicates the stability and structure of metakaolinite. Metakaolinite does not collapse but rather, retains a layered structure. This is because of the fact that, however, the octahedral layer is likely to be changed more than the tetrahedral silica layer during dehydroxylation process, a recent work by S. Lee[107] assumes the rearrangement of the oxygen and vacant sites, which gives stability to the layered structure. Moreover, the TG curve shows that at the calcination temperature of 600 ^{o}C, there is a remarkable weight loss (1.6%) indicating the presence of the

remaining OH group. However, for the 900 ^{o}C calcination temperature, the TG curve indicates negligible weight loss (< 1%) which means the material is completely amorphous.

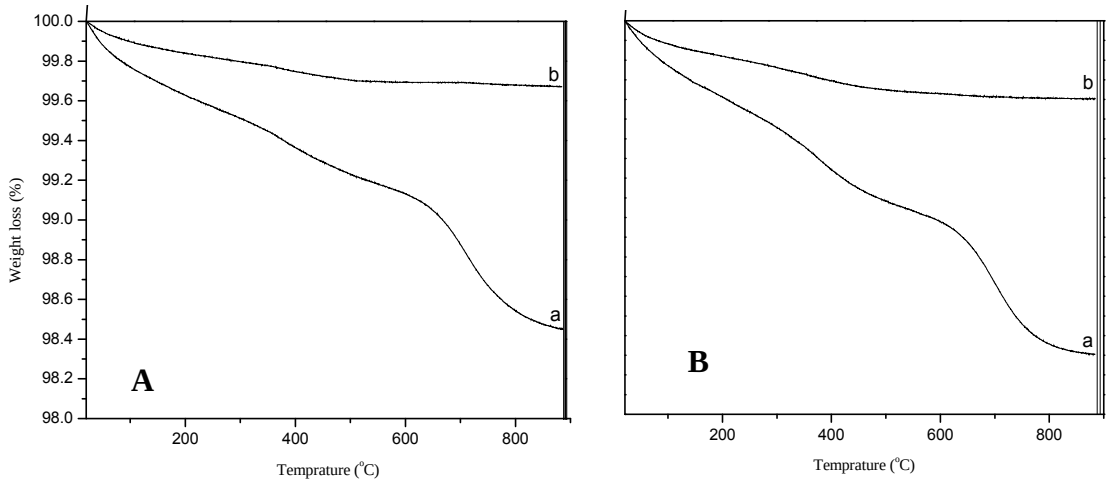

Figure 18: Thermogravimetric analysis of metakaolins obtained from Kaolins A and B at 600 (a) and 900 ^{o}C (b)

4.3. Conventional hydrothermal synthesis

In this section the outcome of different synthesis parameters optimized and systematically analyzed using conventional hydrothermal method are presented. Under this section the effect of different reaction parameters on the crystallinity and morphology of the intended product are briefly discussed.

4.3.1. Effect of metakaolinization temperature

In a first step, a control experiment was conducted for the synthesis of zeolite A in the absence of calcination of kaolins. The synthesis was done following the same protocol as with other synthesis but in the absence of the thermal activation of kaolins. The XRD profile of the synthetic product (Figure 19) indicated no zeolite A formation, rather peaks of the starting kaolin, which remained unconverted are observed. Moreover, the reaction results in the formation of sodalite phase. Therefore, we evaluated the effect of different metakaolinization temperatures on the formation and crystallinity of the synthetic products.

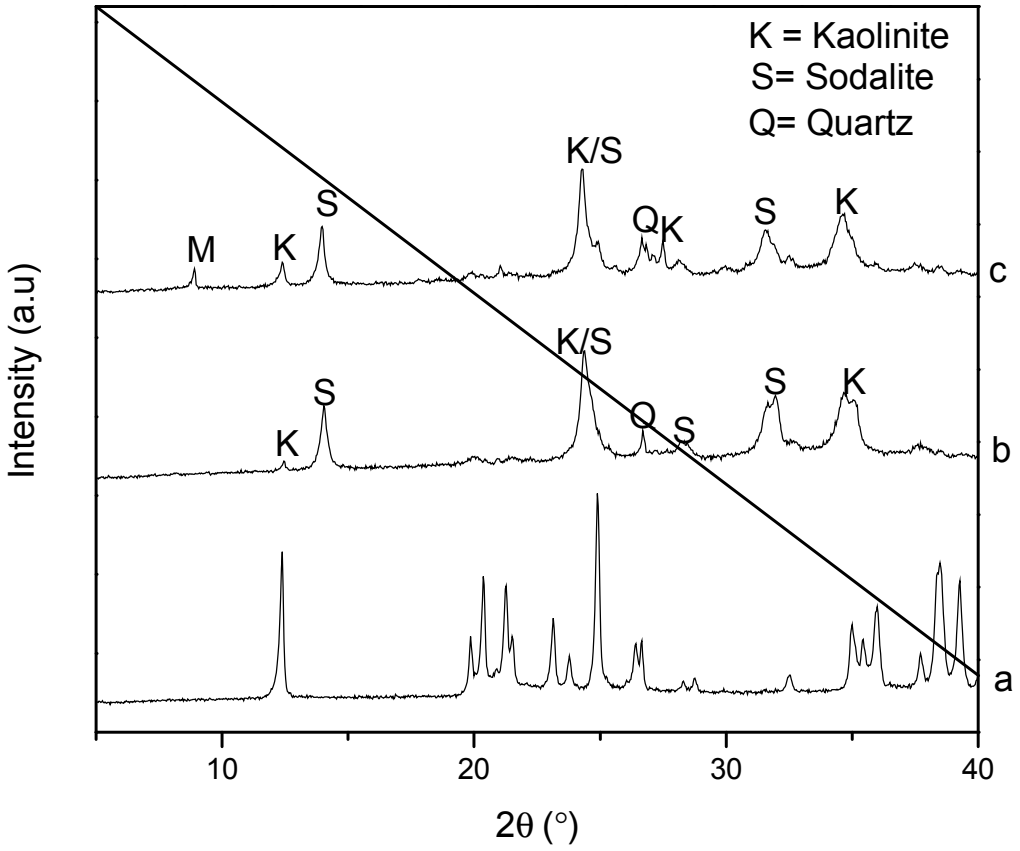

Figure 19: XRD pattern of A kaolin before hydrothermal treatment (a), compared with the hydrothermal synthesis for zeolite A using uncalcined kaolin A (b) and B (c)

The reason behind conducting calcination at different temperatures is to do with the dehydroxylation temperature which is found to have a significant influence on the reactivity towards aqueous NaOH for zeolite formation as well as on the brightness of synthesized zeolite A. These two properties are important in the synthesis of detergent quality zeolite A from kaolin[94]. For the evaluation of the impact of the metakaolinization temperature, initial synthesis conditions were adopted from the literature which involved 4 M concentration of NaOH and crystallization temperature of 100 ^{o}C for 3 h[108]. Using

the above mentioned condition of synthesis, the percent crystallinity (C_{XRD}) calculated from the XRD profiles (Figure 20) revealed in zeolite A having comparable crystallinity of 73 and 75% with calcination temperatures of 600 and 900 ^{o}C, respectively for A type kaolin. Similarly for B kaolin based zeolite A, the crystallinity attained was 66 and 68% for the calcination temperature of 600 and 900 ^{o}C, respectively. Based upon these comparable results, further study was continued with 600 ^{o}C calcination process for metakaolinization.

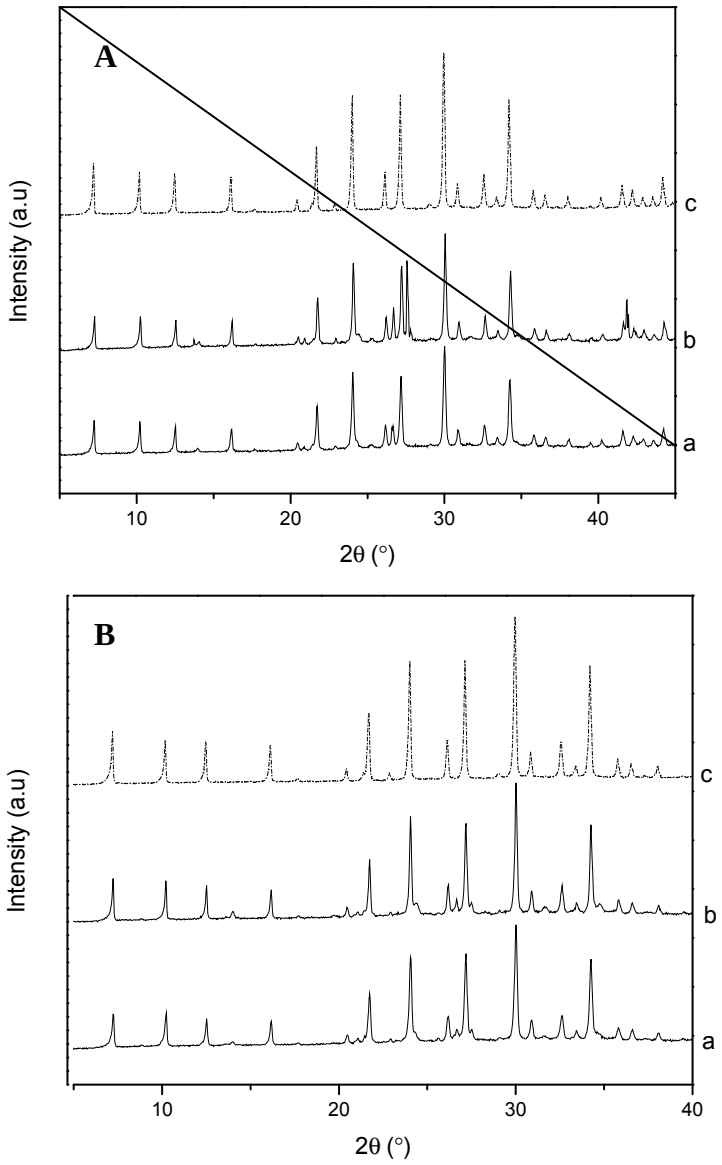

Figure 20: XRD pattern of synthetic zeolite A made with metakaolins formed at different calcination temperatures: (a) 600 ^{o}C, (b) 900 ^{o}C and (c) commercial zeolite A (CZA)

4.3.2. Effect of alkalinity (NaOH)

The concentration of the base used is one of the most important parameter that controls the crystallization of zeolites. The increase in alkalinity causes an increase in the crystallization rate via both nucleation and crystal growth as a consequence of the larger concentration of reactive silicate, aluminates and aluminosilicates species caused by the rapid increments of the solubility of the metakolin[109]. The different compositions of the natural clays require an optimization of NaOH concentration for each source of kaolin. In this study, the concentration of NaOH ranging from 1 M to 6 M was used to produce zeolite A following the treatment of the metakaolin of both raw and purified kaolins at 600 ^{o}C. In this study, the effect of the alkaline concentration was studied by keeping the crystallization temperature at 100 ^{o}C and crystallization time at 3 and 6 h. The metakaolin which is treated with different concentration of NaOH undergoes homogenization for the formation of reaction gel at room temperature (RT) for 10 minutes followed by crystallization for 3 h. The XRD profiles of zeolite A synthesized from the purified A and B type kaolins under different alkaline concentration are compiled in Figure 21. The XRD patterns of 1 M and 2 M alkaline treated reaction products indicated that the x-ray diffraction profile of the synthesized product resembles that of the amorphous starting material metakaolin (Figure 15). This indicated that the alkali concentration used is not sufficient for the zeolitization process. The characteristic XRD peaks of zeolite A started to appear following the alkaline treatment of metakaolin with 2.5 M NaOH with a perfect matching with the characteristic peaks of the commercial zeolite A (SZA) and the literature value[110]. The synthesized zeolite products obtained from 2.5–4 M NaOH concentrations contain zeolite A as the major constituent phase. This is consistent with

the work of Gougazeh and Buhl[57] in which they synthesized zeolite A from natural Jordanian kaolin and it was the main product with the NaOH concentrations of 1.50–3.50 M, whereas hydroxysodalite (HS) and quartz were found as minor phases. This situation is observed for both types of A and B kaolin based zeolite A.

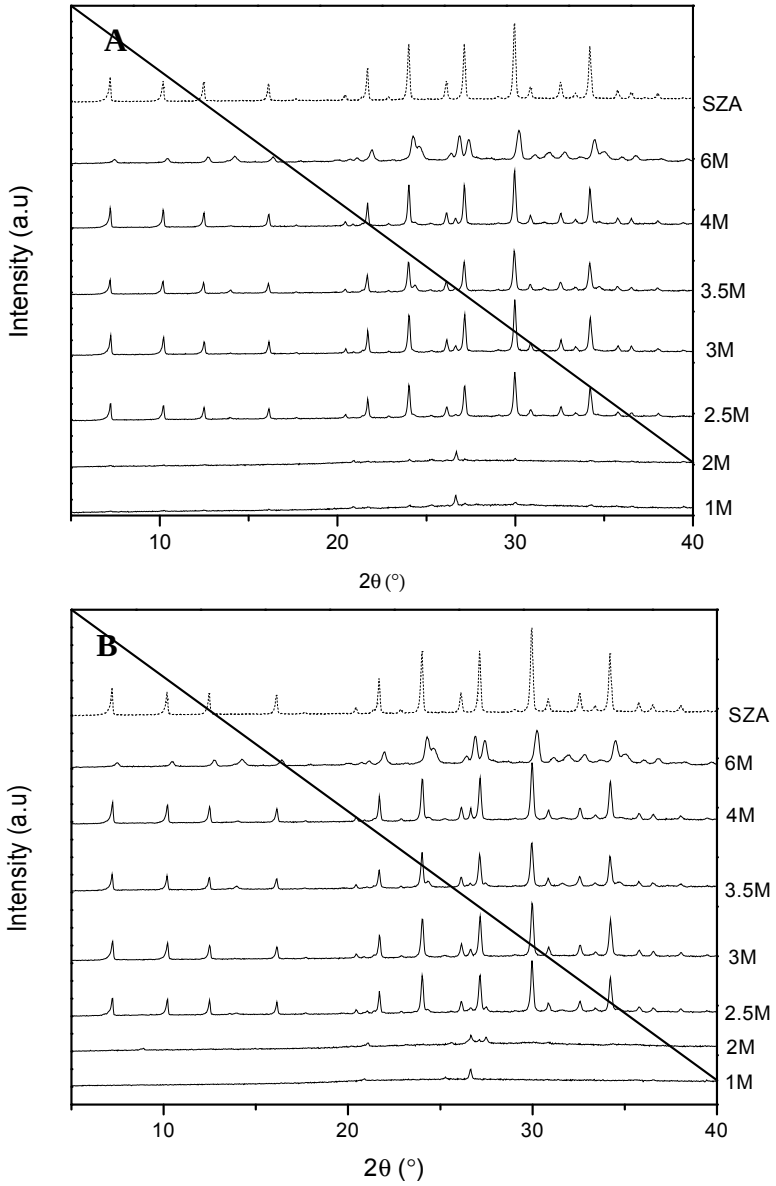

Figure 21: XRD pattern of reaction products at different NaOH concentration using purified kaolin A and B compared to the XRD profile of commercial zeolite A (CZA)

The beginning of the formation of crystals of zeolite A from 2.5 M NaOH treatment reaction product is also confirmed by the SEM micrographic analysis (Figure 22). The SEM images illustrate the presence of some cubic crystals of zeolite A associated with the amorphous aluminosilicate gel.

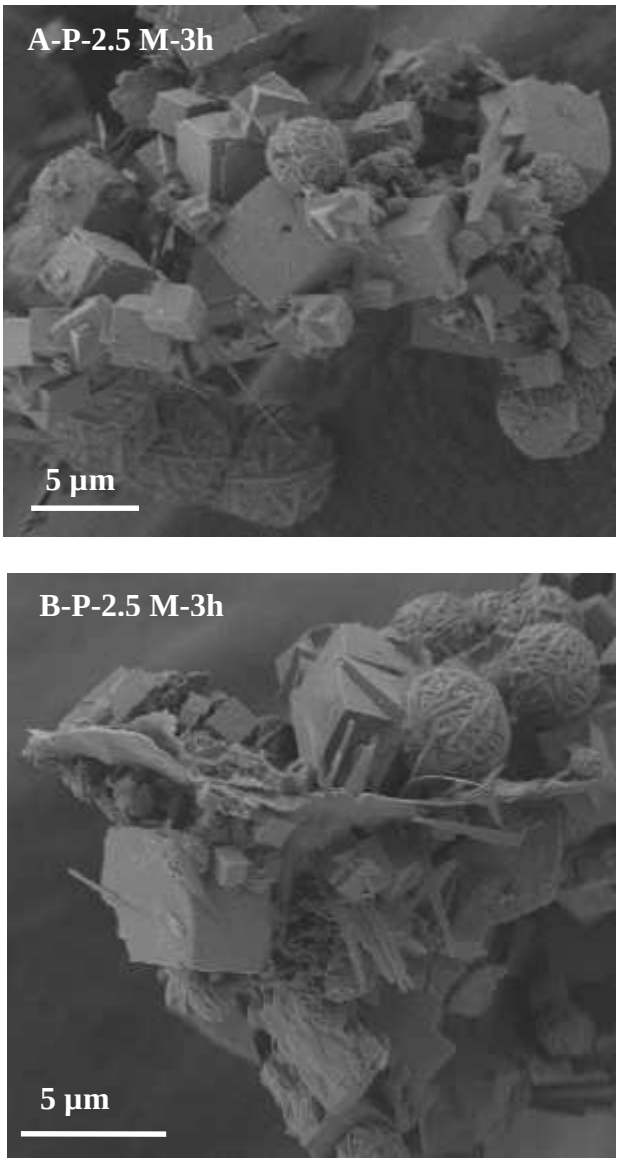

Figure 22: SEM image for 2.5 M NaOH treated metakaolin of A and B type kaolins

The percentage of crystallinity (% C_{XRD}) of the synthesized zeolite A was calculated by comparing the sum of peak intensity of the most five intensive peaks of the synthesized zeolite A (d_{442} at 21.67°, d_{622} at 23.99°, d_{642} at 27.11°, d_{820} at 29.94° and d_{664} at 34.18°) and the commercial zeolite A (SZA) using the following equation[111]:

$$\text{Crystallinity } (\%C_{XRD}) = \frac{\Sigma \text{ Intensity of 5 most intense peaks of product}}{\Sigma \text{ Intensity of 5 most intense peaks of standard}} \times 100$$

Based on this equation, the percent crystallinity of the synthesized zeolite at different concentration of NaOH collected in Table 6. The table shows that the percent crystallinity of synthetic zeolite A increased with increasing the concentration of the base (NaOH) from 2.5 M to 3.5 M and started decreasing beyond 4 M concentration in both 3 and 6 h crystallization times. At higher concentration of the base (6M), the percent crystallinity decreased to < 50 %, particularly for kaolin B based product. This could be due to the formation of other phases other than crystals of zeolite A. From the table it is possible to see that, this situation is more or less similar for both types of kaolin based zeolite products. Further increment of alkalinity, i.e. 3.5, 4 and 6 M does not yield any improvement in the crystallinity of the synthetic products. Hence the optimum concentration of the base in this particular study is 3 M. The molar gel composition for the 3 M NaOH synthetic product is:

$Na_2O: Al_2O_3: 2SiO_2: 37H_2O$

Table 6: The percent crystallinity of synthesized zeolite A

Zeolite A	% C_{XRD}
SZA	100
P-A-2.5M-3h	64
P-A-2.5M-6h	65
P-A-3M-3 h	72
P-A-3M-6 h	71
P-A-3.5M-3 h	65
R-A-3M-3 h	62
P-A-4M-3 h	66
P-A-4M-6 h	63
P-A-6M-3 h	52
P-B-2.5M-3 h	66
P-B-2.5M-6 h	63
P-B-3M-3 h	68
P-B-3M-6 h	68
P-B-3.5M-3 h	62
R-B-3M-3 h	64
P-B-4M-3 h	63
P-B-4M-6 h	66
P-B-6M-3 h	48

From Table 6 it is possible to see that the percent crystallinity (C_{XRD}) obtained with 3 M concentration of NaOH is better than the other concentration of base used in this study. This is further justified by the SEM micrographic analysis results (Figure 23). The SEM

micrograph of kaolin A based synthetic product (P-A-3M-3h) analysis indicates that, cubic shape with rounded edge of crystal of zeolite A having average crystal size of 3.0 µm is obtained, which is in a good agreement with the SEM of commercial zeolite A. This particular morphology and particle size of zeolite A is suitable for the particular application as a detergent builder. Whereas, the SEM micrographic analysis of synthetic product from kaolin B (P-B-3M-3h) indicated the formation of more heterogeneous cubic shaped crystals of zeolite A with sharp edges having an average particle size of 4.0 µm. The zeolite A crystal morphology and particle size difference observed in these two different synthetic products could be a good justification for the difference in composition among the two different kaolins. This result is in a good agreement with the report of Kosanovic et al.[112], which stated that the morphological characteristics of the crystallized zeolite A depend on the combined actions of alkalinity and content of silicon and aluminum in the reaction mixture (expressed by the batch molar ratio y = [SiO_2/Al_2O_3]). Crystal size is also known to be determined by the alkalinity of the system.

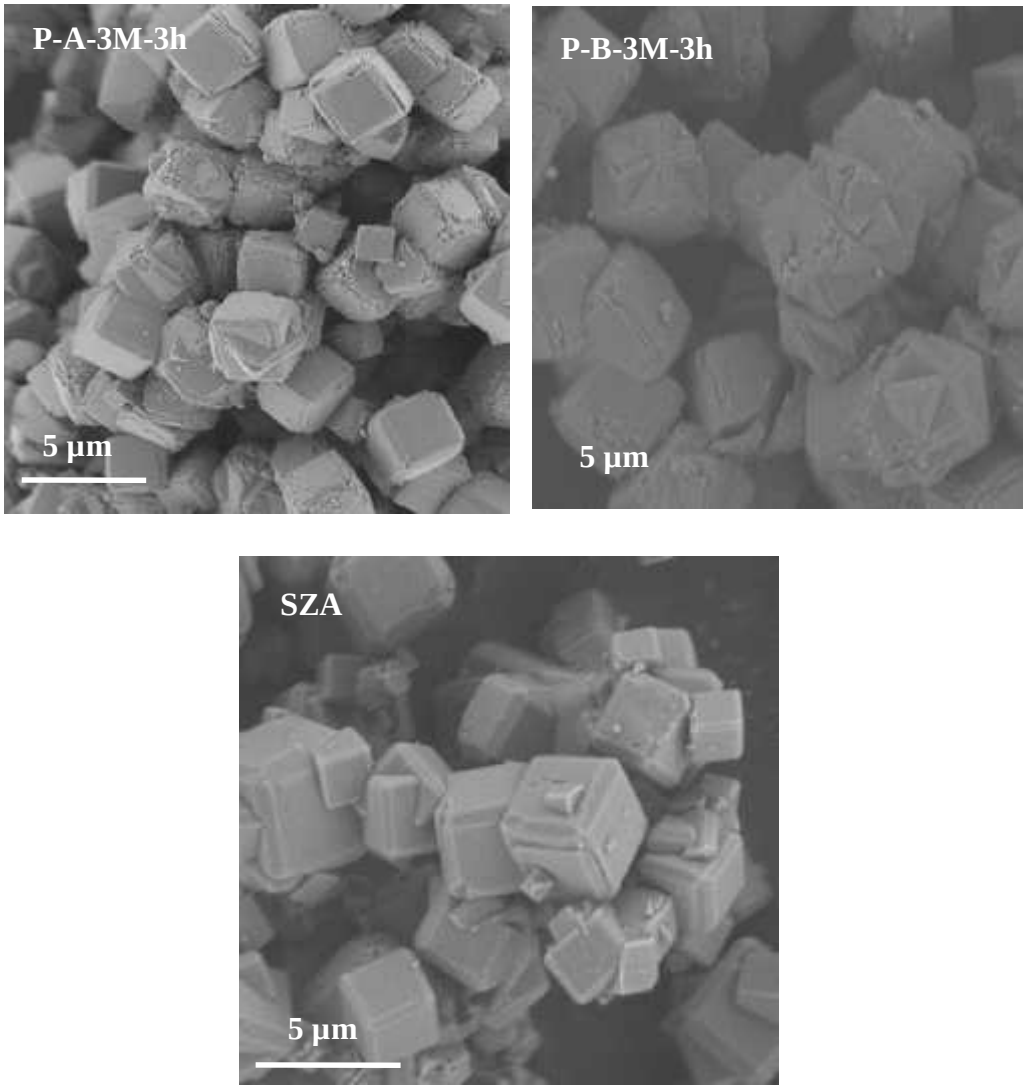

Figure 23: SEM images for 3 M NaOH synthesised zeolite A from kaolin A and B, and compared with commercial zeolite A (SZA)

The ICP-OES elemental analysis result of 3 M NaOH and 3 h crystallization time for the purified kaolin based zeolite A collected in Table 7 shows a Si/Al = 1.1, which is in a good agreement with the Si/Al ratio of commercial zeolite A (SZA). These properties announce the synthetic products could be promising candidates for detergent application

as a detergent builder. Detergent-grade zeolites are characterized by high aluminum content in which a Si/Al ratio of 1 or virtually 1 is achieved. This in turn results in a maximum content of sodium ions which can easily be exchanged for calcium ions, and sometimes other ions which are responsible for water hardness[113]. This is well confirmed by the Na/Al ratio of the synthetic zeolites in Table 7 which indicates the high content of sodium in the synthetic products and verified the zeolite is sodium form zeolite.

Table 7: ICP-OES elemental analysis result of 3M-3h reaction product and commercial zeolite A (SZA)

Zeolite A	**SiO_2**	**Al_2O_3**	**Na_2O**	**Fe_2O_3**	**Si/Al**	**Na/Al**
SZA	33	28.0	17.4	0.02	1.0	1.0
P-A-3M-3h	33.3	26.2	15.4	1.6	1.1	1.0
P-B-3M-3h	29.5	24.0	15.5	1.3	1.1	1.0

Regarding the thermal behavior of the synthetic zeolites made under the conditions of 3 M NaOH and 3 h crystallization time, the thermogravimetric (TGA) result indicates the stability of zeolite A. The graph (Figure 24) depicts loss of water of hydration of about 20% up to 400 ^{o}C and remained stable after this temperature for both types of synthetic zeolites, similar to the commercial zeolite A (SZA). This is an intended property of zeolite A for using it as a builder in detergent and or as adsorbent, since it is typically sold in a hydrate form wherein the weight of the hydrate zeolite is approximately 20-22% water[114].

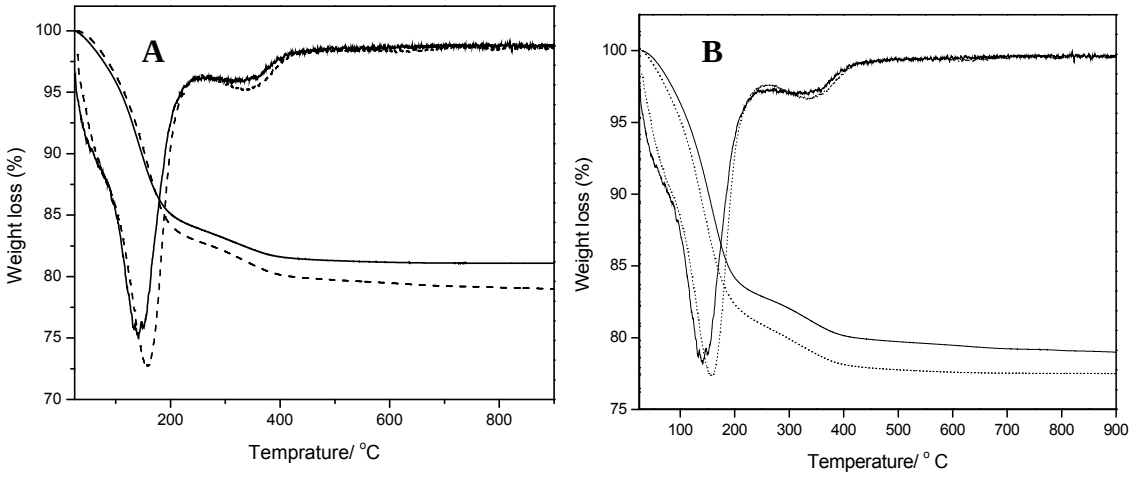

Figure 24: Thermogravimetric analysis (TGA/DTG) of synthetic zeolite A from A and B kaolins(solid line) synthesized using conventional hydrothermal synthesis and compared with commercial zeolite A (dotted line)

As shown in table 6, the concentration of base beyond 3 M could not bring better crystals of zeolite A, rather decreament in the crystallinity was obtained. This was justified by the XRD profile and SEM morphology analysis of 4 M NaOH based synthetic products. The XRD pattern depicted in Figure 25 indicated the presence of weak peaks of cancrinite (CAN) and sodalite (SOD) which could be an indication for the starting of the conversion of the metastable zeolite A to the these phases. Cancrinite and sodalite are known by having a common characterstic peaks at 2θ (°) value of 14.1 and 25.5. The peak at 2θ (°) of 31.9 corresponds to cancrinite phase[110]. This scenario was observed for both kaolins based synthetic products. The result obtained is in a good accord with Buhl et al.[115] study of the transformation of kaolinite to cancrinite. Their study result indicates the full conversion was attained under highly alkaline conditions.

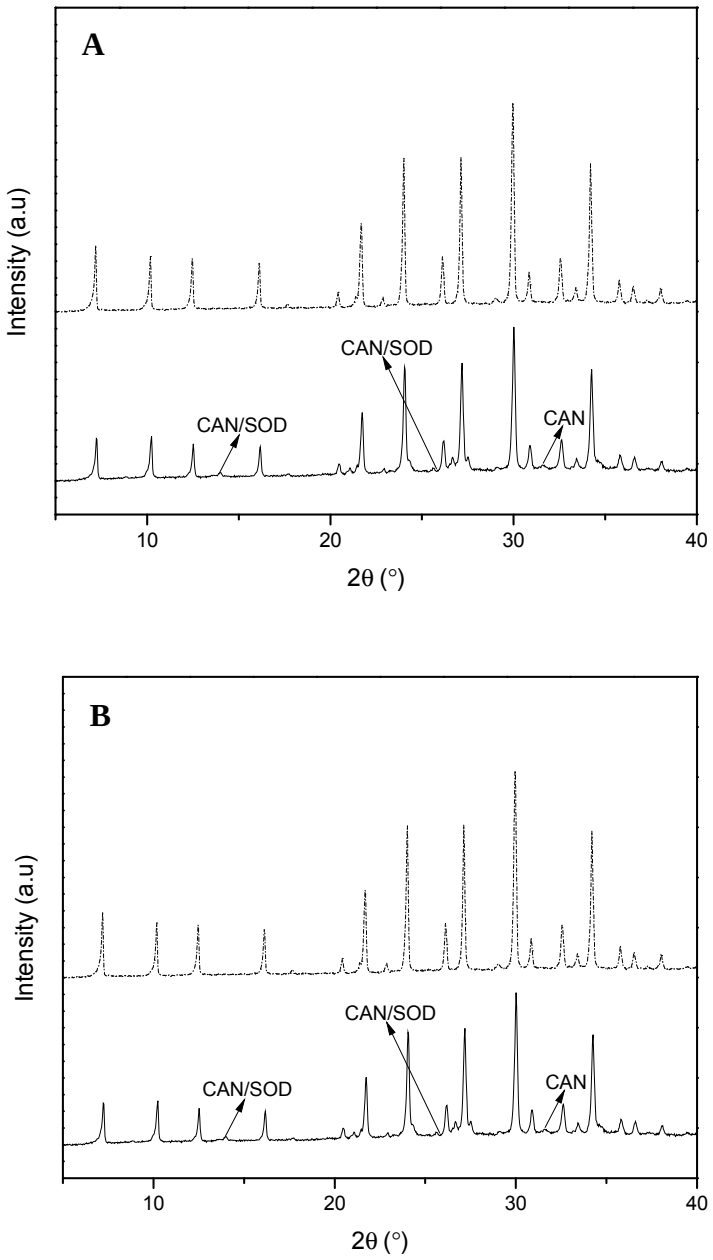

Figure 25: XRD pattern of reaction products at 4 M NaOH concentration using purified kaolin A and B, and compared to the commercial zeolite A (SZA)

The SEM micrographic analysis for this particular concentration (4 M) synthetic products (Figure 26) indicates the loss in the characterstic morphology of zeolite and paving the

way for the formation of lephispheric morphology of cancrinite or sodalite associated to a cubic crystal of zeolite A.

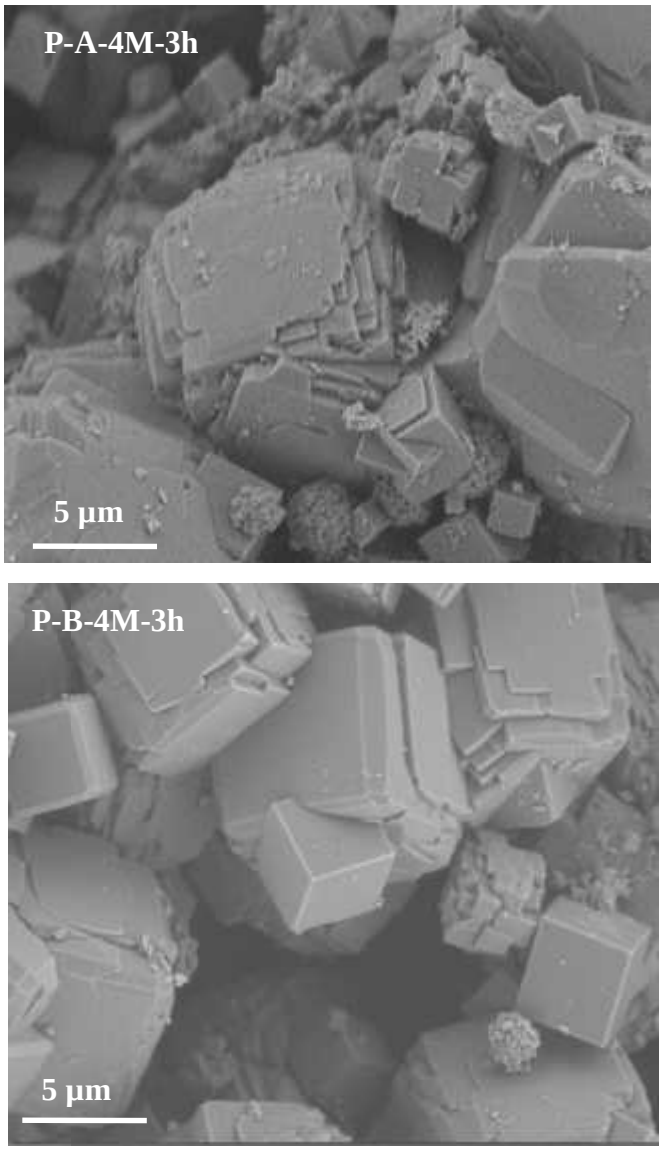

Figure 26: SEM images for 4 M NaOH synthesised zeolite A from purified A and B kaolins

Parallel to the variation of the alkalin concentration, we can also observe the effect of prolonged crystallization time from 3 to 6 h. The XRD profiles (Figure 27) show that

further crystallization time to 6 h produced the characterstic peaks of sodalite phase, which is an indication of the partial transformation of zeolite A to the more thermodynamically stable sodalite phase for both kaolin based synthetic products. Nevertheless, the characteristic peak of quartz at about 26.6º is still observed either at 3 or 6 h reaction time. Similar conversion trend was reported by Novembre et al.[116] during the hydrothermal synthesis of Na zeolites (Na-A, Na-Xand Na-P) and hydroxysodalite using kaolinite. Their study showed the transformation of the Na zeolites to sodalite phase after 8 h of crystallization time. Kwakye-Awuah et al.[117]also observed similar change in their study of the effect of crystallization time on the hydrothermal synthesis of zeolites from kaolin and bauxite. The study result indicated that longer crystallization time resulted in phase change of the zeolites into sodalite. Hence, further study in this work was continued with 3 h of crystallization time.

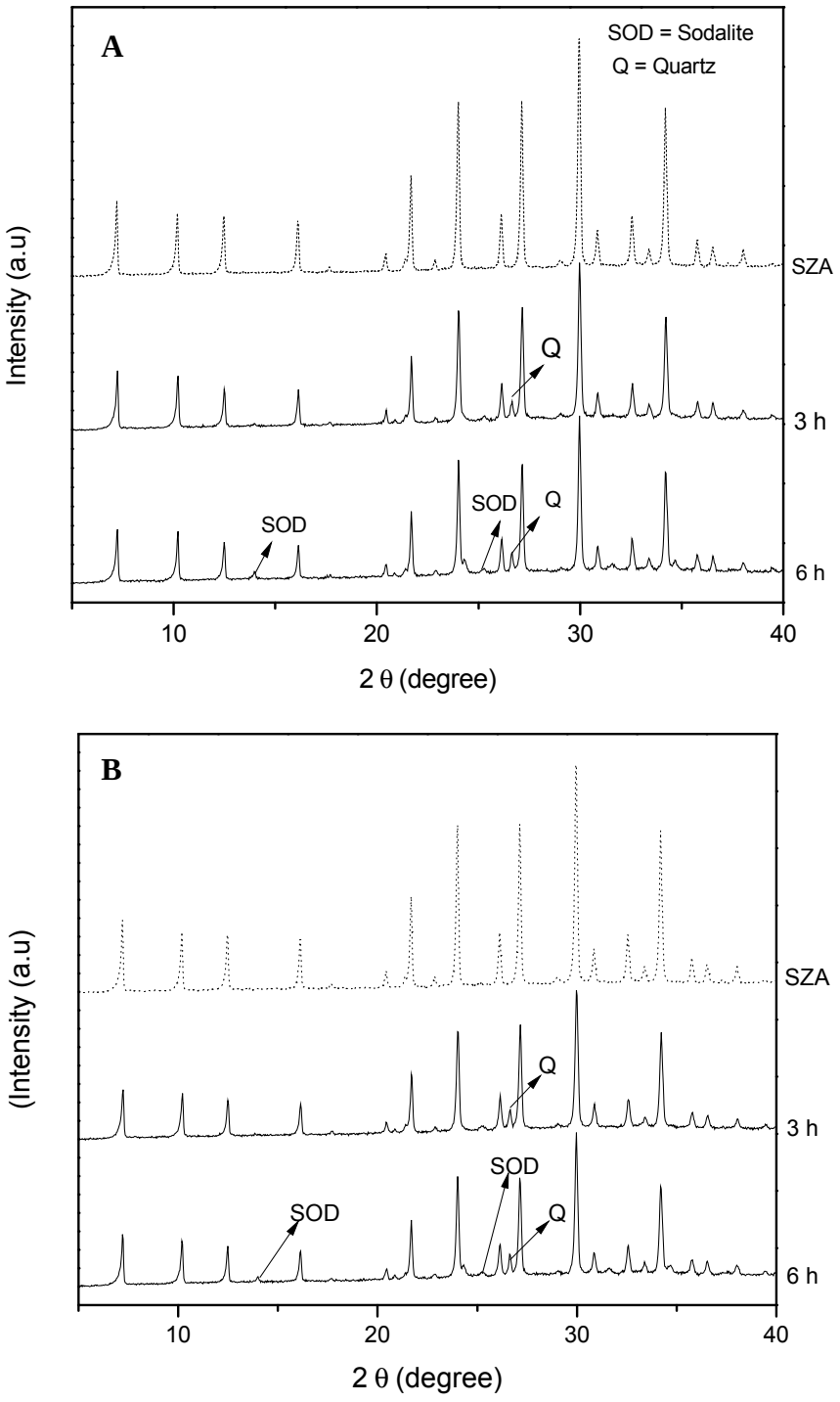

Figure 27: XRD pattern of 3 and 6 h synthesized zeolite A from A and B kaolins and compared with commercial zeolite A (dotted line)

To evaluate the importance of the physical purification of the raw kaolin on the crystallinity of the synthetic products, we have repeated the synthesis with 3 M NaOH at the synthesis condition of 100 ^{o}C/3 h in the absence of any purification processes, using the raw kaolins. The XRD profile analysis result in Figure 55 (Appendices) indicated that the percentage crystallinity (C_{XRD}) decreases for the A kaolin from 72 to 63% and for B type it decreases from 68 to 64% (Table 6). This is due to the presence of impurities like quartz, mica and other phases in the raw kaolin that suppressed the crystallinity of zeolite A. These results reveal the importance of kaolin purification for the conventional hydrothermal synthesis method.

The synthesis with optimized NaOH concentration was also carried out using the kaolin chemically treated (1 M HCl) resulting in a crystallinity which is comparable with the physically treated kaolin Figure 56 (Appendices). The percent crystallinity (% C_{XRD}) of zeolite A obtained under similar synthesis conditions is 79% for A-3M-3 h and 73% for B-3M-3h, which is not significantly different from the crystallinity of the synthetic products made with physically purified kaolins. Hence the chemical treatment was discharged since physical methods are less environmentally harmful.

Finally, the synthesis with low crystallization temperature (80 ^{o}C) has conducted. This was done with the optimum concentration of the base, 3M NaOH and optimum crystallization time (3 h) using both A and B purified kaolins. The XRD profile result demonstrated in Figure 28 shows at crystallization temperature of 80 ^{o}C, low intensity peaks of zeolite A are obsereved. This remarked the starting of the formation of zeolite A. However, high crystallites zeolite A was obtained at the crystallization temperature of 100 ^{o}C. Similar result was reported by A. S. Kovo[118] for the study of the effect of

temperature on the synthesis of zeolite X from Ahoko Nigerian kaolin using novel metakaolinization technique. The study result showed zeolite formation increases with increase in crystallization temperature from 80 to 100 ^{o}C as evident from the increase in the intensity of diffraction peaks. Hence further synthesis in this work is continued with the crystallization temperature of 100 ^{o}C.

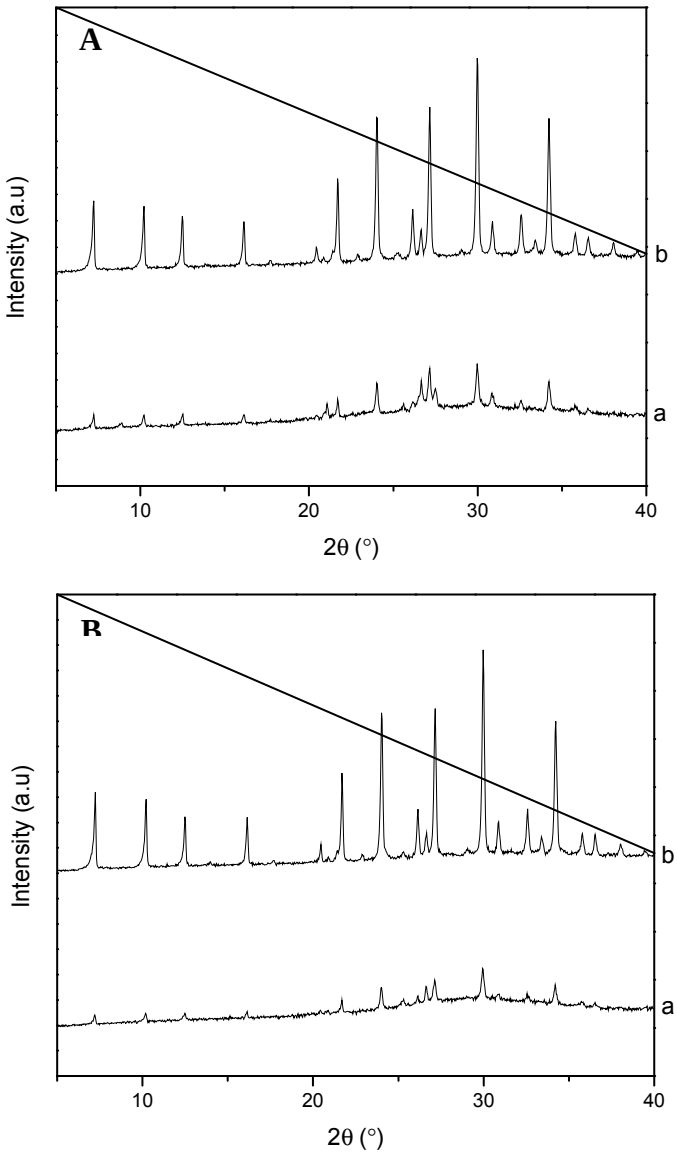

Figure 28: XRD profile of synthetic zeolite A from A and B kaolins at crystallization temperature: (a) 80 ^{o}C and (b) 100 ^{o}C

4.3.3. Effect of gel temperature and aging time

The effect of gel formation temperature and time have been studied in order to fully dissolve the reaction mixture and to make it part of the synthetic products. Doing so, two steps are differentiated. The first one refers to the homogenization of the reaction mixture using magnetic agitation at room temperature (RT) and 50 °C, and the second one involves the aging of the gel for certain period of time under static condition. These two processes were tested for both raw (R) and purified (P) kaolin at 3 M concentration of NaOH, followed by crystallization at 100 ºC for 3 h. Table 8 shows the relative percent crystallinity (% C_{XRD}) calculated from the XRD profiles for the R-3M and P-3M series at RT and 50 °C age formation conditions followed by different aging time (Figure 57, Appendices).

Table 8: Percent crystallinity (C_{XRD}) of zeolite A synthesized from raw (R) and purified (P) A and B type kaolin under different aging times (G)

Zeolite A	Aging time(h)	% C_{XRD}	
	in static	RT	50 °C
R-A-3M-0G-3h	0	72	78
R-A-3M-1G-3h	1	69	79
R-A-3M-3G-3h	3	74	80
R-A-3M-6G-3h	6	78	83
R-A-3M-12G-3h	12	76	76
R-A-3M-24G-3h	24	71	76
P-A-3M-0G-3h	0	76	81
P-A-3M-1G-3h	1	75	82
P-A-3M-3G-3h	3	82	88
P-A-3M-6G-3h	6	84	88
P-A-3M-12G-3h	12	82	85
P-A-3M-24G-3h	24	81	84
R-B-3M-0G-3h	0	62	69
R-B-3M-1G-3h	1	64	66
R-B-3M-3G-3h	3	68	69
R-B-3M-6G-3h	6	68	73
R-B-3M-12G-3h	12	70	70
R-B-3M-24G-3h	24	71	70
P-B-3M-0G-3h	0	61	72
P-B-3M-1G-3h	1	68	75
P-B-3M-3G-3h	3	71	74
P-B-3M-6G-3h	6	76	74
P-B-3M-12G-3h	12	74	75
P-B-3M-24G-3h	24	79	73

The gel formed at 50 °C resulted in better crystallinity compared to that of prepared at RT in all range of synthesis conditions, probably due to the complete dissolution of the metakaolin. Thus, the concentration of dissolved silicate and aluminates ions in the solution increased and reached its critical concentration for the nucleation and facilitated the formation of zeolite A of high crystallinity[119].

The effect of gel aging with time (0, 1, 3, 6, 12 and 24 h) under static condition was also studied for both Raw and Purified A and B kaolins. This is because during aging period, both silica and alumina were completely dissolved into solution and reacted with each other to form some preliminary building blocks. Thus aluminosilicate gel is expected to reorganize chemically and structurally to form the zeolite structure during aging[41]. Based on this, from the table it is possible to see that increament in crystallinity with aging is observed for purified kaolin based synthetic products. In Table 8 the same study in the synthesis with raw kaolin (R series) indicated better crystallinity upon aging compared with the crystallinity result of non aged reaction product (Table 6). Furthermore, the synthesis of zeolite A using the purified kaolin showed better percentage of crystallinity in all synthesis conditions. Therefore purification of the kaolin and removal of some impurities plays a major role on the crystallinity of synthesized zeolite A. However, excessive aging time would result in further dissolution of crystals which will lead to a decrease of the relative crystallinity in all types of synthetic products.

For A type kaolin based synthetic products, the synthesis using the purified kaolin, gel formation at 50 °C and aging the reaction gel for 3 h followed by 3 h crystallization resulted in an optimum crystallinity of about 90%. Whereas, for B type kaolin based synthetic zeolite A, the synthesis using the purified kaolin, gel formation at 50 °C and 1 h

aging followed by 3 h crystallization resulted an optimum percent crystallinity of 75% for B type kaolin. This different result attained from the two different kaolin sources could notice us the same raw materials but from different sources requires different optimization of synthesis parameters. Moreover, for B type kaolin, the percentage of kaolinite in the starting materials is lower (55%) compared to the A type kaolin (77%).

The size and morphology of zeolite particles attained under gel aging was assessed by SEM. The SEM micrographic analysis (Figure 29) for purified A type kaolin based synthetic products, shows the formation of cubic crystal of zeolite A with different particle sizes and homogeneity with different aging time. The first (0 h) aging time product (A-0G) exhibited an average particle size of 4.0 μm with the morphology of cubic edges intergrown crystals. With the 1 h aging product (A-1G), the average particle size of zeolite A crystals decrease to 3.0 μm and the crystals get better homogeneity compared to the 0 h aging product. With the best time of aging product (A-3G) the crystals gets the highest homogeneity as well as smaller in size to the average particle size of 2.0 μm. Moreover in this particular product the number of crystals of zeolite A are larger and have better uniformity compared to the other aging time products. The homogeneity and number of crystals of zeolite A seems to decrease in 6 h aging product (A-6G). Apart from the minor difference observed in different hours of aging time, all the SEM images display a cubic morphology with varying expression of facets and surface terrace, and occasionally intergrown crystals indicating a continuous crystallization process through the whole range of time and generation of crystals of zeolite A with different size during the hydrothermal reaction.

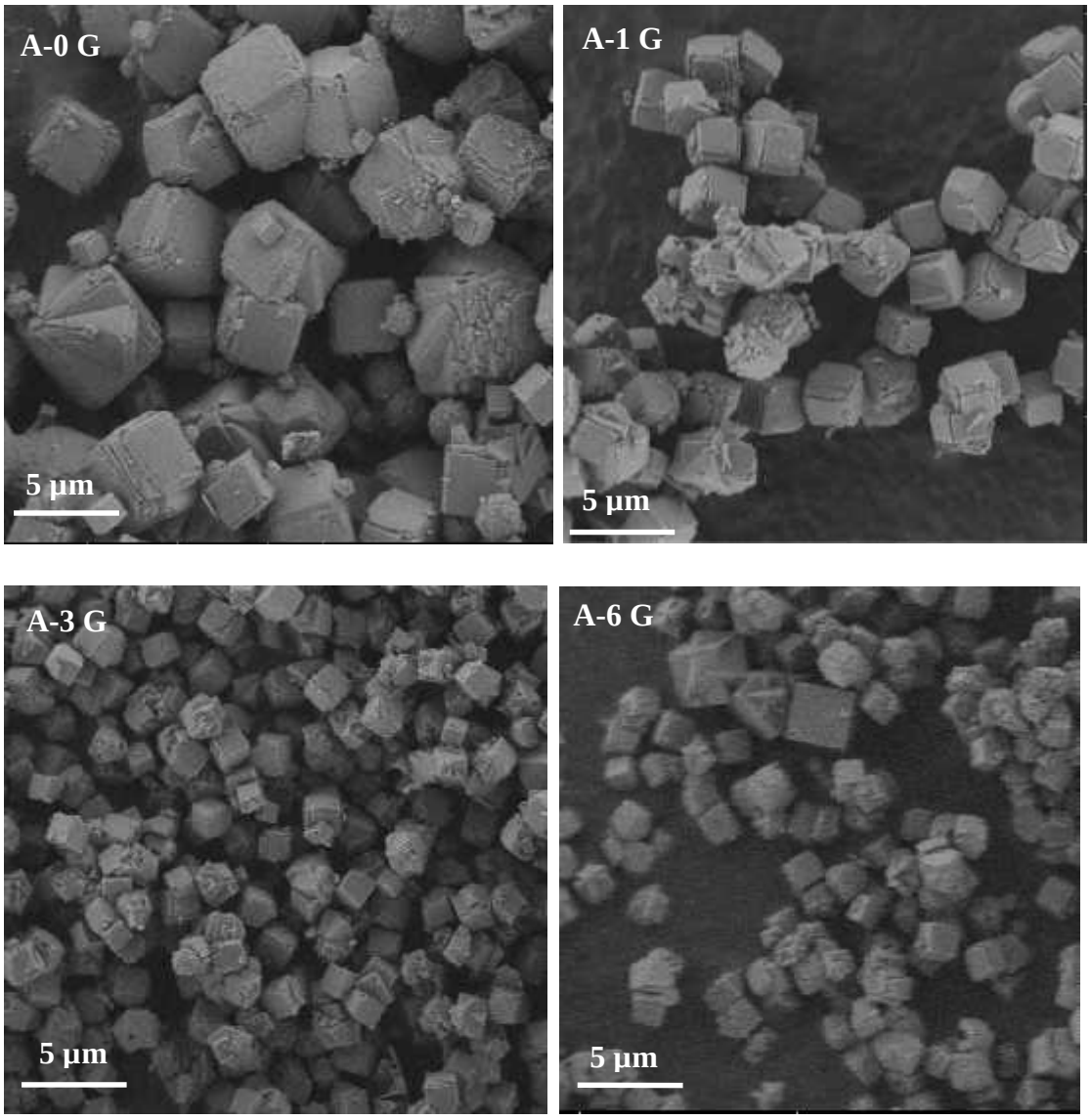

Figure 29: SEM images for A-P-3M-3h series under different aging time (G) 50 °C

The morphological analysis result obtained for the synthetic products based on kaolin B are collected in Figure 30. There is a remarkable difference in crystal size and homogeneity among the synthetic products from the two kaolin sources. For the B kaolin based zeolite A, in all ranges of aging time almost similar particle size and morphology are observed. For instance the average particle size of crystals of zeolite A obtained from 0 h and 1 h aging (B-0G and B-1G) is 3.5 µm. Moreover they exhibited almost similar

particles morphology of intergrowing crystals. As going to the higher aging time (B-6G) the decreament in the average particle size looks insignificant (3.0 μm). Moreover, at the higher aging time (6 G) agglomerated particles with perfectly sharp edge are formed. The considerable morphological difference with the analogous synthetic zeolite A from A type kaolin (Figure 29) could be mentioned to the difference in composition that exists between the two kaolin sources.

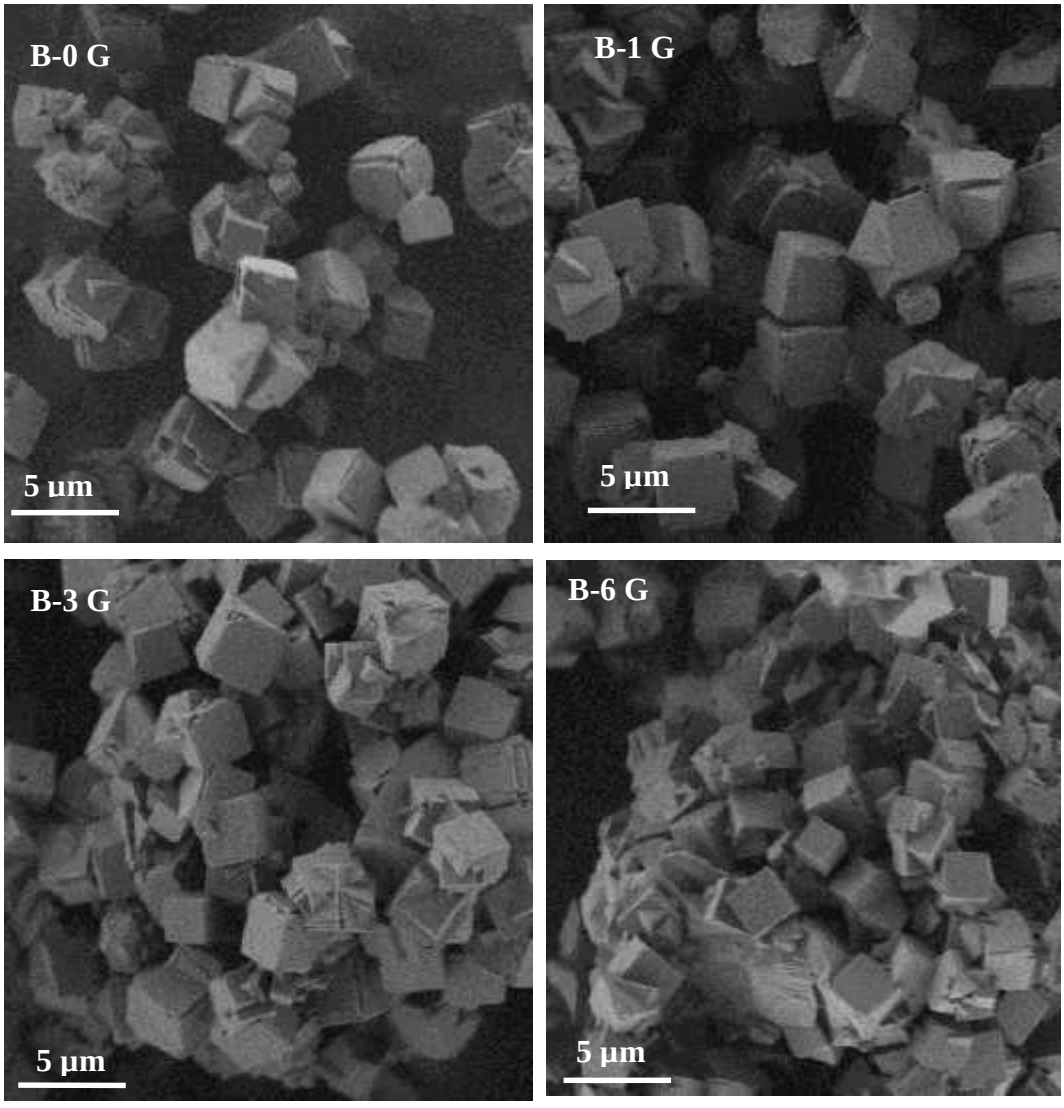

Figure 30: SEM images for B-P-3M-3h series under different aging time (G) at 50 °C

In general, from the SEM image analysis (both Figure 29 and 30), it is possible to see that as the aging time increased the average particle size decreased for both A and B kaolin based zeolite A. This could be as the aging time increasing, the number of nuclei increases against crystal growth. As more nuclei are present, the reagent mass is distributed among more crystals, resulting in smaller crystals on average[120]. Our result is in good agreement with Alfaro et al.[121] who reported the longer aging time of the reaction gel resulted in smaller crystal size of zeolite A compared with the one that is aged for shorter time. Moreover, the crystals are uniform in size compared to the one synthesized without gel aging (Figure 23). Hence, this result indicated that aging time is found to be a crucial factor for the control of the crystal size of zeolite A produced. The ICP-OES elemental analysis result collected in Table 9 for all products under the above mentioned conditions is in a good agreement with the commercial zeolite A.

Table 9: ICP-OES elemental analysis results of zeolite A synthesized under different aging conditions for A and B purified kaolins (wt%)

Zeolite A	**SiO_2**	**Al_2O_3**	**Na_2O**	**Fe_2O_3**	**Si/Al**	**Na/Al**
SZA	33	28.0	17.4	0.02	1.0	1.0
P-A-3M-0G-3h	28.3	24.3	14.0	0.8	1.0	0.9
P-A-3M-1G-3h	30.5	25.3	14.6	1.0	1.0	0.9
P-A-3M-3G-3h	29.4	24.4	13.4	0.9	1.0	0.9
P-A-3M-6G-3h	25.3	24.4	13.9	1.0	1.0	0.9
P-B-3M-0G-3h	31.6	24.8	13.3	0.7	1.1	0.9
P-B-3M-1G-3h	31.3	23.9	13.8	0.7	1.1	0.9
P-B-3M-3G-3h	32.3	25.4	13.5	0.8	1.1	0.9
P-B-3M-6G-3h	32.0	24.4	13.0	0.8	1.1	0.9

From Table 7 it is possible to see that the Si/Al = 1.1 for the particular synthetic product P-A-3M-3h, whereas from Table 9 the Si/Al = 1 for all aging time. This could be due to the dissolving of silica from quartz during aging time and its incorporation in the zeolite A products. This is justified by the decrements in the mass percentage of SiO_2 in the P-A-3M-3h from 33.3 to 25.3% in P-A-3M-1G-3h. This tendency was not observed for the analogous P-B-3M-1G-3h based zeolite A probably due to the different silica composition in the different kaolins sources. Another interesting tendency observed in zeolite A from both types of kaolin is that, after aging, the weight percent composition of Fe_2O_3 became < 1% (Table 9): This could be due to the dissolution in the reaction mixture that could solubilize some of the iron content allowing its removal during washing. It can also be noted from the table, the ratio (Na/Al = 0.9) for all ranges of the gel aged products. The result well confirmed that the synthetic products are mainly sodium ffrrform zeolite A.

4.3.4. Effect of crystallization time

Once the gel temperature and aging time effects were surveyed, a final study was carried out to evaluate the significance of the crystallization time on the crystallinity and overall morphology of zeolite A. Samples were taken at ½ h increments of the gel mixture throughout the 3 h reaction period. The percent crystallinity obtained at different reaction time is depicted in Figure 31. In the early stages of the reaction, the rate of the formation of the zeolite was so slow that percent crystallinity (C_{XRD}) of the reaction product at ½ h is less than 50% for both types of kaolin based synthetic zeolite A. In the first hour, the reaction product exhibited high yield nearly equal to the crystallinity of the best reaction time (3h). Following the first hour of the reaction, the crystallinity of zeolite A slightly

goes down and increasing again at 3 h of crystallization time. This could be due to the competing growth of other phases, although no further investigation in this regard has been pursued in this wok. From the graph it is possible to see that, throughout the crystallization period, zeolite A synthesized from kaolin of A type showed better crystallinity compared to kaolin B based zeolite A.

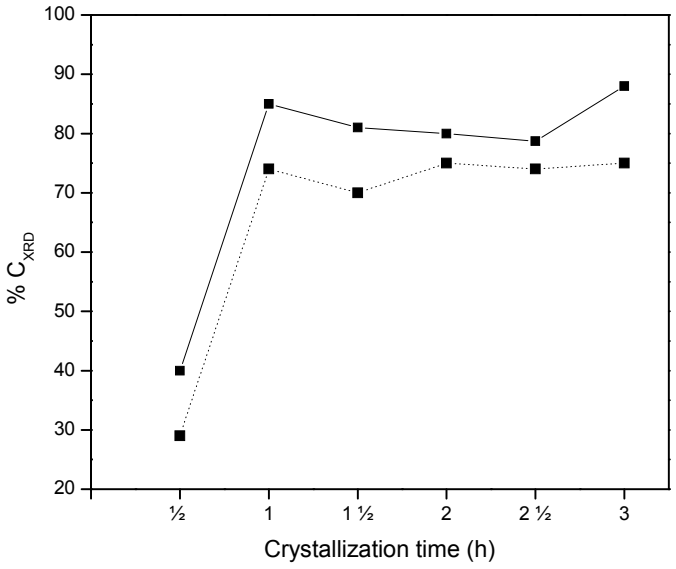

Figure 31: Relative crystallinity (% C_{XRD}) of zeolite A from A kaolin (solid line) and B kaolin (dotted line) versus crystallization time

SEM micrographs (Figure 32) also support the result from the XRD analysis for A type based products. The observations indicated that ½ h synthetic product consist of aggregated amorphous aluminosilicate gel with some cubic crystals of zeolite A. The full cubic morphology of zeolite A started to be observed following 1 h of crystallization time. After 1 h reaction time, a cubic morphology with rounded edge with average

particle size ranging from 2 to 3.0 μm formed. This indicates there is continuous crystallization process through the whole range of time. It also indicated the linear crystal size increments with the crystallization time. The effect of crystallization time on the crystallinity was also better evidenced by the phase composition analysis study. The phase composition of the synthesized zeolite A was quantified for A type kaolin based zeolite A using X-pert high score software (Table 10). The analysis result indicated that the reaction product of the ½ h reaction time is composed of relatively high amount of amorphous aluminosilicate gel compared to the other crystallites sample. However, the crystallite samples showed the presence of amorphous sodium aluminosilicate gel except the 3 h crystallite product.

Table 10: X-pert highscore software analysis result of different crystallization time products.

Sample	Compound	Score (%)
A-P-3M-3G-½h	Zeolite A, NaAlSi	68, 28
A-P-3M-3G-1h	Zeolite A, NaAlSi	77, 19
A-P-3M-3G-1½h	Zeolite A, NaAlSi	79,17
A-P-3M-3G-2h	Zeolite A, NaAlSi	80, 13
A-P-3M-3G-2½h	Zeolite A, NaAlSi	89, 9
A-P-3M-3G-3h	Zeolite A	92, 6

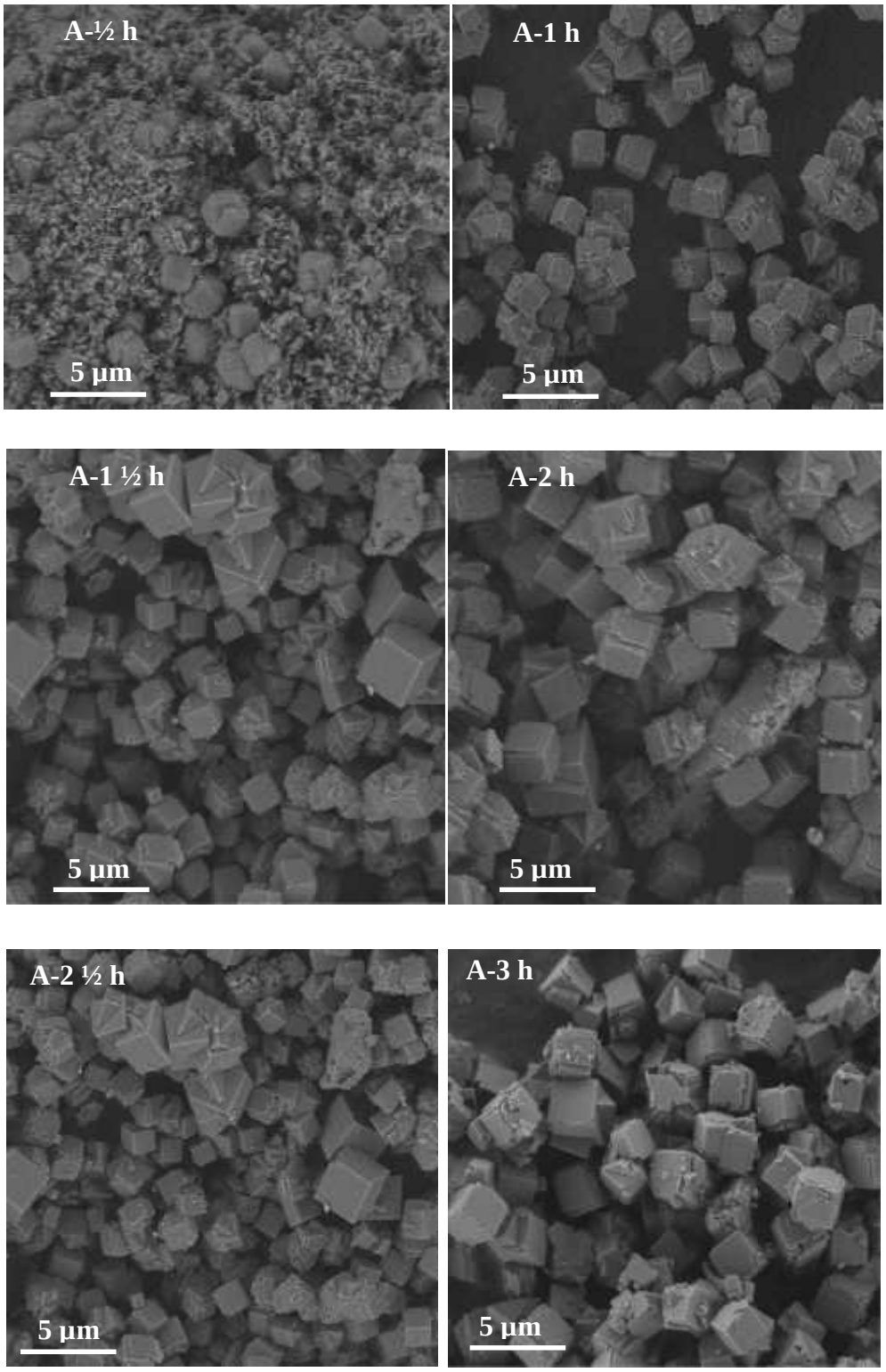

Figure 32: SEM images for A-P-3M-3G-3h series at different crystallization time

Similar to the synthetic products based on A kaolin type, SEM micrographs (Figure 33) analysis of synthetic products from B type kaolin also support the result from the XRD analysis (Figure 31). The slight morphology and particle size difference that is observed in the gel aged synthetic products is also seen while studying the effect of crystallization time. The first ½ h reaction product (B-½ h) is composed of the mixture of amorphous metakaolin and cubic crystals having rounded morphology of zeolite A. Following 1 h reaction time (B-1 h), cubic crystals of zeolite A having cubic shape with sharp edge and average particle size of 3.0 µm is obtained. This is true for both synthetic products at crystallization time of 1½ and 2 h. Slightly rounded edge zeolite A crystals are formed at 2½ h crystallization time. Similar to the synthetic products from A type kaolin, the uniformity in particle size distribution and better morphology of crystals of zeolite A is attained at the optimum crystallization time of 3 h (B-3 h). In all crystallization time, the particle size of zeolite A obtained from B kaolin are systematically larger than those of A type kaolin based products. This may be due to the less content of kaolinite, source of Si and Al, in B kaolin that could faster the nucleation and facilitate for the growing of larger crystal of zeolite A.

In general, from the XRD and SEM micrographic analyses results, the study conducted confirmed that 3 h crystallization time is the optimum crystallization time for both type of kaolin based synthesis.

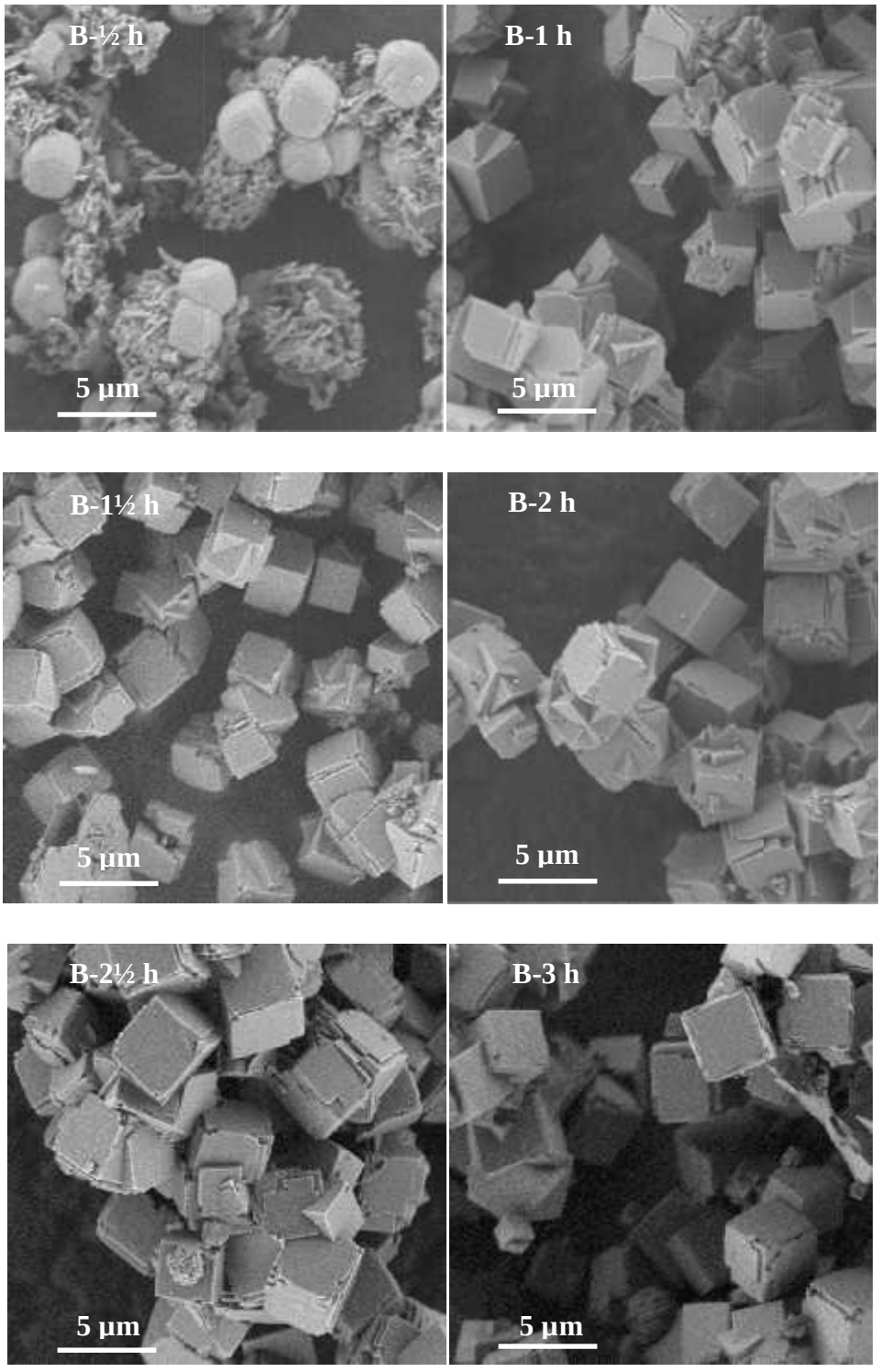

Figure 33: SEM images for P-3M-1G-3h series at different crystallization time

Calcium and magnesium exchange/binding capacity is the most essential criterion to decide the cleaning action of any detergent builder. A builder material possessing higher cation exchange capacity is supposed to excel in water softening, which ultimately results in foaming, thus reducing surface tension between dirt particles and fabric[122]. Hence, the main requirement used for the application of zeolite A in detergent formulation is its cation exchange capacity. The theoretical calcium binding capacity of zeolite A is 352 mg $CaCO_3$/g anhydrous zeolite A or 5.48 meq/g of Ca^{2+} anhydrous zeolite A. Owing to the presence of other competing ions like sodium ions, in the practical detergency washing situation, this level of calcium removal is not achieved[29]. In this study, the calcium removal capacity expressed in mg $CaCO_3$ per gram of anhydrous zeolite A from the solution having a hardness of 500 mg/L $CaCO_3$ is measured and reported. Prior to the CEC measurements of the synthesized zeolite A materials, we have tested the calcium removal capacity of the starting kaolins. The result indicated that the kaolin samples including the commercial sample did not show any calcium removal capacity. This is due to the very low theoretical cation exchange capacity of kaolin (0.001–0.15 meq/g)[72]. It is commonly believed that since permanent negative charge from isomorphous substitution of Al^{3+} for Si^{4+} is insignificant in kaolin, cation exchange occurs due to the broken bonds around the crystal edges, the substitutions within the lattice, and the hydrogen of exposed surface hydroxyls that may be exchanged. Therefore, this indicated the importance of the treatment of the kaolin to use it for such application. The obtained calcium binding capacity results of the synthetic zeolite A from both raw and purified A and B kaolins and the commercial zeolite A are summarized in the Table 11.

Table 11: Calcium exchanged capacity of synthetic zeolite A compared with commercial zeolite A (SZA)

Zeolite A	Calcium removed		Zeolite A	Calcium removed	
	mg $CaCO_3$/g	meqCa^{2+}/g		mg $CaCO_3$/g	meqCa^{2+}/g
SZA	320	5.0			
R-A-3M-3h*	150	2.3	R-B-3M-3h*	160	2.5
R-A-3M-0G-3h	150	2.3	R-B-3M-0G-3h	175	2.7
RA-3M-1G-3h	260	4.0	R-B-3M-1G-3h	230	3.6
R-A-3M-3G-3h	290	4.5	R-B-3M-3G-3h	210	3.3
R-A-3M-6G-3h	290	4.5	R-B-3M-6G-3h	230	3.6
R-A-3M-12G-3h	280	4.4	R-B-3M-12G-3h	220	3.4
R-A-3M-24G-3h	250	3.9	R-B-3M-24G-3h	210	3.3
P-A-3M-3h*	280	4.4	P-B-3M-3h*	190	3.0
P-A-3M-0G-3h	260	4.0	P-B-3M-0G-3h	230	3.5
P-A-3M-1G-3h	240	3.7	P-B-3M-1G-3h	250	3.9
P-A-3M-3G- ½h	170	2.6	P-B-3M-3G- ½h	160	2.5
P-A-3M-3G-1h	220	3.4	P-B-3M-3G-1h	220	3.4
P-A-3M-3G-1 ½h	220	3.4	P-B-3M-3G-1½h	230	3.5
P-A-3M-3G-2h	260	4.0	P-B-3M-3G-2h	220	3.4
P-A-3M-3G-2 ½h	290	4.5	P-B-3M-3G-2½h	225	3.5
P-A-3M-3G-3h	295	4.6	P-B-3M-3G-3h	230	3.5
P-A-3M-6G-3h	290	4.5	P-B-3M-6G-3h	240	3.7
P-A-3M-12G-3h	290	4.5	P-B-3M-12G-3h	232	3.6
P-A-3M-24G-3h	240	3.7	P-B-3M-24G-3h	210	3.3

***** stands for zeolite A made without gel treatment

From the table it is possible to see that the CEC of almost all the synthetic zeolites fulfill the detergent standards with > 160 mg $CaCO_3$/g. Remarkable differences can be extracted

from the different synthesis conditions and the type of kaolin source used for the synthesis. Zeolites A synthesized from raw kaolin without gel aging (R-A-3M-3h* and R-B-3M-3h*) shows low CEC of 150 and 160 mg $CaCO_3$/g. Comparing these two samples with the equivalent P series, a notable increase of the CEC is observed due to the purification process that allowed removing the excess impurities that could suppressed the CEC of the raw kaolin based zeolite. Upon aging, due to the growth of more crystalline zeolite A and thus reaching optimum values of CEC up to 290 mg $CaCO_3$/g in R-A-3M-3G-3h and 295 mg $CaCO_3$/g in P-A-3M-3G-3h for A kaolin based zeolite A. Lower values were obtained for B type kaolin based zeolite A, 230 mg $CaCO_3$/g in R-B-3M-1G-3h and 250 in mg $CaCO_3$/g in P-B-3M-1G-3h. The highest cation exchange capacity of 295 and 250 mg $CaCO_3$/g was exhibited by zeolite A samples of P-A-3M-3G-3h and P-B-3M-1G-3h that could be attributed to the highest crystallinity (90 and 75%) of the samples. This result indicates the importance of gel aging, which resulted in zeolite A having higher crystallinity with smaller and uniform particle size. Moreover, longer aging times, from 3 to 6 and 12 h, showed the best calcium exchange capacity. This could be due to achieving smaller average particle size and uniformity of the particles of zeolite A. These results are well supported by the idea of Micco et al[123]., which states that, for detergent zeolite powder, one strategy to increase Na/Ca exchange rate is to significantly reduce zeolite particle size. The smaller particle size of the zeolite resulted in the higher surface area of the zeolite and brought larger CEC. Further aging to 24 h leads to lower calcium exchange capacity that can be attributed to the formation and predominance of other phases. Nevertheless, sample P-A-3M-3h obtained without any gel treatment shows a rather good performance giving a CEC of 280 mg $CaCO_3$/g. In general zeolite A made

of kaolin type A showed better performance of CEC compared to B type kaolin that could be mentioned to the better quality of this kaolin that gave better quality zeolite A having better crystallinity. In summary, the calcium exchange capacity data are in agreement with the XRD results showing the importance of zeolite crystallinity in view of a potential application. From the XRD data (Figure 31) the ½ h reaction product exhibited the lowest crystallinity (< 50%) which is mainly composed of amorphous sodium aluminosilcate gel (Figure 32), this time reaction product also gave the minimum calcium exchange capacity.

4.4. Alkali fusion followed by hydrothermal synthesis

Given the necessity of activating the kaolin prior the hydrothermal synthesis, alkali fusion followed by hydrothermal condition was adopted for zeolite A synthesis because it would allow larger amounts of aluminosilicates to be dissolved[124]. On top of this, by using this method, we can avoid the steps of purification of the raw kaolins. Figure 34 plots the X ray diffraction patterns of three synthetic zeolite A samples (R-A-3M-3h, P-A-3M-3h and A-F-3M-3h). The first two samples were synthesised by the conventional hydrothermal method and the third one by alkali fusion followed by hydrothermal synthesis method.

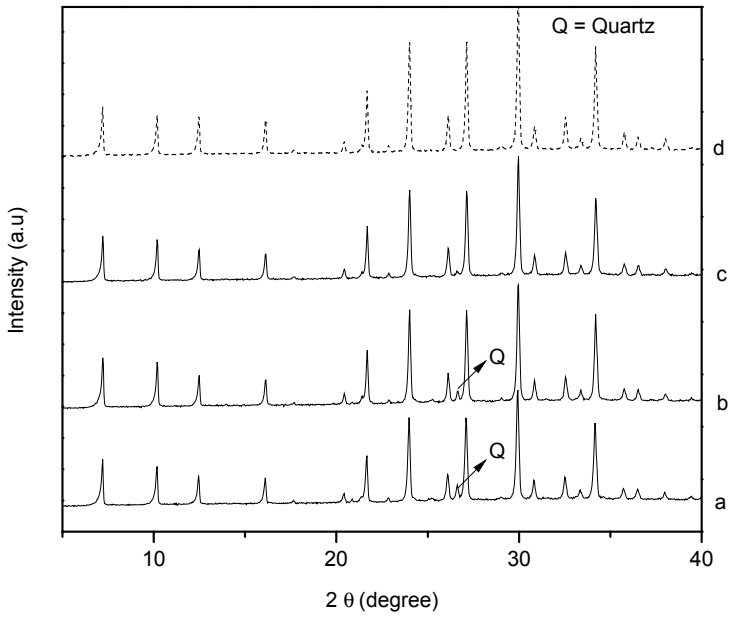

Figure 34: XRD pattern of synthetic zeolite A: (a) R-A-3M-3h, (b) P-A-3M-3h (c) A-F-3M-3h and (d) commercial zeolite

The graph shows fitting of the XRD profiles of all reaction products to the XRD profile of commercial zeolite A and literature[110], although it is possible to follow the changes in

the characteristic peak of quartz at 2θ. The samples prepared using the conventional hydrothermal method both from raw and purified kaolin sources (Figure 34a and 34b) show an intense peak of quartz. Whereas in the XRD profile of the alkali fused product (Figure 34c) this peak is almost negligible. This exciting feature of the alkali fusion method compared to the conventional method could be due to the high efficiency of the alkali fusion technique in extracting silicon from the quartz in a more efficient manner and making it part of zeolite A. This is particularly relevant for B type kaolin based synthetic zeolite A. The result obtained is in agreement with the report of Ríos et al.[41], in which they compared the conventional hydrothermal method with the alkali fusion for the synthesis of zeolite A. In their work, the classic hydrothermal transformation of the starting material produced a mixture of different zeolite-type structures, whereas the alkaline fusion approach promoted the crystallization of pure zeolite A. Moreover, the crystallinity attained by this method in this work is better than the one that was obtained by the conventional method of synthesis with the same synthesis protocols. For instance, the relative percent crystallinity for P-A-3M-3 h is 72% (Table 6) and for A-F-3M-3 h is 84% (Table 13). Similarly for P-B-3M-3 h it is 68% but for the corresponding B-F-3M-3 h the crystallinity is augmented to 83%. This additional improvement in crystallinity attained by alkali fusion followed by hydrothermal method of synthesis can be due to the alkaline activation of metakaolinite following the fusion approach favoured the crystallization of pure zeolite A.

The better crystallinity attained by the alkali fusion synthesis method was further verified using the quantitative analysis of the XRD profile done with X-pert high score software analysis (Table 12). The table shows that the alkali fused products illustrate better score

of zeolite A (81 and 79%) compared to the conventional synthetic product (72 and 68%) for A and B type kaolins based synthetic zeolite A products, respectively.

Table 12: Quantification results of alkali fusion based synthetic products by X-pert High Square software analysis

Samples	**Compound**	**Score (%)**
A-F-3M-3h	Zeolite A	81
B-F-3M-3h	Zeolite A	79

The thermal behaviour of the synthetic zeolites made using the alkali fusion synthesis condition was also analysed (Figure 35). Similar to the conventional hydrothermal synthesis products, it exhibited high thermal stability indicating loss of water of hydration of about 20% up to 400 ^{o}C.

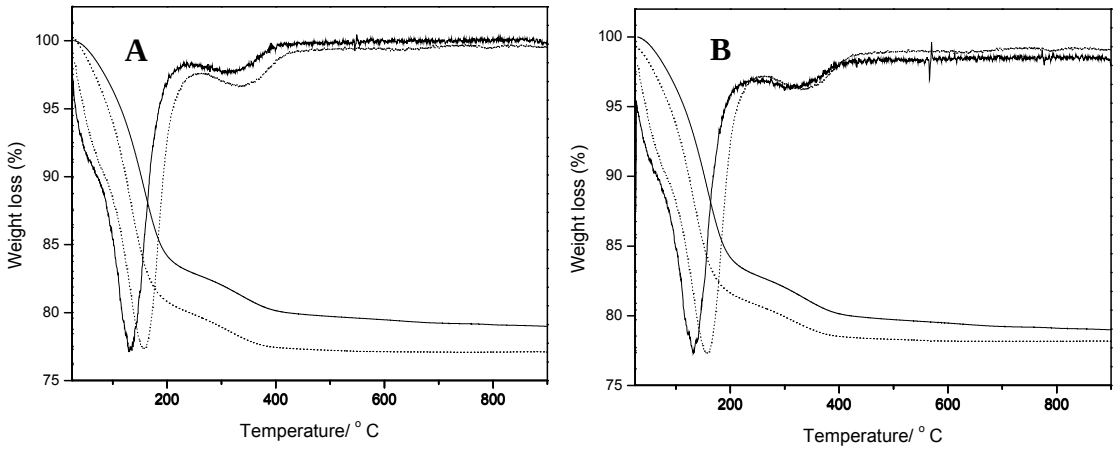

Figure 35: Thermogravimetric analysis (TGA/DTG) of synthetic zeolite A (solid line) synthesized using A and B raw kaolins via alkali fusion method and compared with commercial zeolite A (dotted line)

The SEM morphology analysis of alkali fused synthetic product from both A and B raw kaolins showed the formation of cubic crystals of zeolite A with sharp edges having heterogeneous particle distributions (Figure 36). This result indicated that there is still room for optimization of the synthesis conditions in order to get homogeneous particle size distribution with rounded edges cubed shape zeolite A crystals.

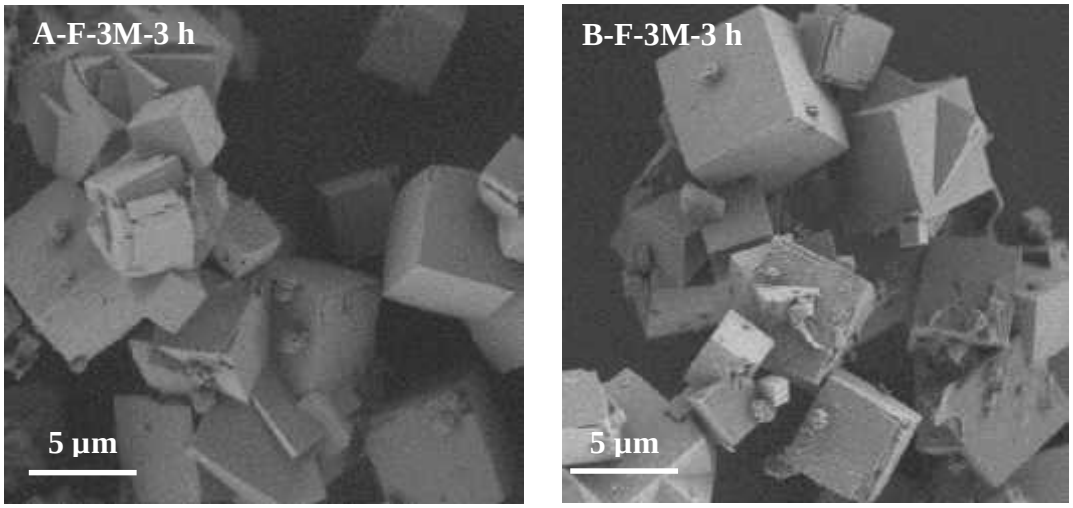

Figure 36: SEM micrographs of Zeolite A obtained by alkali fusion method from A and B raw kaolins

Similar to the conventional hydrothermal synthesis method, in the alkali fusion method of synthesis, the importance of reaction gel aging was studied to get an optimum crystal of zeolite A for the intended application in detergent. Doing so, the reaction gel formed at 50 ^{o}C for 1 h undergo aging for 1, 3, 6, 12 and 24 h. The percent crystallinity (% C_{XRD}) calculated from the XRD profiles is summarized in Table 13. The maximum percent crystallinity (% C_{XRD}) value is obtained for both kaolins based zeolite A at the optimum aging time; 3 h for A type kaolin and 1 h for B based kaolin. From the table it is possible to observe that the alkali fusion method, which did not involve any purification of the kaolin, gave better crystallinity compared to the synthetic product prepared with conventional hydrothermal method (raw and purified) showed in Table 8.

Table 13: Percent crystallinity (% C_{XRD}) of synthetic zeolite A by alkali fusion method.

Zeolite A	% C_{XRD}	Remark
SZA	100	
A-F-3M-3 h	84	
A-F-3M-1G-3h	87	
A-F-3M-3G-3h	91	
A-F-3M-6G-3h	81	
A-F-3M-12G-3h	62	
A-F-3M-24G-3h	0	*
B-F-3M-3 h	83	
B-F-3M-1G-3h	84	
B-F-3M-3G-3h	76	
B-F-3M-6G-3h	60	
B-F-3M-12G-3h	0	*
B-F-3M-24G-3h	0	*

*stands for sodalite phase as a measure product

Apart from this, from Table 13 it is possible to see that the crystallinity of zeolite A decreases with aging time, specially after optimum aging time for both types of raw kaolins. Furthermore, what is new in this method of synthesis is the complete conversion of reaction products to sodalite phase, which is thermodynamically more stable than zeolite A, after 24 h aging time for A type product and 12 h for B type products. Most probably, in the alkali fusion synthesis, the crystals grow faster than in the conventional

hydrothermal synthesis method. However, excessive aging time would result in a rapid conversion of the metastable zeolite A into the other new phase. This was confirmed by the XRD profiles of the synthetic product depicted in Figure 37 at 24 h for zeolite A from kaolin type A and 12 and 24 h for kaolin type B. In this particular aging times, the sodalite phase characterized by its five intense peaks (d_{110} at 14.16°, d_{211} at 24.65°, d_{220} at 28.53°, d_{310} at 31.99° and d_{222} at 35.13°)[110]dominated.

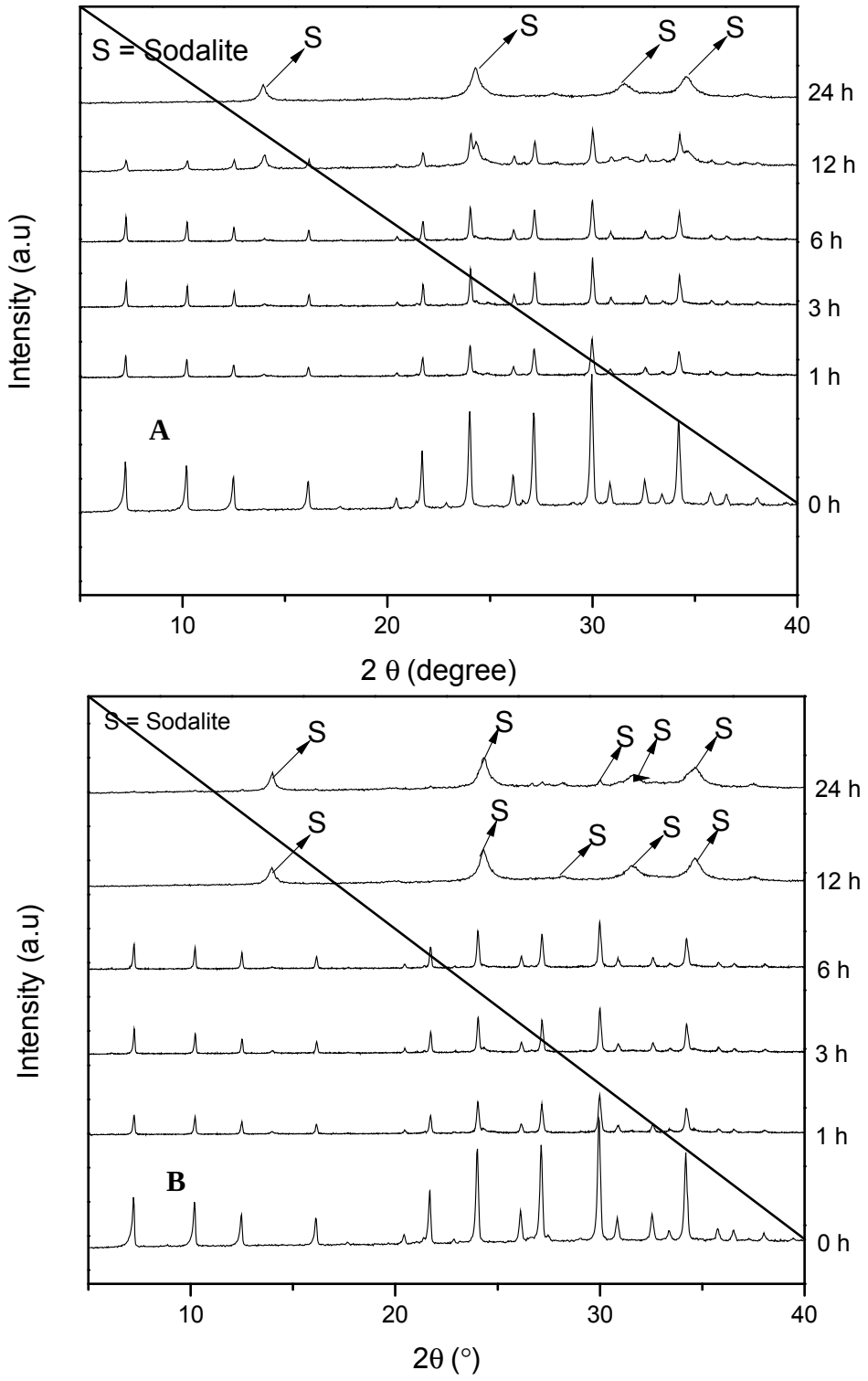

Figure 37: XRD patterns of synthetic zeolite A by alkali fusion from raw kaolin A and B at different aging time

The SEM micrographic analysis of the reaction products by the alkali fusion method is shown in Figure 38. The micrographs of both A-F-3M-3G-3h and B-F-3M-1G-3h revealed cubic shaped crystals of zeolite A with round edge showing average particle size of 4.0 µm. Similar to the conventional method of synthesis with reaction gel aging, crystals of zeolite A gets smaller in size and better homogeneity on the crystal distribution is observed. Moreover, from the micrograph it is possible to see the presence of remaining gel as a small amorphous clusters on the crystals of zeolite A indicating that further nucleation proceeded along with the crystal growth during the hydrothermal reaction. Thus, once again, aging has yielded in optimum properties of zeolite A crystals for using it as a detergent builder in contrast to the sharp edged cubic crystal of zeolite A obtained in the absence of gel aging (Figure 36).

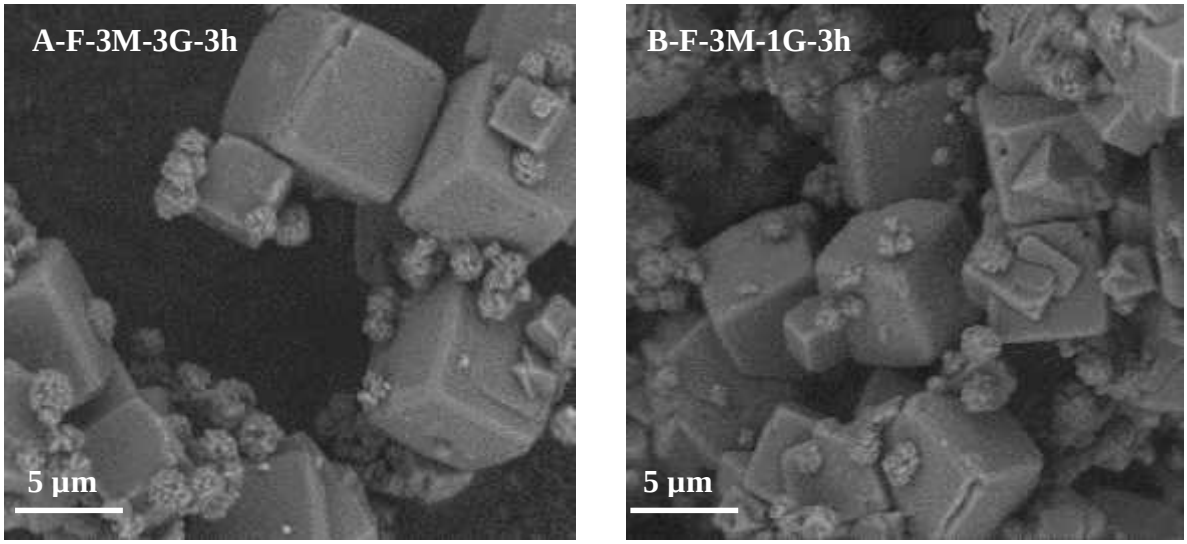

Figure 38: SEM micrographs of Zeolite A by alkali fusion method using raw kaolins A and B with gel aging

The ICP-OES elemental analysis result of the alkali fused product with gel aging is collected in Table 14. The result indicated that the Si/Al ratio in all different aging time products is 1 which is the intended Si/Al ratio for pure zeolite A. This corroborates the complete solubility of silica present in the starting kaolin and quartz by the alkali fusion process. From the table Na/Al is near to 1 alike the commercial zeolite A also evidencing that the synthesized zeolite A is merely sodium form zeolite.

Table 14: ICP-OES elemental analysis result of zeolite A synthesized under different aging conditions by alkali fusion method using raw kaolins A and B

Zeolite A	**SiO_2**	**Al_2O_3**	**Na_2O**	**Fe_2O_3**	**Si/Al**	**Na/Al**
SZA	33	28.0	17.4	0.02	1.0	1.0
A-F-3M-3h	28.6	25.0	15.0	1.0	1.0	0.9
A-F-3M-1G-3h	27.4	25.7	13.8	1.0	1.0	0.9
A-F-3M-3G-3h	27.4	25.0	14.3	1.0	1.0	0.9
A-F-3M-6G-3h	28.6	26.1	14.5	1.0	1.0	0.9
B-F-3M-3h	28.2	24.6	13.8	0.8	1.0	0.9
B-F-3M-1G-3h	28.6	25.7	13.8	0.8	1.0	0.9
B-F-3M-3G-3h	27.2	25.5	13.4	0.8	1.0	0.9
B-F-3M-6G-3h	28.6	26.6	14.4	0.8	1.0	0.9

Finally, the applicability of the products obtained by alkali fusion has been evaluated by the cation exchange capacity (CEC) measurements, and the results are compiled in Table

15. All the synthetic products obtained gave promising calcium removal capacity. Zeolite A obtained using gel aging (A-F-3M-3G-3h and B-F-3M-1G-3h) exhibited the maximum calcium exchange capacity (CEC) of 310 and 300 mg $CaCO_3$/g which is comparable with the commercial zeolite A having the CEC of 320 mg $CaCO_3$/g. These excellent results agree with the high crystallinity attained in these samples (91 and 84% for A-F-3M-3G-3h and B-F-3M-1G-3h, respectively). The obtained CEC result made the synthetic products to be promising candidate for using it as a builder in detergent.[125] From the table it is possible to see that the CEC value decreases with aging time showing again the same tendency as the crystallinity.

Therefore, according to the results obtained by XRD, SEM, ICP-OES and calcium exchange capacity, the synthesis of zeolite A using raw kaolin, either A or B, yields good quality products when using alkali fusion followed by hydrothermal synthesis which implies gel aging. The potential of these optimized products in real applications will be discussed in the next sections.

Table 15: Calcium exchanged capacity of zeolite A synthesized by alkali fusion method.

Zeolite A	Calcium removed		
	mg $CaCO_3$/g	meqCa^{2+}/g	% C_{XRD}
A-F-3M-3h	250	3.9	84
A-F-3M-1G-3h	270	4.2	87
A-F-3M-3G-3h	310	4.8	91
A-F-3M-6G-3h	260	4.0	81
A-F-3M-12G-3h	180	2.8	62
B-F-3M-3h	240	3.7	83
B-F-3M-1G-3h	300	4.7	84
B-F-3M-3G-3h	225	3.5	76
B-F-3M-6G-3h	200	3.1	60

4.5. Conclusions

The syntheses of zeolite A have been successfully carried out from two types of kaolins of Ethiopia named as ‘’A’’ for Ansho and ‘’B’’ for Bombowha kaolins. The synthesis was evaluated via two methods: the conventional hydrothermal and alkali fusion followed by hydrothermal synthesis methods. The optimization of the synthesis parameters for the synthesis of zeolite A included: the concentration of the base NaOH (3 M), the crystallization time (3 h), crystallization temperature (100 ^{o}C), the gel formation temperature and time (50 ^{o}C, 1 h) and gel aging time 3 h for A and 1 h for B type kaolin based zeolite A. The synthesis study involved both raw and purified A and B kaolins. We

have demonstrated the importance of purification of the raw kaolin to minimize the amount of quartz and other impurities in the conventional method of synthesis. However, for the alkali fusion method, the optimum synthesis parameters were achieved using raw kaolin. For the conventional method of synthesis: zeolite A with high crystallinity of about 90 and 75% for A and B type kaolin was obtained using the purified kaolins. Zeolite A having cubic shaped with rounded edge crystals with Si/Al = 1 and cation exchange capacity of 295 and 250 $CaCO_3$/g was obtained from purified A and B type kaolin, respectively. In the alkali fusion method of synthesis, the optimum conditions for the synthesis were similar to the conventional hydrothermal synthesis with the improvement that is obtained with raw kaolin, without purification. Zeolite A with high crystallinity of about 91 and 84% for A and B type kaolins, cubic shaped rounded edge crystals of zeolite A, Si/Al = 1 and cation exchange capacity of 310 and 300 mg $CaCO_3$/ g of anhydrous zeolite, were obtained for A and B type of kaolins, respectively. This method is more efficient in terms in energy demand not only because the purification step is avoided, but for the chemical activation of kaolin which involved metakaolinization at 600 ^{o}C for only 1 h compared to the conventional hydrothermal method which involved 3 h of metakaolinization process.

CHAPTER FIVE

5. Studies on the application of zeolite A in detergents

This chapter focuses on the practical application of the synthetic zeolite A prepared under different conditions in powder detergent as a builder by substituting the environmentally unfriendly phosphate based materials (STPP).

5.1. Introduction

Laundry detergents are compositionally made of at least six groups of components: surfactants, builders, enzymes, bleaching agents, fillers and other minor additives such as dispersing agents, fabric softening clay, dye-transfer inhibiting ingredients, and optical brighteners. Among these components, builders take the share of almost 30% by weight. In today's detergents, builders constitute about 6-25 wt% of liquid detergents and about 20-55 wt% of powder detergent formulations[126]. Thus, builders play a significant role in the detergents market. Among the known builders sodium tripolyphosphate (STPP) has been the most commonly used detergent builder in powder detergents. The job of phosphates is to sequester water hardening alkaline earth metal ions, calcium and magnesium, in favoring of solubilizing, emulsifying and suspending action of surfactants[127]. Although, in the early 1980s the peak consumption of STPP reached more than 1000,000 tones per year, in the late 1980s it has been banned in the USA and Western Europe, because of its eutrophication effects, which is the excessive growth of algae and fungi in water bodies. This led to an intensive worldwide search for the development of acceptable substitutes[60]. The introduction of ion exchange materials such

as, zeolites as detergent builders led to the gradual movement away from phosphate based materials. Zeolites, originally designed as phosphate substitutes for purely ecological reasons, slowly had to meet the demands imposed by modified detergent composition and production technologies. In particular, the trend towards compact detergents increased the demand for zeolite builders systems having high adsorption capacity for liquid components, especially for surfactants[128]. Tested under critical conditions, the phosphate-free detergent containing zeolite even proved superior to the earlier sodium triphosphate method. Systems containing phosphates require precise dosage which must be monitored exactly in relation to the water hardness, otherwise significant fiber incrustation will occur caused by phosphate precipitation. By contrast, zeolite-based systems even at low dosages and elevated water hardness tend to cause only low textile incrustation and deposits on washing machine parts[129]. This robust performance under a wide range of conditions and the high degree of flexibility in formulation terms facilitated the development of the zeolite-based low dosage compact detergents. Alongside its main function (that of softening water) zeolite also has other proven effects in the laundering process. Zeolite A for instance promotes the inhibition of greying through heterocoagulation with dirt particles. Furthermore, zeolites can remove dyes from the washing liquor by heterocoagulation and adsorption. In conjunction with the relatively low sodium concentration associated with zeolite as compared with soluble builders, this leads to a reduced risk of dyes discoloring other items. Zeolite is therefore the builder of choice for special products termed as color detergents[29]. The higher cation exchange capacity and special particle morphology makes zeolites A to be a viable alternative in as a detergent builder. Over the past 20 years, the trend towards compact detergents

increased the demand for zeolite A. The compact detergents of the most recent generation, often also called supercompact and tablet detergents are characterized not only by particularly low dosage and thus high surfactant content, but also by an increase in bulk densities to approximately 700-900 g/l for supercompact and 1000-1300 g/l for tablet types of powder detergents. Irrespective of these vigorous properties of zeolite A, there are various requirements set on a zeolite A to be used as a detergent grade builder. Among these requirements are: the size of the particles, crystal shape, brightness and cation exchange capacity (CEC). In this regard, we evaluate the properties of zeolite A produced from kaolin in terms of CEC, particle size and morphology to be adequate for use as detergent builder. However, problems associated with brightness and iron content are usually encountered when using kaolin for zeolite production[58] and this is also true for the synthetic zeolite A made from kaolin from Ethiopia. In this work, detergent grade zeolite A which has been synthesized from kaolin is used as builder in a formulated powder detergent and its potential was evaluated by analyzing some of its physicochemical properties like foam height, pH value, moisture content and alcohol and water insolubility.

5.2. Formulation of powder detergent

In this particular lab scale formulation of powder detergents the materials used were: Linear alkylbenzene (C12) sulphonate (LABSA), sodium sulphate, soda ash, sodium tripolyphosphate (STPP), sodium silicate, synthetic zeolite A from kaolin of Ethiopia and commercial zeolite A. The materials were mixed and homogenized in a mixing unit. The formulation of 25 g of detergent contains 55% sodium sulphate, 15% LABSA, 8% sodium silicate, 7% soda ash and the remaining 15% is formed by either pure zeolite A or

zeolite A: STPP in 50:50. For this particular formulation, esthetical value additives such as optical brightener, perfumes, preservatives, active enzymes and stabilizer have not been used. In addition, a commercial powder detergent having sodium aluminosilicate as a builder was tested for comparison. The three types of zeolite A samples synthesized using kaolin from Ethiopia were compared with a commercial zeolite A. In this study we have tried to substitute STPP from 50 to 100% by zeolite A in the detergent formulation composition. Based on the type of synthetic zeolite A used for the formulation, the detergent formulated is named as: detergent synthesized with commercial zeolite A (DZAC), detergent made of synthetic zeolite A by conventional hydrothermal method of synthesis from raw Ansho and Bombowha kaolins (DZAR and DZBR, respectively), and for purified Ansho and Bombowha kaolins (DZAP and DZBP, respectively). Finally, detergents were formulated with zeolite A obtained via alkali fusion method using only raw Ansho and Bombowha kaolins (DZAF and DZBF). For all type of the formulated detergents, the synthetic zeolites A used were the one that exhibited the highest calcium removal capacity (CEC), where calcium binding capacity of greater than or equal to ($\geq$ 160 mg $CaCO_3$/g) is the minimum requirement for detergent application.

5.3. Characterization of the formulated detergent

The formulated detergent samples were tested using various physicochemical parameters such as moisture content, foam height, pH measurement and alcohol and water insolubility test, which is adapted from Ethiopian Standard for Soaps and Detergent[130]. The same tests were also conducted on the known commercial powder detergent and the results of their comparative evaluations are presented.

Foam height measurement was done by preparing 1% detergent solution. Thus, 1 g of the detergent is dissolved in 99 mL of real hard water having moderate hardness (120 mg $CaCO_3$/L,). Then 10 mL of the prepared solution was taken and well shaken using a 100 mL measuring cylinder with a glass stopper until the detergent is completely dissolved and forms a foam. The foam height was measured after 10 minutes stability of the foam. The pH of the 1% detergent solution was measured at 25 °C.

For the moisture and volatile content analysis, 5 g of detergent sample was weighed, and dried to constant mass in an oven at 105 ±2°C. This was done until constant mass is attained when successive heating for one hour period shows a difference of not more than 5 mg in the net loss in mass. The % moisture content was calculated using the following equation:

$$\% \text{ Moisture} = \frac{\text{Initial weight} - \text{Final weight of the sample}}{\text{Initial weight of the sample}} \text{ x } 100$$

Insoluble matter in alcohol, i.e. inorganic salts, such as phosphates, sulphates, silicates and carbonates, which are usually present in non-soapy detergent preparations. This was done by weighing 5 g of the detergent material into a beaker, and digested with 50 mL of ethanol, followed by heating on a steam bath for about 2 minutes. Any hard lump was broken down with a glass rod flattened at one end. The solid matter was then allowed to settle and decanted through a sintered glass filter funnel. The alcoholic digestion was repeated in a similar manner with five further consecutive 30 mL portions of boiling ethanol. Each extract was filtered in turn through the same sintered glass funnel and the

residue was washed several times with hot ethanol to remove all the alcohol soluble matter. Finally, the sintered glass funnel was dried with the residue at a temperature of 105 ±2 °C until a constant weight is obtained. The insoluble matter in alcohol is determined using the equation:

$$\% \text{ Insoluble matter in alcohol} = \frac{\text{Mass insoluble in alcohol}}{\text{Initial mass in gram}} \times 100$$

For water insoluble matter analysis, 5 g of detergent sample was weighed and digested with 200 ml of freshly boiled water until sample is completely dissolved. Then, the solution was filtered, dried at 105 ^{o}C and the mass recorded. The residue was washed several times with hot water. The filtrate and the residue were dried for 3 h at 105 ±2 °C. Finally, the water insoluble matter was calculated using the equation bellow.

$$\% \text{ Insoluble matter in water} = \frac{\text{Mass insoluble in water in gram}}{\text{Initial mass in gram}} \times 100$$

5.4. Analysis results of the formulated detergents

The foam height test was used to determine how much foam the detergent can produce. If the foam height is low, then more foam must be added to the detergent. The substitution of STPP by Zeolite A was tested with 50% substitution followed by 100%. The foam height reported included the result of both 50 and 100% substitution. We have used the foam height of the commercial powder detergent as standard. The result obtained is depicted in Figure 39. From the graph it is possible to see that the 50% STTP substitution

by zeolite A exhibited almost the same height as 100% STPP substitution by zeolite A in all formulated detergents. The detergent formulated with synthetic zeolite A from the raw kaolins (DZAR and DZBR) exhibited the lower foam height compared to purified kaolin based and the alkali fused products (DZAP, DZBP, DZAF and DZBF) in both ranges of substitutions. This is directly related with the lower CEC exhibited by the raw kaolin based zeolite A samples (Table 11). Regardless of this, the detergents formulated with the raw A kaolin based synthetic product (DZAR) shows better foam height compared to the raw B kaolin type based zeolite (DZBR) that could be due to the low grade type nature of B kaolin. The detergent made with the purified kaolin based zeolite A (DZAP and DZBP) resulted in better foam height compared to the raw kaolin based zeolite A. This is due to the higher CEC of 290 and 230 mg $CaCO_3$/g exhibited by the particular synthetic products (A-P-3M-3G-3h and B-P-3M-1G-3h), respectively.

On the other hand, the detergent made of alkali fused kaolin based zeolite A (DZAF and DZBF) shows comparable foam height to the foam height of the commercial powder detergent.

This promising result can be accredited to the higher CEC of 310 and 300 mg $CaCO_3$/g anhydrous zeolite A for the particular fused products A-F-3M-3G-3 h and B-F-3M-1G-3 h, respectively. It is also possible to observe from the graph that the detergent made of this alkali fusion method exhibited almost the same foam height in both 50 and 100% substitution and also the same height with detergent made of commercial zeolite A (DZAC) that can be attributed to the better quality and higher calcium removal capacity corresponding to these materials.

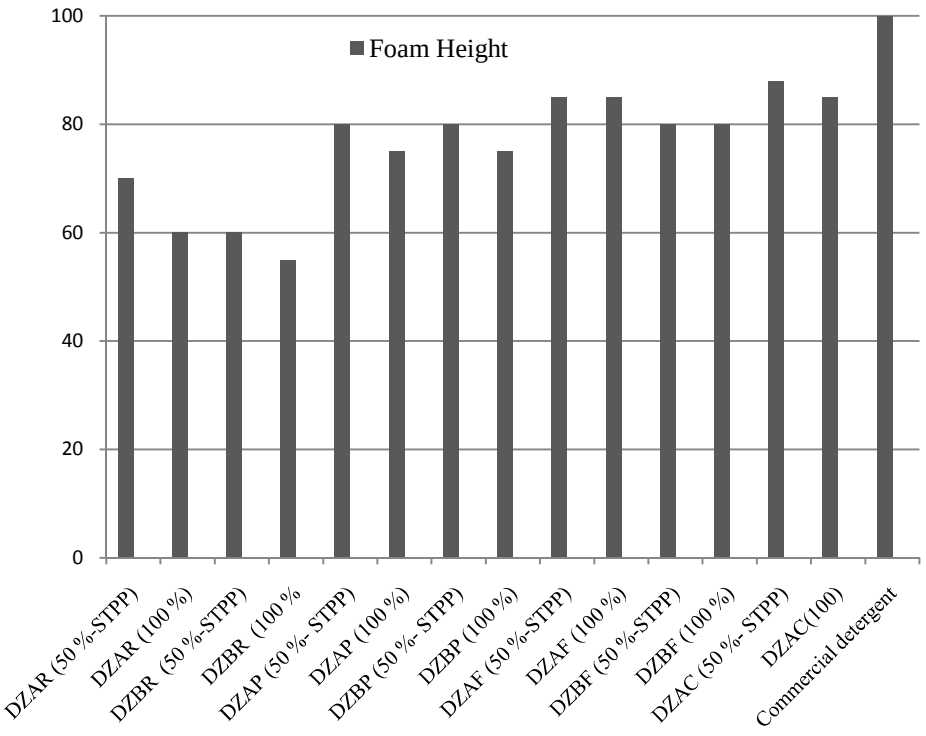

Figure 39: Foam height of 1% detergent solution of synthetic zeolite A and the commercial powder detergent

The pH analysis result of the synthetic detergent in comparison with the commercial one is reported in Table 16. The pH test was carried out on the detergent samples made with 100% of synthetic zeolite A. The results are in good agreement with each other and with the commercial detergent. Moreover, the pH requirement for 1% aqueous solution of industrial detergent determined at 25 ^{o}C shall be not less than 9 and more than 11. In the formulated detergent the data shows that it is in the appropriate required range. The maximum moisture and volatile components content requirement of any commercial synthetic detergent is 13% by mass. From the analysis result, there is remarkable difference between the synthetic zeolite A based detergent and commercial detergent that could be due to the absence of some ingredients and fillers in the synthetic zeolite A

based detergent that could be used to adjust such requirement into the appropriate value. Apart from this, the data, are consistent that they all fall within the same range.

Table 16: pH, moisture content, alcohol and water insolubility analysis result of zeolite A based detergent and commercial detergent.

Detergent type	pH	Moisture content (%)	Alcohol insolubility (%)	Water insolubility (%)
DZAR	10.0	2.3	81.0	17
DZBR	9.8	2.8	84.0	15
DZAP	10.2	2.4	83.0	13
DZBP	9.8	2.4	85.0	13
DZAF	10.1	2.6	85.0	10
DZBF	10.0	2.8	85.0	14
DZAC	10.1	2.2	81.0	11
Commercial	10.1	4.0	77.0	6

The result of alcohol and water insoluble matter analysis of synthetic zeolite A based detergent and commercial powder detergent is also summarized in Table 16. Here the stability of inorganic salts, such as phosphates, sulphates, silicates and carbonates, which are insoluble in alcohol were analysed. This has been done by extracting the material with 99% ethanol. The maximum alcohol insoluble matter requirement for industrial powder detergent is 80% by mass. From the result it is possible to see that the synthetic zeolite A based detergents slightly higher value off the permitted range, although these results could be tuned by varying the specific formulation conditions used to manufacture the detergents. Regardless of this, the obtained results are in good agreement with the commercial sample and indicate the possibility to use these synthetic zeolites for

detergent formulation. From the alcohol insolubility analysis result, the 15% mass loss corresponds to the alcohol soluble component of the detergent, which could be the surfactant linear alkyl benzene sulphonic acid (LABSA). The remaining 85%, which is insoluble in alcohol corresponds to the inorganic ingredients: aluminosilicate, sulphate and carbonates. Appropriate solubility of detergent in water is also another important requirement in washing. The maximum insoluble matter in water should not exceed more than 5-10% by mass. The water insolubility analysis result (Table 16) shows that the synthetic zeolite A based detergent lies in higher ranges, probably due to the chosen formulation. Nevertheless, the results obtained by the sample prepared by alkali fusion shows better results compared to the others that can be remarked to the better quality of these products.

5.5. Conclusions

The role of builders in a formulated detergent is removing of water hardening ions like Mg^{2+} and Ca^{2+} and enhancing the role of surfactants in emulsifying and removing of dirty particles. Based on this, in this section we have discussed the application of synthetic zeolite A from kaolin (Ethiopia) in detergent as a builder. Zeolite A which have been synthesised by two different methods from two different kaolin sources have been evaluated. The analysis result indicated that synthetic zeolite A with the best calcium exchange capacity (CEC) has yielded best results for this particular task. For the conventional hydrothermal synthesis based synthetic products, the good candidate samples were: A-R-3M-3G-3h and B-R-3M-1G-3h with CEC of 290 and 230 mg $CaCO_3$/g and A-P-3M-3G-3h and B-P-3M-1G-3h with CEC of 295 and 250 mg $CaCO_3$/g of anhydrous zeolite A, respectively. For the alkali fusion followed by hydrothermal

synthesis method, the synthetic samples which exhibited exciting performance were: A-F-3M-3G-3h and B-F-3M-1G-3h with CEC of 310 and 300 mg $CaCO_3$/g of anhydrous zeolite A. In general, of all the synthetic zeolite A used in this study, the alkali fused based products show better efficiency as detergent builders that could be due to its better quality and better cation exchange capacity. In spite of this, all synthetic detergent formulated with the synthetic zeolite A showed good detergent performance that could be promising result for using it as a detergent builder.

CHAPTER SIX

6. Studies on the application of zeolite A and other clay based materials in tannery wastewater treatment

6.1. Introduction

Tanning process using chromium compounds is one of the most common methods for processing of hides. Currently more than 90% of global leather production of 18 billion sq. ft is through chrome-tanning process because of the rapid processing, low cost, and better quality of the finished leather products. The function of chromium salts in tanning processes is to form, through complexation with the polypeptide collagen components of leather, a protective layer, which prevents the penetration of water inside the leather pores avoiding putrefaction. In this process about 60-70% of chromium reacts with the hides. In other words, about 30-40% of the chromium amount remains in the solid and liquid wastes, especially spent tanning solutions. The wastewater of tanning process if discharged, without proper treatment, into the sewerage system causes serious environmental impact. This makes tannery effluent containing chromium to be one of the most recognized problems in leather industry that can add chromium pollutant into the environment[131]. According to the report of Chaudry et al.[132] the untreated effluents emanating from the chrome tanning sectional stream in tannery have been found to contain 1500-3000 mg/L of chromium (III), although the discharge limit of chromium (III) in tannery wastewater is 2 ppm. For instance, in India alone about 2000–3000 tone of chromium are disposed into the environment annually from tannery industries, with

chromium concentrations ranging between 2000 and 5000 mg/L in the aqueous effluent[133].

In nature, chromium occurs in two major stable oxidation states Cr(III) and Cr(VI). Although Cr(III) is commonly used for tanning, the very low pH (2.8-3.2), the mechanical process during tanning that could generate heat and post tanning process may facilitate the oxidation of Cr(III) to Cr(VI)[134]. Based on this some countries fixed regulatory limits for the two species. Cr(VI) is known to have 100 fold more toxicity than Cr(III) and soluble in a wider range of pH[135]. It is commonly found in the form of H_2CrO_4, $HCrO_4^-$, CrO_4^{2-}, $Cr_2O_7^{2-}$ and $HCr_2O_7^-$ depending on the pH of the solution and total Cr(VI) concentration in the solution[136]. The toxicity caused by hexavalent chromium is so high that priority is given to regulate this pollutant at the discharge level. Hence, special attention is devoted to this transformation because Cr(VI) causes adverse effects for the human health where it can induce acute and chronic toxicity, neurotoxicity, dermatotoxicity, genotoxicity, carcinogenicity, immunotoxicity, and general environmental toxicity and has been shown to be mutagenic in a number of bacterial systems[135]. Due to this harmful effect of chromium on human and living organisms, the removal and recovery of the chromium content of these wastewaters are necessary for environmental protection[137]. Based on this, several methods have been used for removing of chromium from the tanning wastewater: chemical reduction and precipitation, ion exchange, membrane technologies, adsorption and biological methods.[132, 138-141] Most of these materials and methods suffer from drawbacks such as high capital or operational costs. Therefore, there is a need for the development of a methodology with low cost, easily available materials, which can adsorb and remove chromium economically.

Adsorption and ion exchange are becoming one of the most promising technologies for the removal of metal ions like Cr(III) and Cr(VI) from wastewater. Among these used and developed adsorbents and ion exchangers are activated carbon, fly ash, peat, recycled alum sludge, peanut hulls, resins, biomaterials, clay materials and zeolites. Along with the known ion exchangers, zeolites, both natural and synthetic, deserve a special attention due to their high exchange capacity, reasonable costs and environmentally-friendly nature. Natural zeolites are abundant and low cost resources, which are crystalline hydrated aluminosilicates with a framework structure containing pores occupied by water, alkali and alkaline earth cations. Natural zeolites are environmentally and economically acceptable materials for water treatment. Due to their high cation-exchange ability as well as to the molecular sieve properties, natural zeolites have been widely used as adsorbents in separation and purification processes in the past decades[22]. Even though, it is possible to remove Cr(III) using natural zeolites and other adsorbents, due to its predominantly cationic exchange properties, zeolites cannot remove Cr(VI) anion which is mainly found as oxyanions forms such as chromate (CrO_4^{2-}) and dichromate ($Cr_2O_7^{2-}$) in the solution. Based on this, many works have been done and reported on the modification of natural zeolites for the removal of Cr(VI)[142, 143].

Bentonite is one of clay minerals composed mainly of montmorillonite, a clay mineral of the smectite group, and is produced by in situ devitrification of volcanic ash[144]. Depending on the dominant exchangeable cations present, the bentonites may be referred to as either as calcium bentonite or sodium bentonite. The two varieties exhibit different properties and uses. Due to the presence of exchangeable cations, which are responsible for the presence of adsorption sites, bentonites are also getting attention as adsorbent for

the removal of different pollutant for the environmental remediation. Based on this, a number of study results have been reported on the removal of Cr(III) and Cr(VI) from aqueous solution using bentonites and modified bentonites[145, 146].

Hydrotalcites (HT), also known as layered double hydroxides (LDH), are anionic clays with positively charged octahedral hydroxide layers, which are neutralized by interlayer anions and water molecules, and which are generally formulated as $[M^{2+}_{1-x}M^{3+}x(OH)_2](A^{m-})_{x/m}\cdot nH_2O$, where M^{2+} and M^{3+} are di- and tri-valent cations, respectively, A^{m-} is an anion whose charge is m-. Magnesium-aluminum hydrotalcite with the formula $[Mg_6Al_2(OH)_{16}]^{2+}.CO_3^{2-}.4H_2O$, and a layered structureis stable up to 400 °C. They are structurally formed by brucite-like ($Mg(OH)_2$) sheets where isomorphous substitution of Mg^{2+} by a trivalent cation like Al^{3+} produces a positive charge in the layer that is compensated by anions, which occupy the interlayer space along with water molecules. Hydrotalcite-like materials with similar properties can be obtained by substituting Mg^{2+} by other divalent cation keeping the same structure. The cation nature, the ratio M^{3+}/M^{2+}, the synthesis method, among others determine the properties of the layered double hydroxides[147]. Hydrotalcites, as many clays, may be expanded introducing compounds between the layers. The interlayer spaces in carbonate and nitrate exchanged hydrotalcites are either 2.9 or 4.0 Å, respectively[148]. One of the most exploited property of hydrotalcites is the so called ‘‘memory effect” which consists in the spontaneous structural reconstruction of the original layered structure after being calcined and then put in water or aqueous solutions containing different anions[149]. This memory effect can be used effectively to remove harmful anions including chromate anion from wastewater solutions. There are generally two mechanisms for adsorption of

chromate in HT, the first of them is the already mentioned, memory effect, where the HT is calcined at high temperatures i.e. 350–800 ºC for several hours, resulting in mixed metal oxide which is more precisely a solid solution of the two metal oxides. The layer structure is lost during the calcination. When this material is put in contact to a Cr(VI) aqueous solution, the HT recovers its layered structure and the chromate anions are trapped within the HT layers[150]. The second mechanism, anion exchange, does not require calcination and it is simply based on equilibrium between the anions within the HT layers and the bulk solution. Memory effect mechanism generally is much more efficient than anion exchange, giving adsorption capacities for Cr(VI) ca. 10 times higher than the latter[151].

The leather industry is becoming one of the booming industrial sectors in Ethiopia that contributes substantially towards the national economy. According to the Ethiopian leather evaluation final report by UNIDO (2012), there are 26 tanneries in Ethiopia and almost all of them employ chrome tanning[152]. According to the Ethiopian Environmental Pollution Control Proclamation No.300/2002, the limit for total chromium and Cr(VI) from tannery wastewater to the environment is 2 mg/L and 0.1 mg/L, respectively[153]. However, the challenge coming with the expansion of tanneries is the management and treatment of effluents coming out from these factories. To overcome this national problem it needs high efficient and low cost adsorbent from locally available cheap resources.

By taking into account this national environmental challenge, synthetic zeolite A made of locally available kaolin and other locally available natural and synthetic adsorbents have

been tested for the treatment of the tannery wastewater collected from domestic tanneries, as well as from synthetic water with chromate (CrO_4^{2-}) in solution.

6.2. Materials and methods

Among the tested adsorbents, in our work we focused on evaluating the removal capacity of our synthesized zeolite A from different kaolin of Ethiopia[91]. For comparison purposes, we evaluated as well the raw kaolins from Ansho and Bombowha, two natural zeolites: one collected from Ethiopia (ET-7) kindly donated by Prof. Solomon Taddesse, School of Earth Sciences, AAU and the other one is from Mexico (clinoptilolite) donated by Prof. Pedro Bosch, two bentonites (from Ledi and Mille deposits) donated by the Directorate of Research and Development of the Ministry of Mines and mixed oxides (Hydrotalcite and nano Hydrotalcite (HT/SiO_2)) kindly donated by Prof. Pedro Bosch and Dr. Geolar Fetter from Universidad Nacional Autonoma de Mexico (UNAM). All raw adsorbents obtained in powder form, were crushed and sieved to the particle size fraction 75-125 µm and prepared for the experiments. Chromium wastewater was directly obtained from the directorate of Leather Industry Development Institute (LIDI) containing more than 2000 mg/L of Cr(III). Model synthetic Cr(VI) solution was prepared in our lab using potassium dichromate ($K_2Cr_2O_7$). All other chemicals used were reagent grades.

HT and nano-HT/SiO_2 preparation

The mesoporous material SBA-15 was used as SiO_2 support in the synthesis of nano-hydrotalcite (nano-HT), 10.5 g of calcined SBA-15 were dispersed in NaOH (2 M) and aluminum and magnesium nitrates solutions (2.5 M) in 50 mL of distilled water. The

reactive amounts were calculated for a molar ratio Mg/Al = 3 and SiO_2/HT = 7/3 (w/w)[154]. The mixture was treated in a microwave autoclave at 80 °C and 200 W for 10 minutes (MIC-I Sistemas y Equipos de Vidrio S.A. de C.V).

Preparation of standards and analysis of chromium (III) solution

Standard solutions containing 1, 2, 3 and 4.0 ppm of Cr(III) were prepared for calibration by appropriate dilution of a 1000 mg/L stock solution of chromium (III). Analytik Jena ZEEnit700 P model flame atomic absorption spectrophotometer (FAAS) was used to measure the concentration of chromium before and after adsorption experiment. To minimize the uncertainty in measurements, the sample amounts were accurately weighed and the dilution factor (correction) was taken into consideration.

Chromium (III) adsorption experiments

Adsorption experiments were carried out in batch mode at 25 ±0.5 ˚C with continuous stirring at 500 rpm. A total of 10 mL of wastewater was treated with adsorbent with varying adsorbent dosage from 2 g/L to 100 g/L and a total contact time of 24 h. All mixing vessels were kept sealed throughout the duration of each isotherm test in order to minimize evaporation of water. In order to correct for any adsorption of chromium on the container surface, control experiments were carried out in the absence of adsorbents. All samples were filtered prior to analysis. The first few milliliters of the filtered samples were discarded in order to minimize the effect of any adsorption that may occur on the filter paper. The pH of the samples at all isothermal temperatures was measured but the solution was not buffered. This procedure was adopted in order to analyze the cations behavior in a real wastewater situation, that is, with variable pH. The chromium in

solution and that adsorbed was determined by mass balances according to the following equation:

$$\% \text{ Removal of chromium} = \frac{C_o - C_f}{C_o} \times 100$$

Where; C_o and C_f are the concentration of Cr(III) in the sample solution before and after the treatment.

Adsorption capacity (q_e) which is defined as the amount of adsorbate retained per mass of adsorbent was calculated using the following expression:

$$q_e = \frac{(C_{eq} - C_o)V}{m}$$

Where V is the volume of solution treated and m is the mass of adsorbent utilized.

Adsorption results and discussion

The chromium concentration in the tannery wastewater was 2036 mg/L. The result of this study showed that the wastewater of tannery process is one of the most important sources of environmental pollutants as the concentration of chromium in the wastewater is extremely high that it is more than 1000 fold to its maximum limits that could be released into the environment and it needs great attention from health and environmental aspect. In this study all the sample reactor pH was constant at values around 4 which indicated that dealumination of the zeolite or precipitation of hydroxides could be in principle neglected. A comparative study of the removal efficiencies of the synthetic zeolite A with the other natural adsorbents is conducted. The Cr(III) removal efficiency of different adsorbents used is summarized in Table 17.

Table 17: Cr(III) removal (%) from tannery wastewater using different adsorbents

Adsorbent	Dosage rate (g/L)		
	25	**50**	**100**
A-Kaolin	–	–	0
B-Kaolin	–	–	0
Bentonite (Mille)	–	–	17.1
Bentonite (Ledi)	–	–	30.8
ET-7	43.5	50.4	53.5
R-A-3M-3 h	84.9	92.0	99.8
R-B-3M-3 h	87.0	94.0	99.6

The table shows that the raw kaolins show null performance of Cr(III) removal that can be explained by the very low cation exchange capacity of the kaolins (Table 11). Betonites present relatively low Cr(III) removal that can explained by low content of exchangeable ions in the natural bentonites (Table 18). However, from the table it is possible to see that there is a remarkable difference in the Cr(III) removal among two bentonite samples. The Ledi bentonite sample shows better removal efficiency compared to the Mille bentonite sample that could be mentioned to the presence of better number of Cr(III) exchangeable cations in the Ledi bentonite sample. The weight percent composition of exchangeable cations from ICP-OES analysis of the bentonite samples indicates, relatively higher compostion of Na and K in Ledi sample.

Table 18: ICP-OES analysis result of natural bentonites and zeolite in weight %

Sample	Si	Al	Ca	Na	Mg	K	Fe	Ti	Si/Al
Bentonite (Mille)	27.8	7.0	0.8	1.21	1.70	0.8	6.0	0.5	3.8
Bentonite (Ledi)	23.9	8.0	1.2	1.56	1.41	1.3	6.9	1.0	2.9
ET-7	25.6	13.1	0.43	10.6	0.06	-	0.09	-	1.9

In our attempt to evaluate natural zeolite for Cr(III) removal, we have tested natural zeolite from Ethiopia (ET-7). The X-ray diffraction pattern of this sample showed a mixture of two structures: Natrolite and Analcime (Figure 40). Natrolite with a unit cell formula of $Na_2Al_2Si_3O_2(H_2O)_2$ shows to be the main component and Analcime ($Na(AlSi_2O_6)(H_2O)$) which gives small XRD intensities is the minor component[155].

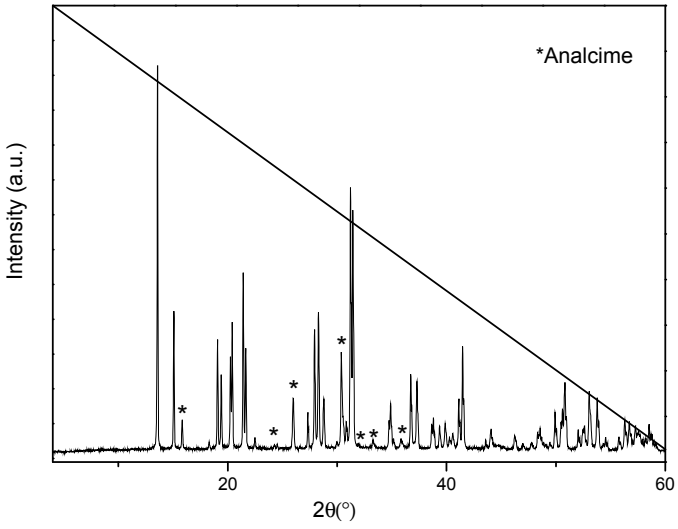

Figure 40: XRD pattern of ET-7

From Table 17, the natural zeolite (ET-7) exhibited moderate Cr(III) removal efficiency at the higher dosage rate (50 and 100 g/L). This is due the presence of interchangeable cations that can exchange with Cr^{3+} ion. Table 18 indicates the highest Na wt% composition compared to the bentonite samples which can be easily exchanged with Cr(III) and responsible for its removal. Moreover, from the ICP-OES analysis result (Table 18) it is possible to see that ET-7 revealed the lowest Si/Al ratio (1.9) compared to the bentonite samples. This further confirmed the better cation exchange capacity of the material.

Among all adsorbents used, the best chromium removal efficiency is exhibited by the synthetic zeolite A both from Ansho and Bombowha kaolin. The synthetic zeolite A samples used in this chromium removal study are the low quality type having the lower crystallinity of 62% (R-A-3M-3 h) and 64% (R-B-3M-3 h). In the adsorbent dose of 100 g/L both zeolites types revealed almost 100% removal. This is demonstrated in Figure 41. As shown in the figure, the deep blue color due to chromium is almost completely removed after treatment with zeolite A. Even at low dosage rate (25 g/L) the chromium removal is more effective than any other adsorbent tested. In this particular study, the Cr(III) concentration of 2036 mg/L in the original wastewater was reduced to 10.1 mg/L in the final water. This indicates that by increasing the adsorbent does it is possible to tune the treatment according to each factory in order to reach the Ethiopian Environmental Protection Authority (EEPA) limit of 2 mg/L.

Figure 41: Tannery wastewater before (left) and after (right) treatment with R-B-3M-3 h

Effect of adsorbent dosage

The effect of adsorbent dosage on the removal of chromium from the tannery wastewater is studied using the best adsorbent zeolite A (R-B-3M-3 h). Results are shown in Figure 42. The adsorption efficiency increases with the increments in the dosage from 2 g/L to 100 g/L keeping the temperature (25 ^{o}C), contact time (24 h) and initial chromium concentration (2036 mg/L) constant. Maximum removal of 99.8% was observed with adsorbent dose of 100 g/L. Increasing the percentage of adsorption with adsorbent dose is due to the increase in adsorbent surface area and availability of more adsorption sites. This means more mass available, more the contact surface offered to the adsorption. This

is expected because the higher dose of adsorbent in the solution, the greater availability of exchangeable sites for the ions, i.e. more active sites are available for binding of Cr ions[145]. However, the adsorption capacity (q_e) decreases while increasing the adsorbent dosage (Figure 42). The drop in adsorption capacity while increase in adsorbent dose can be attributed to adsorption sites remain unsaturated because the number of available adsorption sites increases[156].

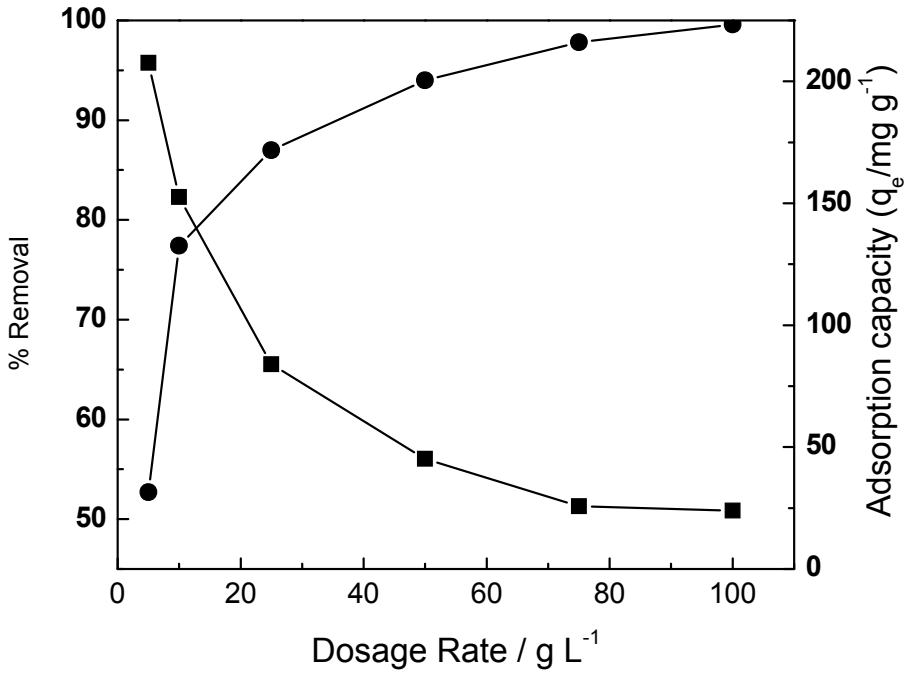

Figure 42: Chromium removal from tannery wastewaters using R-B-3M-3 h

Adsorption Kinetics

The kinetic study for the removal of chromium was carried out via the batch method and with different contact times. Chromium wastewater from tannery was treated at adsorbent dosage of 25 g/L (1.25 g in 50 ml). The suspension was stirred using magnetic stirrer with constant and vigorous agitation speed. During the study, the temperature was kept

constant at 25 ^{o}C. 0.5 mL aliquots of the solution with adsorbent suspended were withdrawn at different time intervals (from 10 to 2880 min). The solid phase was then separated by centrifuge followed by filtration. The total sampling volume did not exceed 5% of the total solution volume.

Adsorption kinetics describes the solute uptake rate as function of the contact time of the adsorbate on the adsorbent. There are essentially three stages in the adsorption process by porous adsorbents. (1) solute transfer from the bulk solution to the external surface of the sorbent through a liquid boundary layer (film resistance), (2) solute transfer from the sorbent surface to the intraparticle active sites (intraparticle resistance), and (3) interactions of the solute with the available sites on both the external and internal surfaces of the sorbent (reaction resistance). One or more of the above mentioned stages may control the rate at which the solute is adsorbed and the amount of solute that is adsorbed onto the sorbent.

Hence, in the present study, the kinetics of chromium removal from the tannery wastewater into synthetic zeolite A was carried out to understand the behavior of the adsorbent. Kinetics of adsorption is shown in Figure 43 as adsorption capacity at different contact times. The experimental results showed rapid initial adsorption rate for the first 3 h adsorption experiment followed by a slower rate until an asymptote is reached at about q_t = 80 mg g^{-1}. A similar trend has been reported by T. R. Choudhury et al.[157] in which there was no significant change in equilibrium concentration after 6 h for the adsorption of Cr(III) from aqueous solution by groundnut shell.

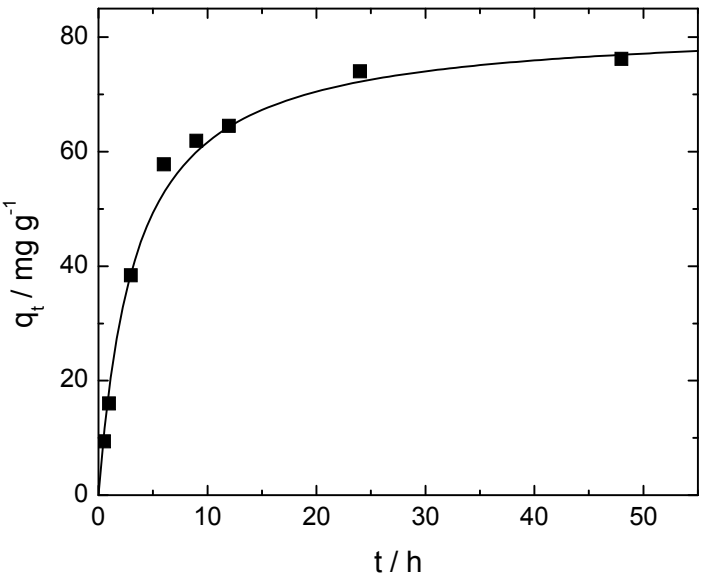

Figure 43: Adsorption kinetics for Cr(III) removal using R-B-3M-3 h

This phenomenon can be explained by the fact that initially, the adsorption sites are open and the metal ions interact easily with the sites and hence a higher rate of adsorption is observed. Moreover, the driving force for adsorption (the concentration difference between the bulk solution and the solid-liquid interface) is higher initially and this leads to a higher adsorption rate. However, after the initial period, slow adsorption is due to slower diffusion of solute into the interior of the adsorbent and the overall saturation of adsorbing site of the adsorbent. The results demonstrated that around 90% of the metal ions were removed after 24 h of adsorption that could be taken as equilibrium time. Further contact time (48 h adsorption) did not give significant change i.e. the equilibrium is reached.[158] This trend emphasizes that sorption times have important effects on the removal efficiency, which increases significantly with increasing zeolites contact time with the Cr(III) solution. This is a consequence of the molecular sieve property of the

zeolites, where the larger size Cr(III) species needed more time to exchange with sodium cation that is neutralized in the pore of the zeolite framework.

The kinetics of sorption that defines the efficiency of sorption of chromium was modeled by several kinetic models[159]. The experimental data fitted best to a pseudo-second order kinetics, where the rate of adsorption is proportional to the square of the driving force, that is the difference between the adsorption capacity at a time *t*, q_t and the adsorption capacity at infinite time (at equilibrium), $q_{\text{ã}}$: The fitting yielded the following parameters:

Kinetic constant: $k_2 = 3.6\text{x}10^{-3}$ g mg^{-1} h^{-1}

Adsorption capacity at $t = \infty$, $q_\infty = 82.3$ mg g^{-1}

Adsorption Isotherm and adsorption mechanism

Adsorption data are usually described by adsorption isotherms. Adsorption isotherms relate adsorption capacity (metal uptake per unit weight of adsorbent, q_e) to the equilibrium adsorbate concentration in the bulk fluid phase (c_e). Some of the most utilized adsorption isotherms are:

The linear model, which describes the accumulation of solute by sorbent as directly proportional to the solution concentration:

$$q_e = k_{\text{DC}e} \qquad (1)$$

The Langmuir model assumes that the uptake of metal ions occurs on a homogenous surface by monolayer adsorption without any interaction between adsorbed ions. The Langmuir isotherm is given by:

$$q_{eq} = \frac{q_m b c_{eq}}{1 + c_{eq}} \qquad (2)$$

q_m (maximum adsorption capacity) and b are fitting constants for the Langmuir equation. The Freundlich isotherm is the most widely used non-linear sorption model and is given by the general form:

$$q_{eq} = k_f c_{eq}^{1/n} \qquad (3)$$

k_f and n (sorption intensity) are fitting constants for the Freundlich equation[160].

Figure 44 show a representation of q_e vs Ce for the adsorbents, zeolite A synthesized from kaolin along with the commercial Zeolite A.

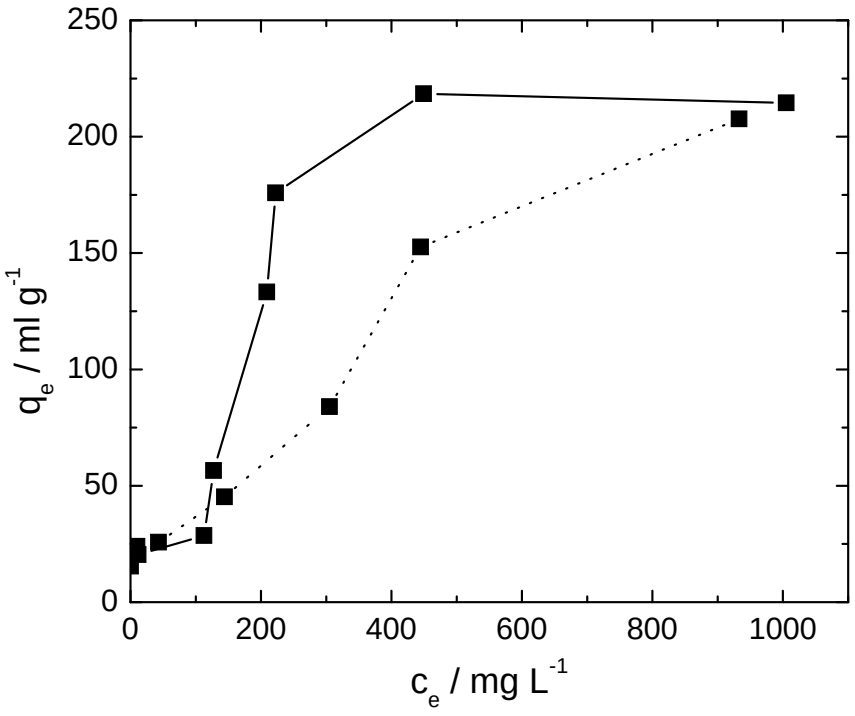

Figure 44: Adsorption isotherm for Cr(III) removal by R-B-3M-3 h (solid line) and commercial zeolite A (dotted line)

However, the equilibrium data did not fit to any of the models proposed in the literature. Moreover, the S-shape of the graphics is very unusual for adsorption processes indicating a complex mechanism of adsorption. Another anomaly observed is that, from the theoretical cation exchange capcity (CEC) of Na form of this zeolite A, the expected maximum adsorption capacity for Cr(III) is about 95 mg/g of zeolite. However, the experimentally obtained result indicated that the Cr(III) adsorption capacity was about 200 mg/g at the lower adsorption dose (Figure 42). This unexpected high adsorption capacity attained at the lower adsorbent dose was further investigated by XRD in order to verify whether the zeolite remains stable or else the zeolite is collapsed leading to pure surface adsorption. The XRD profiles of the zeolite A recovered after the adsorption experiment at different adsorbent dose are proved in Figure 45.

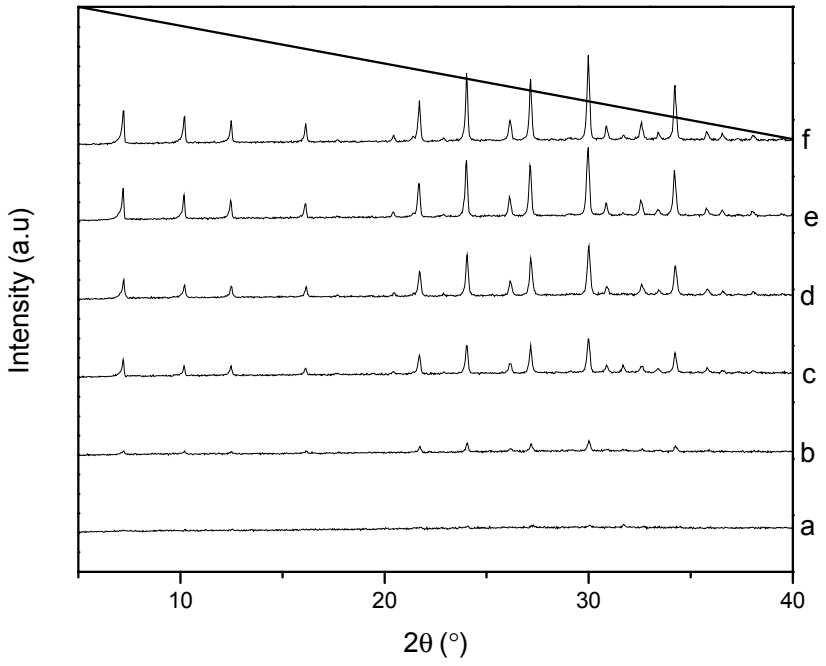

Figure 45: XRD patterns of R-B-3M-3 h after adsorption experiment with different doses. (a) 5 g/L (b) 10 g/L (c) 25 g/L (d) 50 g/L (e) 75 g/L and (f) 100 g/L

The X-ray diffraction analysis of the zeolite samples after chromium uptake points out a distinct behaviour for the different adsorbent dosages. The XRD results indicated that at lower dosages (5 and 10 g/L) the synthetic zeolie A loses its crystallinity. This situation may favor the co-precipitation of Cr(III) in the form of chromium silicate, $Cr_2(SiO_3)_3$ or other amorphous solid material that augmented the adsorption capacity of the lower adsorbent doses up to 200 mg/g. However, for the higher adsorbent doses (25, 50, 75 and 100 g/L) the XRD profile shows that the zeolite remained crystalline after chromium removal experiment. Moreover, from Figure 42 it is possible to see that the adsorption capacities for the higher adsorbent doses are less than the theoretical cation exchange capacity (95 mg/g). So it is possible to say that the removal mechanism is merely due to cation exchange for these higher adsorbent doses.

The situation observed for the synthetic zeolite A (R-B-3M-3 h) is also true for the commercial zeolite A (CZA) used in the Cr(III) removal from tannery wastewater. The XRD pattern analysis of the low dosage (5 g/L) indicated the absence of the characteristic peaks of zeolite A (Figure 46). For the higher doses (25, 50 and 100 g/L), zeolite A survived the high concentration of Cr(III). Hence, the higher adsorption capacity attained at the lower adsorbent doses for both commercial and synthetic zeolite A verified that the removal mechanism is not merely ion exchange. M. Pansinii et al[161]., similarly reported structural collapse during chromium removal from waste water by ion exchange using zeolitic rock containing phillipsite and chabazite. Their assumption for the structural collapse is may be caused in some instances by the unfavourable environment determined by the presence of a Brønsted acid, but may be also due, as demonstrated in this investigation, to the framework-cation interaction.

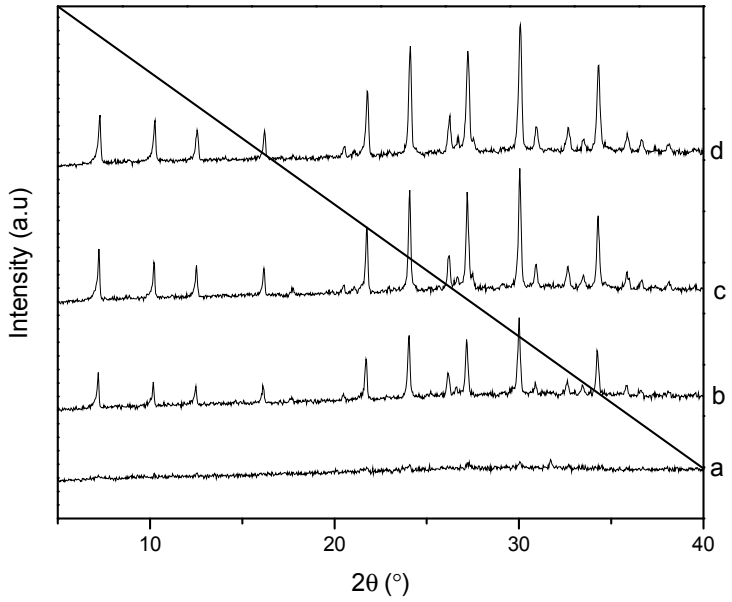

Figure 46: XRD patterns of the commercial zeolite A after adsorption experiment with different adsorbent doses: (a) 5 g/L (b) 25 g/L (c) 50 g/L (d) 100 g/L

The relative percent crystallinity (C_{XRD}) summarized in Table 19 shows that as the adsorbent dose increases, the crystallinity increases for both synthetic zeolite A and commercial, which could be mentioned to the effect of Cr(III) solution concentration. This means the higher adsorbent dosage shows better survival of high chromium (III) concentration.

Table 19: Percent crystallinity (C_{XRD}) of zeolite A after Cr(III) removal

Adsorbent dose (g/L)	C_{XRD} (%)	
	Synthetic	Commercial
100	40	25
75	34	-
50	25	24
25	19	17
10	9	-
5	-	-

Generally, from the adsorption isotherm data (Figure 44), the equilibrium data did not fit to any of the models proposed in the literature. As we observed from the isotherm graph the data looks as if it follows normal trend for the first three isotherm points (higher adsorbent doses), but the isotherm points get scattered for the higher points (lower adsorbent doses), this scenario is true for both types of zeolites used as an adsorbent, specially for the commercial zeolite A (dotted line). Therefore, this different removal mechanisms exhibited at different adsorbent doses and related to the crystallinity of the zeolite could be plausible reason for the unfitting of the isotherm data to any of the proposed model.

Further electron microscopy studies were carried out in order to understand the adsorption of chromium by the synthetic zeolite A. Spherical aberration (C_s) corrected Scanning Transmission Electron Microscopy coupled with High Angular Annular Dark

Field detector (C_s-corrected STEM-HAADF) instead of conventional TEM was chosen due to the high analytical power of this mode, while maintaining atomic resolution using the C_s corrector in the condenser system. Besides, it has to be mentioned that low silica zeolite like zeolite A is extremely unstable under the electron beam due to the large amount of water contained in the structure[162], thus, a precise control on the exposure to the electron beam has to be taken into account. Figure 47 shows Cs-corrected STEM-HAADF images of synthetic zeolite A (R-B-3M-3 h).

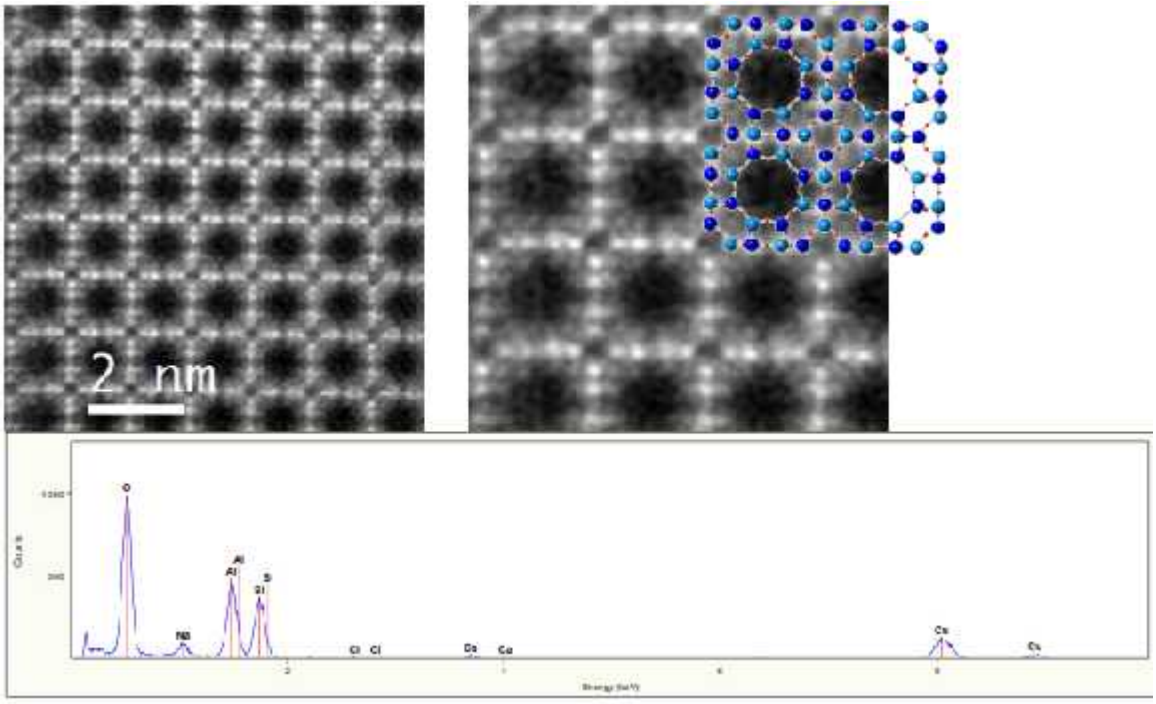

Figure 47: Cs-corrected STEM-HAADF images and EDS spectrum of R-B-3M-3 h

The image shows the perfectly arranged structure of zeolite matching with the overlayed model. The dark contrast in this mode corresponds to the parts of the material with no electron density, that is, zeolite alpha cages, linked to each other by sodalite cages, in

which the four-membered rings can clearly be observed in brighter contrasts. Moreover, the EDS spectrum also displays the zeolite A framework compositions, Si, Al, O and Na.

The zeolitic framework of the chromium ion-exchanged material (Figure 48) is exactly the same, meaning that in this particular sample (100 g/L) the crystallinity of the zeolite A remains stable. The EDS spectrum which displays the composition of Cr-exchanged zeolite A shows the presence of Cr in addition to the zeolite framework elements (O, Si, Al, Na) which corroborates the absorption of chromium. However, it is not possible to observe any contrast inside the cages, probably due to the low amount of Cr atoms that do not yield sufficient electron density to inverse the contrast.

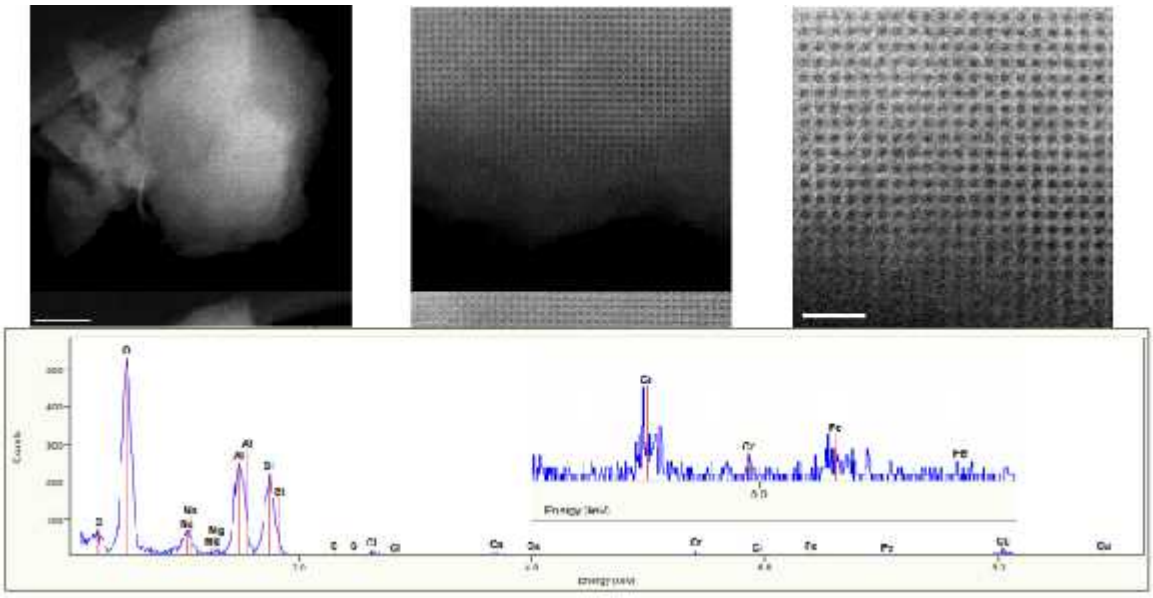

Figure 48: Cs-corrected STEM-HAADF images and EDS spectrum of Cr(III) exchanged R-B-3M-3 h

6.3. Removal of Cr(VI) from synthetic wastewater

Preparation of standards and analysis of Cr(VI) solution

In order to improve the sensitivity of UV-Vis towards Cr(VI), a complexation agent, 1, 5-diphenyl carbazide (DPC) is used. 0.25 g of DPC was taken and dissolved with small amount of 95% ethanol. This solution was further diluted to 100 mL with distilled water. 0.360 g of potassium dichromate ($K_2Cr_2O_7$), analytical grade, and 1 L distilled water were used to prepare a stock solution of 1000 mg/L Cr(VI) solution. A series of eight standards were prepared by taking aliquots of 0.1, 0.2, 0.3, 0.4, 0.5, 0.7, 1 and 1.25 mL from the stock solution into 100 mL measuring flasks. They were acidified with 5 mL of 0.2 N sulfuric acid. Then 1 mL of freshly prepared 1, 5-DPC solution was added to each standard and a pink color was immediately developed. The solution was completed by adding water until the mark. The standard solutions were analyzed with UV-Visible spectrophotometer with 1cm quartz cell. The absorbance measurements were performed in the range of 400-700 nm. The absorption maxima were observed at 540 nm as shown. A calibration curve is done by plotting the absorbance at the maximum vs the concentration of Cr(VI) in mg/L. A slope of 0.200 ± 0.026 is obtained (Figure 49).

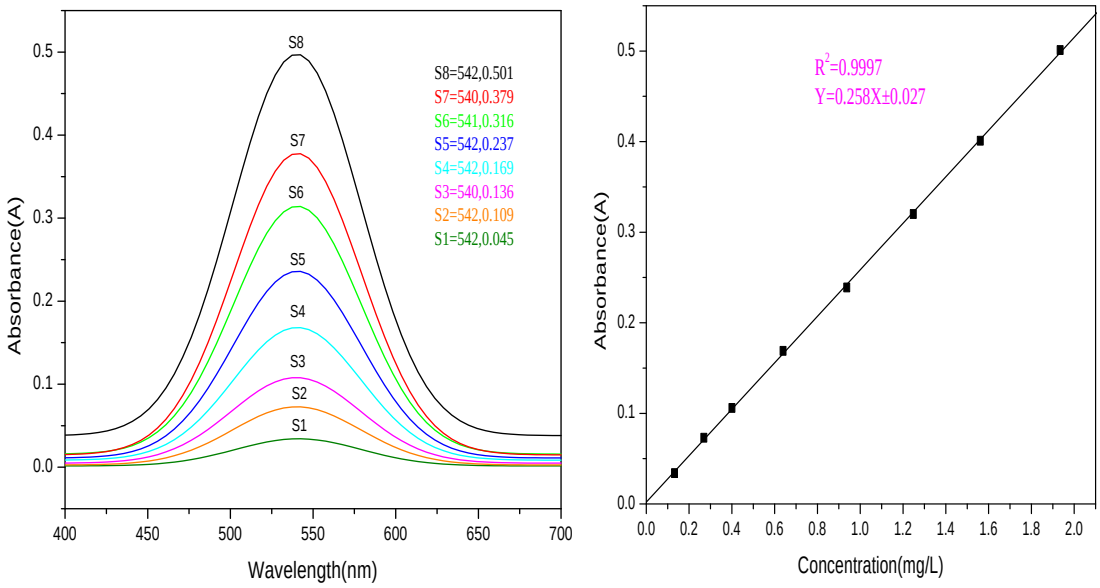

Figure 49: Spectral data and calibration curve of Cr(VI) standard solutions

Chromium (VI) adsorption experiment

For adsorption experiment, 4 mg/L of Cr(VI) solution was prepared by weighing 11.3 mg of $K_2Cr_2O_7$ and diluting it in 1000 ml volumetric flask. Then 2.5 ml of the solution was poured into each glass vials which had 25 mg of the different adsorbents (Clinoptilolite, ET-7, zeolite A, bentonites (Ledi and Mille) and mixed oxides (hydrotalcite and nano-hydrotalcite). Each vial containing the adsorbent and adsorbate was left for a contact time of 24 h under vigorous stirring. Then solutions were taken to centrifuge to separate the supernatant solution from the residue. Finally the supernatant solution was immediately analyzed by adding 0.5 mL of 0.2N H_2SO_4 and 2.5 mL 1.5-DPC to each solution in order to improve the sensitivity towards UV-Vis measurement. These amounts were accurately weighed in order to determine the dilution factor (correction). The absorbance was recorded at 540 nm and the concentration of each solution was calculated using the

calibration curve. For the adsorption isotherm experiments 20 mg of nano-HT/SiO_2 and 20 mL of Cr(VI) solution (adsorbent dose 1 g/L) at different concentrations were used. Adsorption removal (% removal) was calculated using similar expression used in Cr(III) removal. In order to be sure that all the Cr(VI) removed from the solution has been done by adsorption instead of other mechanisms (such as Cr(VI) degradation), the remaining solution of an adsorption experiment was analyzed for total chromium by Atomic Absorption Spectrometry. This control experiment revealed that the concentration of total chromium matched to concentration of Cr(VI) by UV-Vis spectrophotometry within experimental error, indicating that no degradation occurred.

Adsorption results and discussion

In this part we have also attempted to evaluate the potential of natural adsorbents and synthetic zeolite A for Cr(VI) removal following the promising result obtained from tannery wastewater treatment. Table 20 collects a summary of the data obtained from the adsorption experiment. In this experiments, solutions of 4 mg/L of Cr(VI) and different adsorbent dose were chosen. The contact time between the Cr(VI) solution and the adsorbents were not optimized, thus set at 24 h where we assume that the saturation or equilibrium has been reached. The obtained results shows us indirectly the chemical properties of each material, being these properties are the determining factor for the adsorption capacity for a chromate ion in the solution.

Table 20: Cr(VI) removal (%) from model synthetic wastewater using different adsorbents

Adsorbent types		Adsorbent dose (g/L)	(% Removed)
Natural zeolite	Clinoptilolite	10	74.4
	ET-7	10	67.7
Synthetic zeolite A		10	26.3
Bentonites	Ledi	10	89.3
	Mille	10	90.2
Hydrotalcite		10	100
		5	88.7
		2	87.8
		1	85.4
nano-HT/SiO_2		10	100
		5	98.6
		2	96.3
		1	94.6

In principle zeolites are known to be cationic exchangers, thus they should not accept anions, however both natural zeolites (ET-7 and Clinoptilolite) show good (68 to74%) adsorption capacity for chromate ion. The following mechanisms may be proposed to explain this result. 1) Most zeolites found in nature may contain impurities and they are not as neat as synthetic zeolites. The impurities are randomly located throughout the

structure of the zeolite and they may retain the chromate ions from the solution and or they may reduce Cr(VI) to Cr(III) and facilitate its removal by exchanging with the negatively charged zeolite framework. 2) The defect sites present in the structure of natural zeolites contribute to the removal of chromate ion. The chromate ion from the solution can enter to the missing part of the zeolites and can be stuck into the pore. So the removal of Cr(VI) could be observed due to these reasons. In contrast to the natural zeolite, the synthetic zeolite A exhibited the minimum chromate anion removal of 26% that could be due to the predominantly cation exchange properties of zeolites. However, the un expected removal could be due to the presence of impurities in the synthetic zeolite coming from the synthesis from kaolin that can help in the removal of Cr(VI). Interesting removal result which is about 90% is attained by the natural bentonites. The higher removal efficiency of these natural bentonites can be due to the presence of extra framework cations responsible for the reduction of Cr(VI) to Cr(III) and facilitate its removal. The ICP-OES elemental analysis of these bentonites sample (Table 18) indicates the presence of 6 and 7 wt% of Fe that can be responsible for the reduction of chromate anion into Cr(III) and assist its removal by either ion exchange mechanism and/or precipitate Cr(III) as chromium hydroxide, or chromium iron hydroxide. Similar study result was reported by S. A. Wanees et al.[145] in their investigation of the adsorption potential of activated carbon and bentonite for removal of Cr(VI) ions from wastewater. The study result showed bentonite was found to be more effective (76% removal) than activated carbon, under the same experimental conditions.

The other important adsorption result is obtained by the mixed oxides (hydrotalcite and nano-hydrotalcite). The hydrotalcite and nano-hydrotalcite show better adsorption

capacity than the rest of adsorbent mentioned above. Table 20 shows the adsorption removal (% rem) of HT and nano-HT/SiO_2 for a 4 mg/L solution of Cr(VI) at different dosage rates. The Cr(VI) removal is significantly high for both adsorbents even at low dosage rates. For 10 g/L the adsorption removal is 100% in both cases but upon decreasing the dosage rate to 1 g/L the adsorption removal is only decreased down to 85.4% for HT and 94.6% for nano-HT/SiO_2. Similar results are obtained by Lazaridis and Asouhidou[163] for dosage rates ranging from 0.2 to 0.5 mg/L. However, it is possible to observe that nano-HT/SiO_2 exhibits better adsorption capacity than HT, for the same conditions evaluated. The higher adsorption capacity of the latter can be then attributed to the considerable smaller size of the crystals, which would favor adsorption kinetics and would minimize possible hindrances between the layers of HT. Despite the insignificant differenc among the two adsorbents, the removal can be mentioned to the memory effect and ion exchange properties of these materials. The memory effect which consists in the spontaneous structural reconstruction of the original layered structure after being calcinated and then put in water or aqueous solutions containing chromium anions. When hydrotalcite are calcined, the layers become slept together by removing the interlayer distance. After in contact with anionic solution the mixed oxides will start to attain their former structure or reform again and they can start to retain anions (in our case CrO_4^{-2}) easily from the solution (Scheme 7).

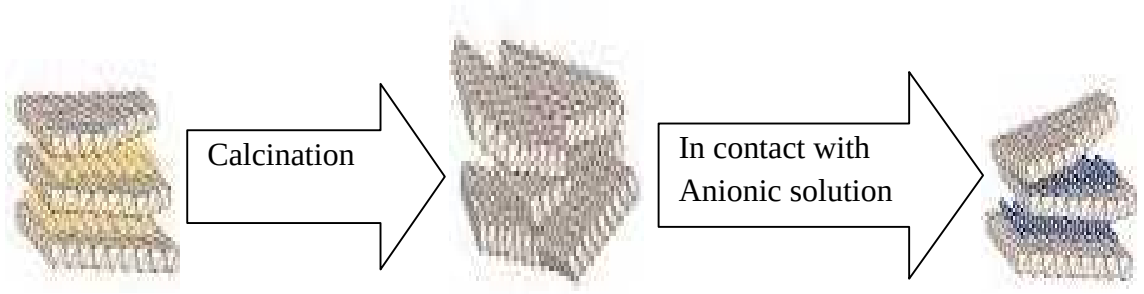

Hydrotalcite Mixed oxide Hydrotalcite

Scheme 7: Schematic diagram for memory effect of hydrotalcite

In the aim to prepare nano-hydroxytalcite, a newly developed synthesis route has been explored in with the hydrotalcite supported on a SBA-15. The final composite SBA-15/HT has the desired functionality in the pores surface, along with large pore size that will allow the chromate ion to move through the channels. The nature of the adsorption mechanism of HT and nano-HT could be initially characterized by X ray diffraction of the solids before and after exposing them to the CrO_4^{-2} solution (Figure 50). The memory effect when using HT versus the anion exchange route followed by nano-HT/SiO_2 could be explained following the structure of the layers in both cases. Figure 50a collects the XRD patterns of conventional HT after calcination, and upon CrO_4^{-2} removal. The profile of HT calcined at 500 ºC shows the loss of the layered structure, showing intensities due to the crystalline mixed oxide formed upon the collapse of the layers. When the HT calcined is exposed to a water solution of Cr(VI) the spontaneous structural reconstruction of the original layered structure takes place due to the adsorption of the CrO_4^{-2} anions that become the scaffold for the cationic layers. The XRD profile of HT exposed to 4 mg/L of Cr(VI) solution can be indexed to the typical layered structure of

hydrotalcite. The presence of Cr in this solid could be corroborated by ICP giving 0.24 weight % Cr. In the case of the composite the nanometric nature of the HT is envisaged by the presence of broad diffraction peaks with very low intensity (Figure 50b). The high background is also indicative of the amorphous nature of the SiO_2 support with no diffraction observed at low angle, which corroborates that the initial SBA-15 structure is no longer hexagonal after the synthesis of the nano-HT. Nevertheless, since this material is not calcined prior the adsorption experiment, there is no change in the overall profile. On the contrary, the XRD profile is identical after adsorption of 4 or 10 mg/L of chromate anions. The profiles could be indexed again as the layered structure of HT, and the presence of identical structure before and after adsorption experiment corroborates that in this case, the mechanism is by anion exchange with no change in the d-spacing between the layers. Once again, the presence of Cr in these solids could be corroborated by elemental analyses (ICP), obtaining 0.38 wt% in the 4 mg/L and 1.29 wt% in 10 mg/L Cr(VI) solution using the nano-HT/SiO_2 adsorbent.

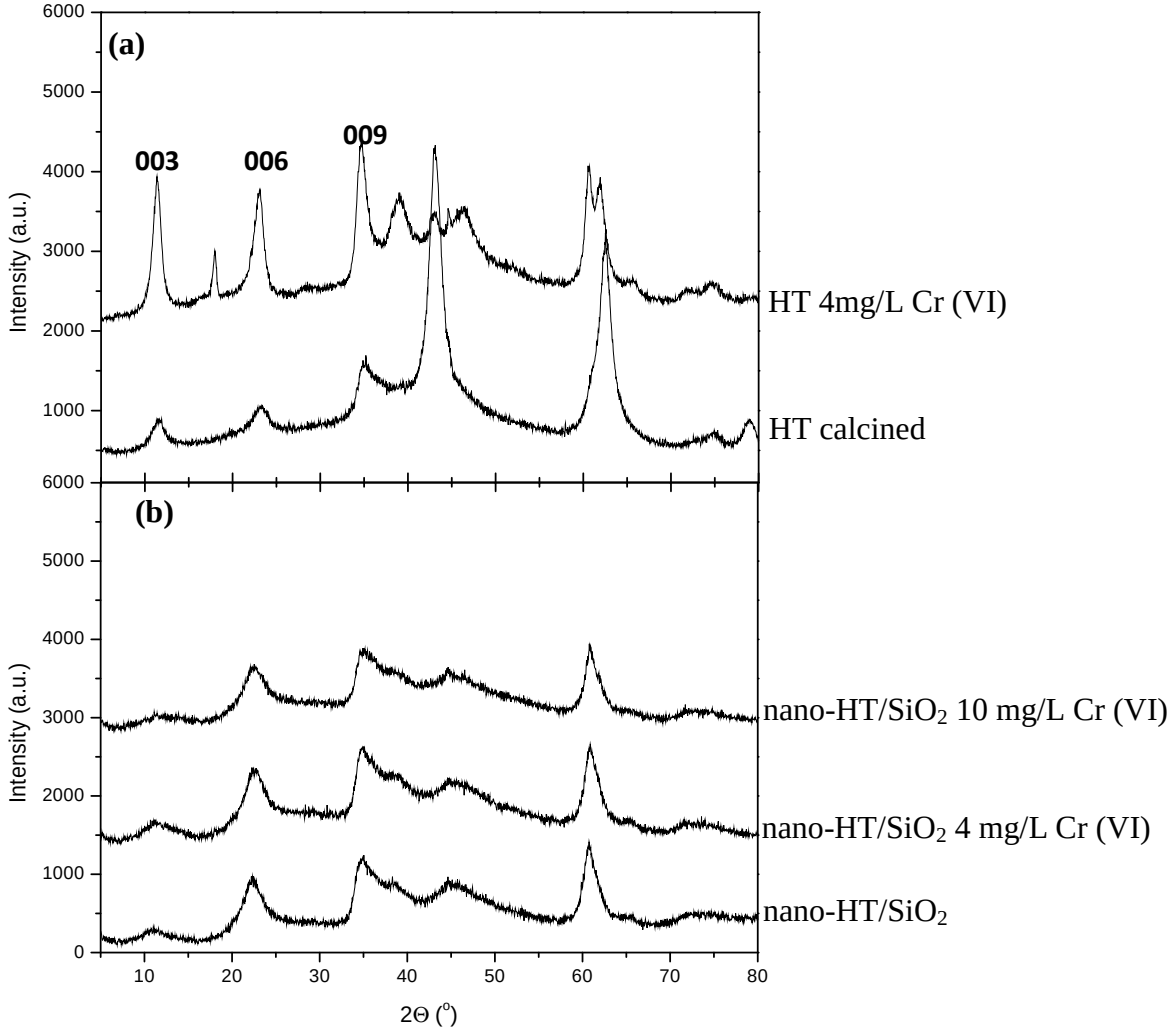

Figure 50: XRD pattern of HT (a) and nano-HT/SiO_2 (b) before and after chromium removal

Further electron microscopy studies were carried out in order to understand the nature of the HT and nano-HT/SiO_2. Besides, it has to be mentioned that HT are extremely unstable under the electron beam due to the large amount of water contained in the layered structure[164], thus, a precise control on the exposure to the electron beam has to be taken into account. This mode yields to images with dark background, while the solid

shows light contrast, and thus the brighter areas are commonly directly related to the higher atomic number of the elements. Low magnification STEM-HAADF images already allow observing different morphology of the particles forming the adsorbent. In the case of conventional HT (Figure 51a), the particles are uniform and rather large, although in the composite sample (Figure 51b), within the same range of magnification, it is possible to observe the agglomerated nature of the particles, showing an uneven surface and morphology.

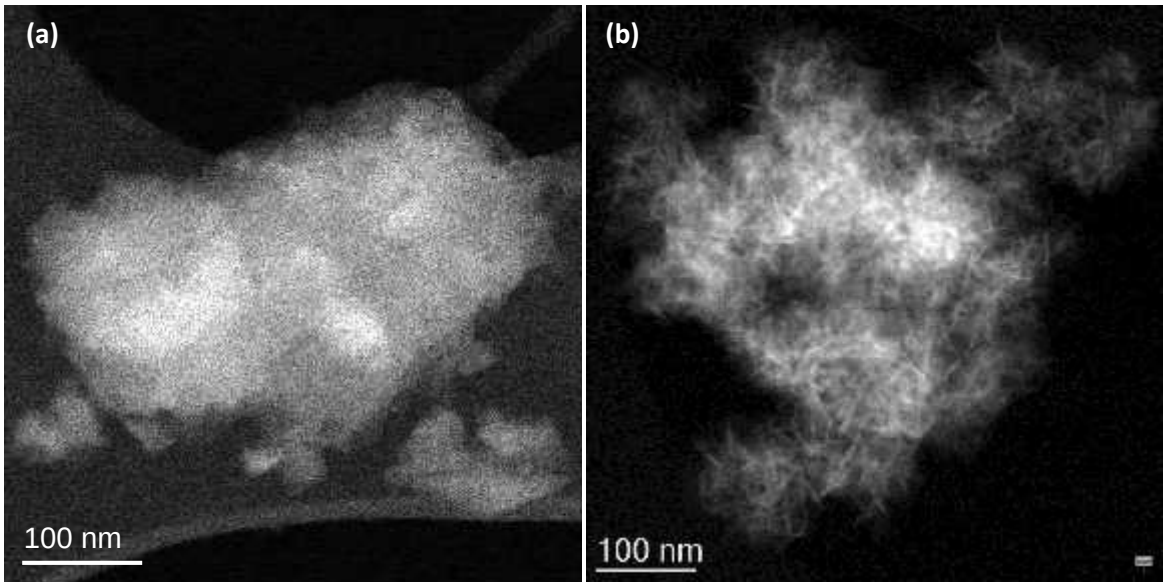

Figure 51: C_s-corrected STEM-HAADF low magnification images of HT (a) and nano-HT/SiO_2 (b)

A closer look to conventional HT reveals uniform crystals (Figure 52a) with layered structure with d-spacings of 0.64 nm (Figure 52b). The microscopy study was carried out after Cr(VI) removal in 4 mg/L solution, thus small amount of Cr could be detected by

EDS, although the layered structure analyzed seems to be perfectly recovered after calcination, proving the memory effect mechanism.

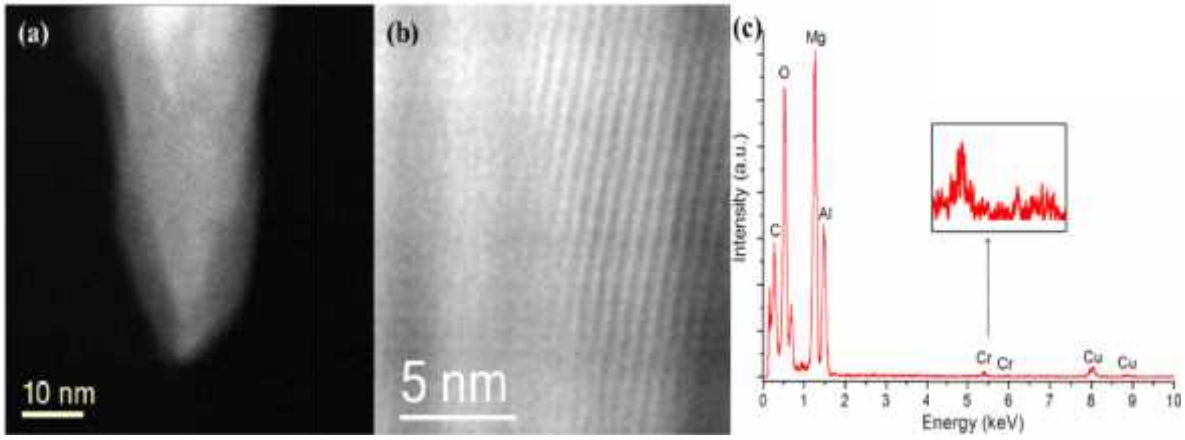

Figure 52: (a) Cs-corrected STEM-HAADF image of the HT particle. (b) HT showing the layers that form the structure with interlayer d-spacing of 0.64nm. (c) EDS spectrum which displays the HT composition, Al, Mg and O, and corroborates the absorption of Cr

Figure 53a and b show the high magnification images of nano-HT/SiO_2 in which due to the high-resolution achieved three layers with d-spacing of 0.62nm (Figure 53a) can be observed. Given the lack of stability of these materials, this result implies an unprecedented high resolution imaging of hydrotalcites most probably due to the strength provided by the SiO_2 support. EDS analyses was conducted in the area imaged as Figure 53b, yielding the Mg, Al in the ratio expected by the HT structure, and Si coming from the support, as well as Cr in a higher amount than before since this sample was observed after 10 mg/L adsorption experiment.

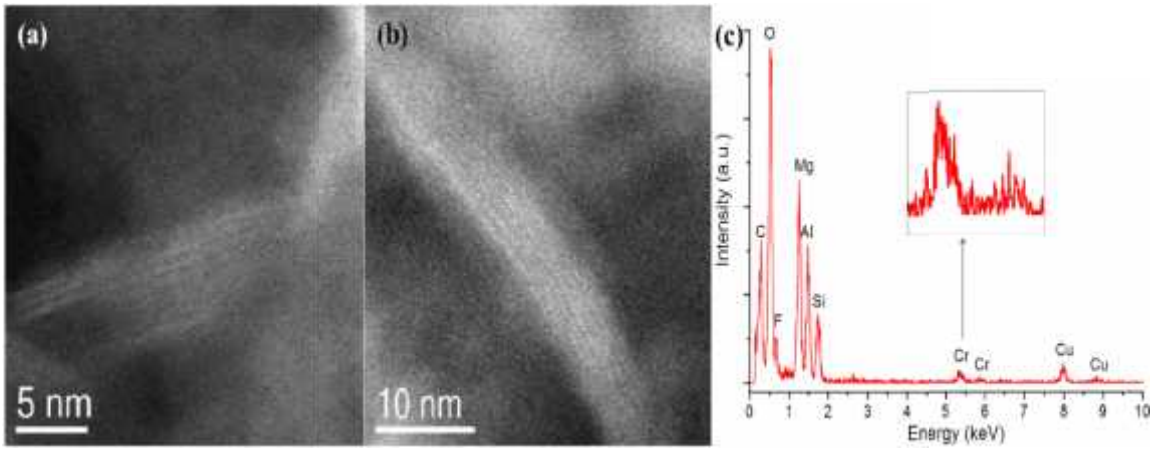

Figure 53: (a) and (b) High-resolution images of 50 nm nano-HT/SiO_2 crystals revealing the interlayer d-spacing of 0.62nm. (c) EDS spectrum which displays the composition of the composite: Si, Al, Mg and O, and corroborates the absorption of Cr

In this study, the behavior of the equilibrium of adsorption between adsorbates and adsorbents was rationalized by studying the adsorption isotherms. Figure 54a shows the adsorption capacity expressed in percent of Cr(VI) removed vs the initial concentration for a dosage rate of 1 g/L. As expected, for low initial concentrations, the proportion of chromium removed is high (> 80%) and it decreases upon increasing initial concentration. The adsorption isotherm is represented in Figure 54b that plots the relationship between the equilibrium capacity, q_{eq} of the adsorbent (expressed in mg of Cr(VI) per gram of nano-HT/SiO_2) and the concentration of the solution in equilibrium. Representation of $\ln q_e$ vs $\ln c_e$ fits to a straight line, indicating that the data are described by a Freundlich isotherm. From the slope and zero intercept of the fitting the Freundlich parameters can be obtained: n = 3.5 ± 0.3; k_f = 3.35 ± 0.14. The report by He et al[165] compares Cr(VI) adsorption of a supported nano-structured HT to adsorption on the same

neat HT powder. They fit adsorption data to Langmuir and Freundlich isotherms obtaining values of R^2 higher for the fitting to the former. However, a closer look to the fittings reveals that only the neat HT fits to the Langmuir isotherm whereas the nanostructured material fits to the Freundlich isotherm. The Freundlich constants obtained (n = 2.24; k_f = 3.73) are comparable to those in this work. The fact that these nanostructured materials do not fit a Langmuir model, suggests a non-uniform surface, which is consistent to their arrangement in nanocrystallites.

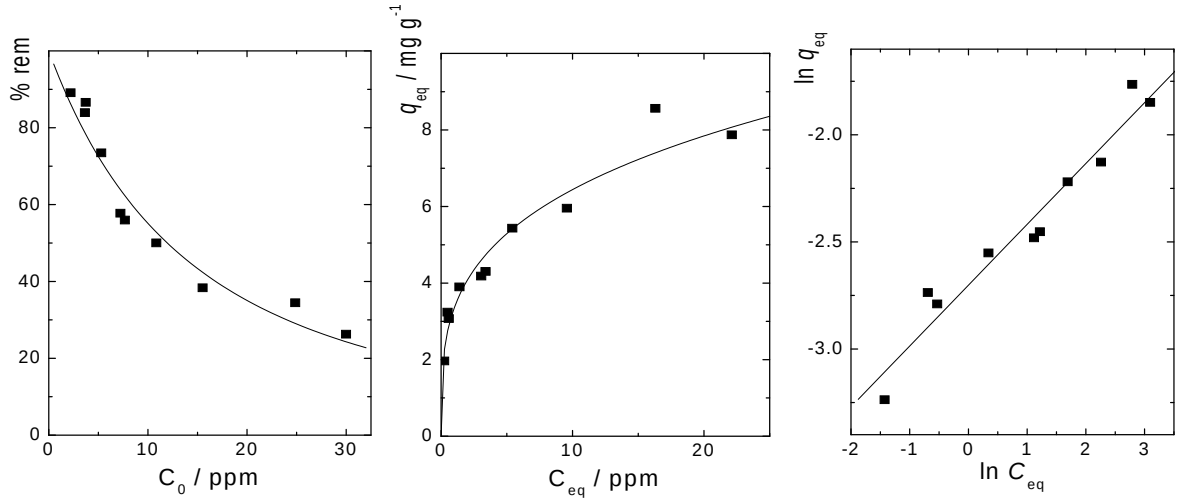

Figure 54: (a) Cr(VI) % removal from solutions at different concentrations. (b) Adsorption isotherm (q_{eq} vs equilibrium concentration). (c) Linearized Freundlich Adsorption isotherm (ln q_e vs ln c_{eq})

6.4. Conclusions

The adsorption capacity of different adsorbents for Cr(III) and Cr(VI) was studied using batch adsorption method. The removal of Cr(III) from tannery wastewater having initial concentration of 2036 mg/L was conducted using different adsorbents. Among all adsorbents used, the maximum Cr(III) removal was attained by the synthetic zeolite A. For the removal capacity of zeolite A and adsorption isotherm study, the adsorbent dosage was varied from 2 to 100 g/L in 10 mL of tannery wastewater in a closed vial until the equilibrium is attained. Adsorption kinetics study was also conducted to understand the behavior of the adsorbent. The results showed that with increase in adsorbent dose, the percentage adsorption of Cr(III) was increased. Maximum removal of 99.8 % and adsorption capacity of 200 mg/g was attained with adsorbent dose of 100 and 5 mg/L respectively. Moreover the adsorption isotherm data could not fit to any of the adsorption models probably due to the different removal mechanism attained at different adsorbent doses. The kinetics study result indicated that the maximum adsorption was attained in the first 3 h adsorption and the experimental data fitted best to pseudo-second order kinetics. In the Cr(VI) removal study, two natural zeolites: Clinoptilolite and ET-7 give an unusually good result that could be related to the presence of impurity and or defect sites responsible for the reduction of Cr(VI) and Cr(III). However, the synthetic zeolite A exihibited small removal capacity, that could be due to the dominate effect of cation exchange property in the synthetic zeolites. In this study two natural bentonites exhibited highest removal efficiencies of about 90%, that could be due to the presence of iron that can reduce Cr(VI) to Cr(III) and responsible for its removal. The best result was shown by the mixed oxides (Hydrotalcite and nano-hydrotalcite).

7. General summary and conclusion

- In this study, characterization and purification of two raw kaolins from Ethiopia; Ansho (A) and Bombowha (B) kaolins has done. Despite, the presence of quartz and mica as an impurity, the characterization result indicated the raw kaolins are mainly composed of the intended kaolinite mineral. Ansho kaolin is better type kaolin compared to the corresponding Bombowha kaolin. However, the synthesis of zeolite A has conducted using both raw and purified kaolins.
- Following the characterization and purification task, the optimization of the synthesis parameters and synthesis method has done to get the optimum crystals of zeolite A. Based on this, two methods of zeolite A synthesis from kaolins has undertaken: the conventional hydrothermal synthesis and alkali fusion followed by hydrothermal synthesis methods. The synthesis parameters optimized were: metakaolinization temprature, alkali concentration, crystallization time and temprature, gel formation temprature and time and gel aging time. The optimization result revealed that the best synthesis conditions were: metakaolinization temprature (600 ^{o}C), alkali concentration (3M), crystallization temprature and time (100 ^{o}C/ 3h) and gel formation at 50 ^{o}C and gel aging time (3 h for A kaolin and 1 h for B kaolin). Although, both methods of synthesis yield optimum crystals of zeolite A (cubic shape with rounded edge), alkali fusion method of synthesis gave zeolite A having high crystallinity (91%) and high cation exchange capacity (310 mg $CaCO_3$/g) which makes it the best synthesis method.
- The other most important work was the investigation of the practical application of the synthesized zeolite A in the manufacturing of powder detergents and for Cr(III) removal from tannery wastewater and Cr(VI) from aqueous solution of chromium in comparison

with other locally available natural adsorbents. The application test indicated promising result in powder detergent as a builder by substituting the environmentally unfriend material sodium tripolyphosphate (STPP). The other exciting application result obtained by the synthetic zeolite A was in the removal of Cr(III) from tannery wastewater. The adsorption result indicated 99.8% removal in the adsorbent dose of 100 g/L. Natural zeolite and clay materials were more efficient in the removal of Cr(VI) from synthetic chromate solution.

8. References

1. S. M. C. Auerbach, K.A.; Dutta, P.K., *Handbook of Zeolite Science and Technology*, Marcel Dekker, Inc.: New York, NY, USA, 2003.

2. Y. Zheng, X. Li and P. K. Dutta, *Sensors*, 2012, **12**, 5170-5194.

3. S. Kulprathipanja, *Zeolites in Industrial Separation and Catalysis*, Wiley-VCH Verlag GmbH & Co. KGaA: Weinheim, Germany, 2010.

4. M. E. Davis, *Chemical Engineering, California Institute of Technology, Pasadena, California 91125, USA*, 2002, **417**.

5. V. H. Bekkum, Flanigen, E.M., Jacobs, P.A., Jansen, J.C., *Introduction to Zeolite Science and Practice.*, 2nd edn., Elsevier, Amesterdam, 1991.

6. W. P. Ruren Xu, Jiong Yu, Qisheng Huo, Jiesheng Chen. , *Chemistry of Zeolites and Related Porous Materials: Synthesis and Structure*, John Wiley & Sons, Singapore, 2007.

7. R. M. Barrer., *Hydrothermal Chemistry of Zeolites.*, 1st edn., Academic Press, New York, 1982.

8. M. Ackley, *Microporous and Mesoporous Materials*, 2003, **61**, 25-42.

9. R. M. Barrer, *Pure and Applied Chemistry*, 1979, **51**, 1091-1100.

10. L. B. M. Ch. Baerlocher, D.H. Olson, *Atlas of Zeolite Framework Types.* , 6th edn., Elsevier, Amsterdam, 2007.

11. D. W. Breck, *Zeolite Molecular Sieves: Structure, Chemistry and Use*, John Wiley & Sons, New York, 1974.

12. A. Dyer, in *Geological Magazine*, Cambridge University Press, New York, 1988, vol. 126, pp. 446-447.

13. B. D. Zdravkov, J. J. Čermák, M. Šefara and J. Janků, *Central European Journal of Chemistry*, 2007, **5**, 385-395.

14. N. K. K. O. Miki Niwa, *Springer Series in materials science* 2010, **141**, 1-97.

15. M. J. Climent, A. Corma and S. Iborra, in *Zeolites and Catalysis*, Wiley-VCH Verlag GmbH & Co. KGaA, 2010, pp. 775-826.

16. J. Weitkamp, *Solid State Ionics*, 2000, **131**, 175-188.

17. A. Primo and H. Garcia, *Chemical Society Reviews*, 2014, **43**, 7548-7561.

18. A. Dabrowski, *Advances in Colloid and Interface Science*, 2001, **93**, 135-224.

19. E. Erdem, N. Karapinar and R. Donat, *Journal of Colloid and Interface Science*, 2004, **280**, 309-314.

20. K. P. Kitsopoulos, *Clays and Clay Minerals*, 1999, **47**, 688-696.

21. R. P. Townsend, *Pure and Applied Chemistry*, 1986, **58**, 1359—1366.

22. K. Margeta, N. Z. Logar, M. Šiljeg and A. Farkaš, *Natural Zeolites in Water Treatment – How Effective is Their Use*, 2013.

23. F. Moattar and S. Hayeripour, *International Journal of Environmental Science and Technology*, 2013, **1**, 45-50.

24. J. Weitkamp, S. Ernst and L. Puppe, in *Catalysis and Zeolites: Fundamentals and Applications*, eds. J. Weitkamp and L. Puppe, Springer Berlin Heidelberg, Berlin, Heidelberg, 1999, pp. 327-376.

25. F. A. M. L.B. Sand, *Natural Zeolites: Occurrence, Properties and Use*, Pergamon Press, Oxford, 1978.

26. D. G. Bogdan Bogdanov, Krasimira Angelova, Yancho Hristov, *International Science conference, Stara Zagora, Bulgaria*, 2009.

27. M. R. Consulting, in *Market Review and Forecast*, Market Publishers Ltd., 2014, p. 58.

28. M. V. C. S. Kundu, S. Rajendiran, Ajay and A. Subba Rao, *Current Science*, 2015, **108**, 1320-1325.

29. V. N. E. Avenue, *ZEODET*, 2000.

30. R. A. Rakoczy and Y. Traa, *Microporous and Mesoporous Materials*, 2003, **60**, 69-78.

31. C. Fruijtier-Pölloth, *Arch Toxicol*, 2009, **83**, 23-35.

32. W. G. a. S. C. Parker, *The Journal of Physical Chemistry C*, 2010, **114**, 9739-9747.

33. S. Y. a. M. Lach-hab, *The Journal of Physical and Chemical Reference Data*, 2010, **39**.

34. K. P. Lillerud, *Verified Synthesis of Zelolitic Materials.*, 2nd edn., Elsevier, Amesterdam, The Netherlands, 2001.

35. J.-Q. Wang, Y.-X. Huang, Y. Pan and J.-X. Mi, *Microporous and Mesoporous Materials*, 2014, **199**, 50-56.

36. Ö. Andaç, M. Tatlıer, A. Sirkecioğlu, I. Ece and A. Erdem-Şenatalar, *Microporous and Mesoporous Materials*, 2005, **79**, 225-233.

37. M. Y. K. Byrappa, *Handbook of Hydrothermal Technology.*, Norwich, New York, U.S.A., William Andrew Publishing, LLC, 2001.

38. A. Palcic, B. Subotic, V. Valtchev and J. Bronic, *Crystal Engineering Communication*, 2013, **15**, 5784-5791.

39. P. Cubillas and M. W. Anderson, in *Zeolites and Catalysis*, Wiley-VCH Verlag GmbH & Co. KGaA, 2010, pp. 1-55.

40. C. G. Pope, *Microporous and Mesoporous Materials*, 1998, **21**, 333-336.

41. C. A. Ríos, C. D. Williams and M. A. Fullen, *Applied Clay Science*, 2009, **42**, 446-454.

42. T. Bein, *Chemistry of Materials* 1996, **8**, 1636-1653.

43. A. G. F. D Renzo, P. Trens, F. Fajula, *Handbook of porous materials.* , Weley-VCH, 2002.

44. A. C. Jiri Cejka, Stacey Zones, *Zeolites and Catalysis: Synthesis, Reactions and Applications*, Wyley-CVH, Weinheim, 2010.

45. R. R. X. a. X. S. Liu, *Acta Chimica Sinica*, 1984, **42**, 227–232.

46. Q. Li, Y. Zhang, Z. Cao, W. Gao and L. Cui, *Petroleum Science*, 2010, **7**, 403-409.

47. C. S. Cundy and P. A. Cox, *Microporous and Mesoporous Materials*, 2005, **82**, 1-78.

48. Y. Li and W. Yang, *Journal of Membrane Science*, 2008, **316**, 3-17.

49. T. R. Bhardwaj Deepesh, Khare S. Purnima, Goswami Yogesh and Srivastva Pankaj, *Research Journal of Chemical Science*, 2013, **3**, 1-4.

50. P. N. A. Gualtieri, G. Artioli and J. Hanson, *Physics and Chemistry of Minerals*, 1997, **24**, 191–199

51. X.-d. Liu, Y.-p. Wang, X.-m. Cui, Y. He and J. Mao, *Powder Technology*, 2013, **243**, 184-193.

52. R. M. Mohamed, A. A. Ismail, G. Kini, I. A. Ibrahim and B. Koopman, *Colloids and Surfaces A: Physicochemical and Engineering Aspects*, 2009, **348**, 87-92.

53. P. K. Rewadee Anuwattana, *Journal of hazardous materials*, 2009, **166**, 227-232.

54. D. N. Khadse Shaila, Patil Pralhad, Panhekar Deepa, *International Research Journal of Environment Science*, 2015, **4**, 93-99.

55. V. Sanhueza, U. Kelm and R. Cid, *Journal of Chemical Technology & Biotechnology*, 1999, **74**, 358-363.

56. S. M. Holmes, A. A. Alomair and A. S. Kovo, *RSC Advances*, 2012, **2**, 11491-11494.

57. M. Gougazeh and J. C. Buhl, *Journal of the Association of Arab Universities for Basic and Applied Sciences*, 2014, **15**, 35-42.

58. G. García, W. Aguilar-Mamani, I. Carabante, S. Cabrera, J. Hedlund and J. Mouzon, *Journal of Alloys and Compounds*, 2015, **619**, 771-777.

59. S. H. Park, J.-K. Yang, J.-H. Kim, C.-B. Chung and G. Seo, *Green Chemistry*, 2015, **17**, 3571-3578.

60. M. M. Crutchfield, *Journal of the American Oil Chemists' Society*, 1978, **55**, 58-65.

61. R. Sharma, D. P. Bisen, U. Shukla and B. G. Sharma, *Recent Research in Science and Technology*, 2012, **4**, 77-79.

62. B. N. V. Shafranovskii I I, Springer, 1962, vol. 351.

63. P. Forman, *Archive for History of Exact Sciences*, **6**, 38-71.

64. J. M. H. Brent Fultz, Springer-Verlag Berlin Heidelberg, 2013, pp. 1-59.

65. H. Stanjek and W. Häusler, *Hyperfine Interactions*, 2004, **154**, 107-119.

66. J. H. BrentFultz, *Transmission Electron Microscopy and Diffractometry of Materials*, 4th edn., Springer Berlin Heidelberg, 2013.

67. V. L. P. Somsubhra Ghosh, B. Sowjanya, P. Srivani, M. Alagaraja, David Banji *Asian Journal of Pharmaceutical Analysis*, 2013, **3**, 24-33.

68. K. R. J. Mamatha Veeramachaneni, *Journal of Advanced Pharmacy Education & Research*, 2013, **3**, 516-522.

69. D. J. E. A. Michael Dunlap, *Facility for advanced instrumentation,U. C. Davis*, 1997, 1-51.

70. T. Radeti, *Fundamentals of Scanning Electron Microscopy and Energy Dispersive X-ray Analysis in SEM and TEM*, University of Belgrade Faculty of Technology and Metallurgy, Beograd, Serbia, 2011.

71. J. Czarnecki and J. Šesták, *Journal of Thermal Analysis and Calorimetry*, 2000, **60**, 759-778.

72. C. Ma and R. A. Eggleton, *Clays and Clay Minerals*, 1999, **47**, 174-180.

73. M. S. Bernhard Welz, *Atomic Absorption Spectrometry*, 3rd edn., 2007.

74. N. R. Bader, *RASAYAN Journal of Chemistry*, 2011, **4**, 49-55.

75. W. Wan, C. Xiao and X. Zou, in *Mesoporous Zeolites*, Wiley-VCH Verlag GmbH & Co. KGaA, 2015, pp. 425-460.

76. D. J. Smith, in *Nanocharacterisation*, The Royal Society of Chemistry, 2015, pp. 1-29.

77. M. B. Ward, N. Hondow, A. P. Brown and R. Brydson, in *Nanocharacterisation*, The Royal Society of Chemistry, 2015, pp. 108-157.

78. A. R. Lupini, S. N. Rashkeev, M. Varela, A. Y. Borisevich, M. P. Oxley, K. van Benthem, Y. Peng, N. de Jonge, G. M. Veith, T. J. Pennycook, W. Zhou, R. Ishikawa, M. F. Chisholm, S. T. Pantelides and S. J. Pennycook, in *Nanocharacterisation*, The Royal Society of Chemistry, 2015, pp. 30-79.

79. J. Z. Ihab H. Farag, *IRACST – Engineering Science and Technology An International Journal* 2012, **2**, 188-194.

80. K. S. Hui and C. Y. Chao, *Journal of hazardous materials*, 2006, **137**, 401-409.

81. A. R. Chaudhuri, G. K. Dey and T. K. Pal, *Chemical Engineering & Technology*, 2002, **25**, 91-95.

82. M. P. Moisés, C. T. P. da Silva, J. G. Meneguin, E. M. Girotto and E. Radovanovic, *Materials Letters*, 2013, **108**, 243-246.

83. Q. Miao, Z. Zhou, J. Yang, J. Lu, S. Yan and J. Wang, *Frontiers of Chemical Science and Engineering in China*, 2009, **3**, 8-11.

84. W. E. Parham, *Clay Mineralogy and Geology of Minnesota's Kaolin Clays.* , Minnesota Geologicla Survey, Minneapolis, 1976.

85. T. K. Valentyn Sviderskyi, *chemistry and chemical technology*, 2013, **7**.

86. H. H. Murray, *Developments in Clay Science, 2*, 2007, **2**, 9-69.

87. D. E. H. A J Bloodworth, C J Mitchell, *Mineralogy and petrology group, British geological survey, Nottingham, United kingdom*, 1993.

88. O. L. A. Abel O. Talabi, Oluwatoyin O. Akinola, *Research Journal in Engineering and Applied*, 2012, **1**, 327-333.

89. J. C. Miranda-Trevino and C. A. Coles, *Applied Clay Science*, 2003, **23**, 133-139.

90. C. C. J. G. Thompson, *Clays and Clay Minerals*, 1985, **33**, 490-500.

91. L. Ayele, J. Pérez-Pariente, Y. Chebude and I. Díaz, *Microporous and Mesoporous Materials*, 2015, **215**, 29-36.

92. C. Belver, M. A. Bañares Muñoz and M. A. Vicente, *Chemistry of Materials*, 2002, **14**, 2033-2043.

93. I. A. Biljana, Mitrovic Ljiljana, Milicic, *Hemijska industrija*, 2010, **64**, 351-356.

94. S. Chandrasekhar, *Clay Minerals*, 1996, **31**, 253-261.

95. T. P. G. Kakali, S. Tsivilis, E. Badogiannis, *Applied Clay Science*, 2001, **20**, 73-80.

96. P. R. S. Ramaswamy, *Journal of Minerals & Materials Characterization & Engineering*, 2011, **10**, 1007-1025.

97. O. A. Ajayi, S. S. Adefila, *International journal of scientific and technology research*, 2012, **1**, 13-18.

98. S. Ayele, *Ministry of Mines Geological Survey of Ethiopia.*, December, 2011, 1-13.

99. T. R. M. a. Agency, in *Brochure*, January 2014.

100. T. M. Haile Michael Fentaw, *Applied Clay Science* 1998, **13**, 149-164.

101. T. R. Yager, *U.S Minerals Yearbook.*, 2011.

102. E. Costa, A. De Lucas, M. A. Uguina and J. C. Ruiz, *Industrial & Engineering Chemistry Research*, 1988, **27**, 1291-1296.

103. E. I. Basaldella, R. M. Torres Sánchez and M. S. Conconi, *Applied Clay Science*, 2009, **42**, 611-614.

104. S. B. G. B. Mitra, *The American mineralogist*, 1969, **54**, 1408-1418.

105. G. Varga, *Építőanyag.*, 2007, **59**, 4-8.

106. S. Sperinck, P. Raiteri, N. Marks and K. Wright, *Journal of Materials Chemistry*, 2011, **21**, 2118-2125.

107. Y. J. K. Sujeong Lee, and Hi-Soo Moon, *Journal of American Ceramic Society*, 2003, **86**, 174-176.

108. M. Alkan, Ç. Hopa, Z. Yilmaz and H. Güler, *Microporous and Mesoporous Materials*, 2005, **86**, 176-184.

109. C. A. Rios, C. D. Williams and M. J. Maple, *BISTUA*, 2007, **5**, 15-26.

110. J. B. H. M.M.J. Treacy, *Collection of Simulated XRD Powder Patterns for Zeolites*, 4th edn., Elsevier, Amsterdam, The Netherlands, 2001.

111. S. U. M. JS Udhoji. A K Bansiwal, S S Rayalu, *Journal of scientifc and indystrial research*, 2005, **64**, 367-371.

112. S. Bosnar, J. Bronić, Đ. Brlek and B. Subotić, *Microporous and Mesoporous Materials*, 2011, **142**, 389-397.

113. S. M. Kuznicki, T. W. Langner, J. S. Curran and V. A. Bell, Google Patents, 2002.

114. B. B. D. Georgiev, I. Markovska, Y. Hristov, *Journal of Chemical Technology and Metallurgy*, 2013, **48**, 168-173.

115. J.-C. Buhl, C. Taake, F. Stief and M. Fechtelkord, *Reaction Kinetics and Catalysis Letters*, **69**, 15-21.

116. D. Novembre, B. Di Sabatino, D. Gimeno and C. Pace, *Clay Minerals*, 2011, **46**, 339-354.

117. E. V.-K. B. Kwakye-Awuah, R. Buamah, I. Nkrumah, C. Williams *International Journal of Scientific & Engineering Research*, 2014, **5**, 734-741.

118. A. S. Kovo, *Chemical Engineering Communications*, 2012, **199**, 786-797.

119. Z. Zhou, G. Jin, H. Liu, J. Wu and J. Mei, *Applied Clay Science*, 2014, **97–98**, 110-114.

120. D. V. a. A. K. Jolanta Donėlienė, *Scientific Journal of Riga Technical University*, 2010, **22**, 30-34.

121. S. Alfaro, C. Rodríguez, M. A. Valenzuela and P. Bosch, *Materials Letters*, 2007, **61**, 4655-4658.

122. B. S. Sekhon and M. Sangha, *Reson*, 2004, **9**, 35-45.

123. R. J. H. D. J. Micco, *U.S. Patent 2003/0050219 A1*, 2003.

124. N. M. Musyoka, R. Missengue, M. Kusisakana and L. F. Petrik, *Applied Clay Science*, 2014, **97–98**, 182-186.

125. L. Ayele, J. Perez-Pariente, Y. Chebude and I. Diaz, *New Journal of Chemistry*, 2016, **40**, 3440-3446.

126. C. J. Adams, A. Araya, S. W. Carr, A. P. Chapple, P. Graham, A. R. Minihan and T. J. Osinga, in *Studies in Surface Science and Catalysis*, eds. H. G. Karge and J. Weitkamp, Elsevier, 1995, vol. 98, pp. 206-207.

127. Y. Yu, J. Zhao and A. E. Bayly, *Chinese Journal of Chemical Engineering*, 2008, **16**, 517-527.

128. D. Bajpai and V. K. Tyagi, *Journal of Oleo Science*, 2007, **56**, 327-340.

129. G. Browne, *US/19864534876.*, 1986.

130. *Compulsory Ethiopian Standard (CES 105), 1st edition. Published by Ethiopian Standards Agency ICS: 71.100.40* 2013.

131. A. A. Belay, *Journal of Environmental Protection*, 2010, **01**, 53-58.

132. O. T. A. A. M. Ashraf Chaudry, *ScienceTechnology and Development*, 2013, **32**, 48-55.

133. P. Ghosh, R. Kumar, A. N. Samanta and S. Ray, *Asia-Pacific Journal of Chemical Engineering*, 2013, **8**, 645-656.

134. J. H. Sharphouse, *Leather Technician's Handbook*, Leather Producer's Association, 1983.

135. A. Zayed and N. Terry, *Plant and Soil*, 2003, **249**, 139-156.

136. C. Maldaner, V. Martins, R. Bertolo and R. Hirata, *Procedia Earth and Planetary Science*, 2013, **7**, 958-961.

137. K. J. Sreeram and T. Ramasami, *Resources, Conservation and Recycling*, 2003, **38**, 185-212.

138. A. M. N. Abass Esmaeili, Reza Vazirinejad, *American Journal of Applied Sciences*, 2005, **2**, 1471-1473.

139. C. Covarrubias, R. García, R. Arriagada, J. Yánez and M. T. Garland, *Microporous and Mesoporous Materials*, 2006, **88**, 220-231.

140. N. F. Fahim, B. N. Barsoum, A. E. Eid and M. S. Khalil, *Journal of hazardous materials*, 2006, **136**, 303-309.

141. R. A. J Raghava Rao, B Madhan, Balachandran Unni Nair and T Ramasami *Journal of American Leather Chemists Association*, 2004, **99**, 197-204.

142. M. Ghiaci, R. Kia, A. Abbaspur and F. Seyedeyn-Azad, *Separation and Purification Technology*, 2004, **40**, 285-295.

143. C. Covarrubias, R. García, J. Yánez and R. Arriagada, *J Porous Mater*, 2007, **15**, 491-498.

144. S. Hillier and D. G. Lumsdon, *Clay Minerals*, 2008, **43**, 477-486.

145. A. M. M. A. Salah Abdel Wanees, Mohamed S. Adam and Mamdouh A. Mohamed, *Chemistry Journal*, 2012, **2**, 95-105.

146. L.-n. Shi, X. Zhang and Z.-l. Chen, *Water Research*, 2011, **45**, 886-892.

147. C. T. Gore, S. Omwoma, W. Chen and Y.-F. Song, *Chemical Engineering Journal*, 2016, **284**, 794-801.

148. P. B. Maria Teresa Olguin, Dwight Acosta and Silva Bulbulian, *Clays and Clay Minerals*, 1998, **46**, 567-573.

149. J. C. A. A. Roelofs, A. J. van Dillen and K. P. de Jong, *Catalysis Today*, 2000, **60**, 297-303.

150. Z. H.-Y. ZHAO Ce, WANG Ya-Ju, LIU Ping-Le, LI Yu-Qin, YANG Yong-Jie, *Journal of inorganic materilas*, 2011, **26**, 874-880.

151. S. Martinez-Gallegos, H. Pfeiffer, E. Lima, M. Espinosa, P. Bosch and S. Bulbulian, *Microporous and Mesoporous Materials*, 2006, **94**, 234-242.

152. M. UNIDO; Boario, *Technical assistance project for the upgrading of the Ethiopian leather and leather products industry* . , Vienna, 2012.

153. G. W. Giorgis, Federal Negarit Gazeta of the Federal Democratic Republic of Ethiopia, Addis Ababa, Ethiopia, 2002, vol. Proclamation No. 300/2002, pp. 1959-1966.

154. A. Perez-Verdejo, A. Sampieri, H. Pfeiffer, M. Ruiz-Reyes, J. D. Santamaria and G. Fetter, *Beilstein journal of nanotechnology*, 2014, **5**, 1226-1234.

155. L. Gómez-Hortigüela, J. Pérez-Pariente, R. García, Y. Chebude and I. Díaz, *Separation and Purification Technology*, 2013, **120**, 224-229.

156. N. G. H. Adhena Ayaliew Werkneh, Hayelom Dargo Beyene, *American Journal of Applied Chemistry*, 2014, **2**, 128-135.

157. K. M. P. Tasrina Rabia Choudhury, Md. Nurul Amin, M.Ali, S.B Quraishi, A.I.Mustafa, *Journal of Environmental Science and Water Resources* 2012, **1**, 144-115.

158. M. Valix, W. H. Cheung and K. Zhang, *Adsorption*, 2008, **14**, 711-718.

159. G. McKay, *Chemical Engineering Science*, 1984, **39**, 129-138.

160. S. Rengaraj, C. K. Joo, Y. Kim and J. Yi, *Journal of hazardous materials*, 2003, **102**, 257-275.

161. M. Pansini, C. Colella and M. De Gennaro, *Desalination*, 1991, **83**, 145-157.

162. A. Mayoral, T. Carey, P. A. Anderson, A. Lubk and I. Diaz, *Angewandte Chemie*, 2011, **50**, 11230-11233.

163. N. K. Lazaridis and D. D. Asouhidou, *Water Research*, 2003, **37**, 2875-2882.

164. I. Diaz and A. Mayoral, *Micron*, 2011, **42**, 512-527.

165. S. He, Y. Zhao, M. Wei, D. G. Evans and X. Duan, *Industrial & Engineering Chemistry Research*, 2012, **51**, 285-291.

9. Appendices

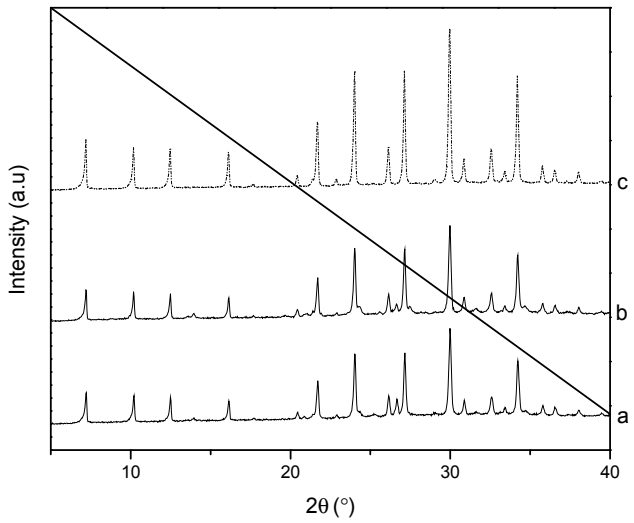

Figure 55: XRD patterns of reaction products using raw kaolins (a) R-A-3M-3h (b) R-B-3M-3h and (c) commercial zeolite A (SZA)

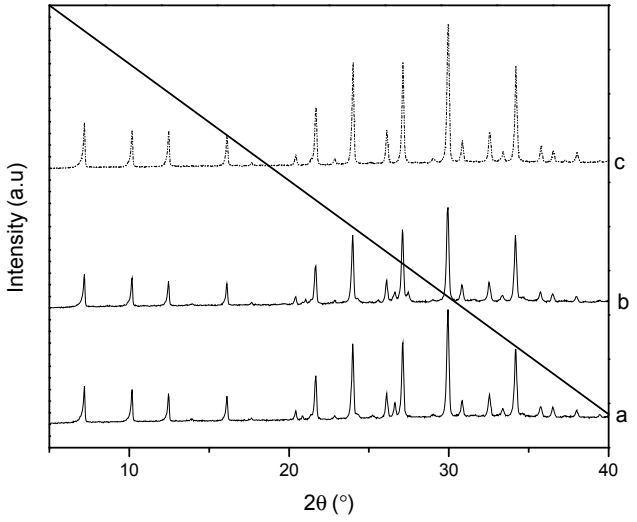

Figure 56: XRD patterns of reaction products using kaolin treated with 1 M HCl (a) A-3M-3h (b) B-3M-3h and (c) commercial zeolite A (SZA)

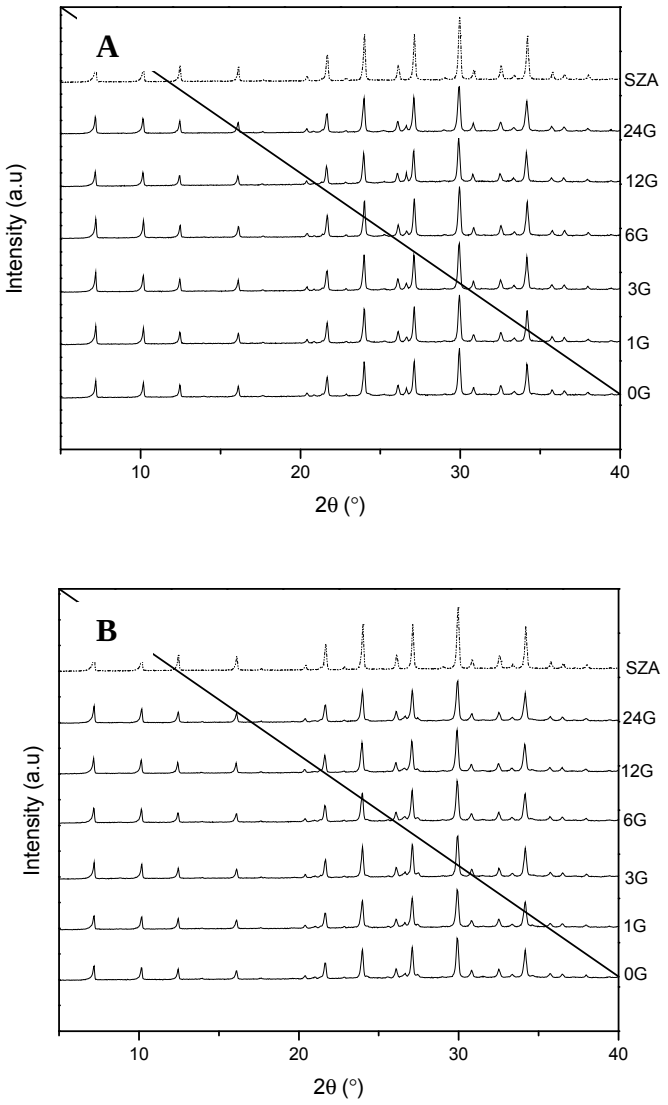

Figure 57: XRD patterns of reaction products with aging effect

Publications

1. Eduardo Perez, **Lijalem Ayele**, Girum Getachew, Geolar Fetter, Pedro Bosch, Alvaro Mayoral, Isabel Diaz. Removal of chromium(VI) using nano-hydrotalcite/SiO_2 composite. *Journal of Environmental Chemical Engineering* 3 (2015) 1555-1561.
2. **Lijalem Ayele**, Joaquín Perez-Pariente, Yonas Chebude, Isabel Díaz. Synthesis of zeolite A from Ethiopian kaolin. *Microporoporous and Mesoporous Materials* 215 (2015) 29-36.
3. **Lijalem Ayele**, Joaquín Pérez-Pariente,Yonas Chebude, Isabel Diaz. Synthesis of Zeolite A using kaolin from Ethiopia and its application for detergents. *New Journal of chemistry* 40 (2016) 3440-3446.
4. **Lijalem Ayele**, Joaquín Pérez-Pariente, Yonas Chebude, Isabel Díaz. Conventional versus alkali fusion method of synthesis of Zeolite A from low grade kaolin. *Applied Clay Science* 132-133 (2016) 485-490.
5. **Lijalem Ayele**, Eduardo Perez, Joaquín Pérez-Pariente, Yonas Chebude, Isabel Diaz. Synthesis of Zeolite A from Kaolin of Ethiopia and its application in Cr(III) removal from tannery wastewater. *Microporoporous and Mesoporous Materials 18th IZC* Invited paper (submitted).